

**SINGLE MOLECULE FLUORESCENCE:  
FROM PHYSICAL FASCINATION TO  
BIOLOGICAL RELEVANCE**

The research presented in this thesis was carried out at the Biophysical Techniques Group, within the Faculty of Science and Technology as part of the program of the BMTI institute of the University of Twente, the Netherlands and in collaboration with the Genetics and Cellbiology Department of the Erasmus University Rotterdam, the Netherlands.

The work was supported financially by the Technology Foundation STW of the Netherlands (Grant no. TTN.4881) and by the 'Vrouwen aan de UT' program.

Cover:

From the upper left corner, in clockwise direction, 16 successive scanning confocal images are shown obtained from a single fluorescent Cy5 molecule. The cartoon in the page center is an author's representation of the NER mechanism.

ISBN: 90-365-1901-2

---

Copyright © 2003, by G.M.J. Segers-Nolten

**SINGLE MOLECULE FLUORESCENCE:  
FROM PHYSICAL FASCINATION TO  
BIOLOGICAL RELEVANCE**

PROEFSCHRIFT

ter verkrijging van  
de graad van doctor aan de Universiteit Twente,  
op gezag van de rector magnificus,  
prof. dr. F.A. van Vught,  
volgens besluit van het College voor Promoties  
in het openbaar te verdedigen  
op vrijdag 16 mei 2003 om 15.00 uur

door

Gezina Maria Johanna Segers-Nolten  
geboren op 21 juli 1956  
te Oldenzaal

Dit proefschrift is goedgekeurd door:

promotor: Prof. Dr. J. Greve

copromotor: Prof. Dr. J.H.J. Hoeijmakers

assistent-promotor: Dr. C. Otto

Nemt nich altied de makkelijkste weg,  
want doar he'j gen voldoening van.



# Contents

<b>1 Introduction</b>	1
1.1 Aim of this thesis	2
1.2 Single molecule fluorescence detection	3
1.3 Single molecule fluorescence detection methods	13
1.4 Confocal fluorescence microscope	15
1.5 Nucleotide excision repair	21
1.6 Outline of this thesis	24
1.7 References	24
<b>2 Characterization of fluorophores used in single molecule fluorescence microscopy</b>	31
2.1 <i>Green fluorescent protein mutants</i>	32
2.1.1 Materials and methods	34
2.1.2 Results	35
2.1.3 Discussion and conclusions	44
2.1.4 References	45
2.2 <i>Cyanine dyes</i>	47
2.2.1 Materials and methods	49
2.2.2 Results	50
2.2.3 Discussion and conclusions	59
2.2.4 References	60
2.3 <i>Alexa dyes</i>	62
2.3.1 Materials and methods	64
2.3.2 Results	64
2.3.3 Discussion and conclusions	68
2.3.4 References	68
<b>3 Structure, dynamics and interaction of single DNA and protein molecules</b>	71
3.1 General introduction	72
3.1.1 <i>Structure of 4-way junction DNA from single molecule FRET</i>	73
3.1.2 Materials and methods	76
3.1.3 Results	78
3.1.4 Discussion and conclusions	88
3.1.5 References	89
3.2 <i>Diffusion of DNA in an agarose matrix</i>	90
3.2.1 Materials and methods	90
3.2.2 Results	93
3.2.3 Discussion and conclusions	98
3.2.4 References	99

3.3	<i>Immobilization of DNA in an agarose matrix by protein binding</i>	100
3.3.1	Materials and methods	100
3.3.2	Results	102
3.3.3	Discussion and conclusions	105
3.3.4	References	106
3.4	<i>Colocalization of NER proteins and DNA</i>	107
3.4.1	Localization of single molecules in confocal fluorescence microscopy images	107
3.4.2	Discussion and conclusions	110
3.4.3	References	111
<b>4</b>	<b>Single molecule study on nucleotide excision repair: complex formation of XPA/RPA with bubble-DNA</b>	113
4.1	Introduction	114
4.2	Materials and methods	115
4.3	Results	117
4.4	Discussion	123
4.5	References	125
<b>5</b>	<b>Single molecule study on nucleotide excision repair: DNA binding specificity of XPA, RPA and XPC</b>	127
5.1	Introduction	128
5.2	Materials and methods	129
5.3	Results	131
5.4	Discussion and conclusions	137
5.5	References	140
<b>6</b>	<b>General discussion and future prospects</b>	143
6.1	Confocal fluorescence microscope	144
6.2	Fluorophores	145
6.3	Alternative optical single molecule methods to study NER	146
6.4	Confocal single molecule microscopy and NER	146
6.5	References	149
	Summary	151
	Samenvatting	153
	List of abbreviations	155
	Nawoord	157
	Curriculum vitae	158



# 1

## INTRODUCTION

*In this chapter the purpose of the research described in this thesis will be given. Background information will be provided with respect to single molecule fluorescence in general, frequently used fluorophores and single molecule detection methods. The Confocal Fluorescence Microscope used in our single molecule fluorescence studies will be described as well as the biological application, which is the Nucleotide Excision Repair process. The chapter will end with an outline of this thesis.*

## 1.1 **Aim of this thesis**

Until about 15 years ago, it only was possible to perform investigations on ensembles of molecules in solution. Traditional biological, biochemical and physical methods, like electrophoresis, chromatography, microscopy and spectroscopy provided valuable information on many biological systems. With these methods the average properties of a population of molecules are determined. Usually individual molecules present in a sample behave in an unsynchronized way. In an ensemble only a small fraction of the molecules may be active during the time of observation and thus contribute only in some extent to the final outcome. To investigate in more detail the characteristic behavior of only the active participants in a reaction it is required either to synchronize the reaction or to study the individual components. The interest in the functioning of individual molecules resulted in the development of several single molecule methods mainly based on the detection of force and/or optical signals. At present the most widely used optical and spectroscopical single molecule detection methods are: Near Field Optical Microscopy (NSOM), Total Internal Reflection Fluorescence Microscopy (TIRFM) and Scanning Confocal Fluorescence Microscopy.

In this thesis the possibilities of Scanning Confocal Fluorescence Microscopy will be shown for the study of the architecture and functioning of complex biological structures. In particular it will be shown how Scanning Confocal Fluorescence Microscopy can contribute to our knowledge of interactions between proteins and DNA in the macromolecular assembly that is formed during Nucleotide Excision Repair (NER). NER is a vitally important process, because it takes care of the elimination of a variety of frequently occurring damages from genomic DNA.

In the following paragraphs we will discuss the basic principles of fluorescence, and in particular aspects of single molecule fluorescence. In relation to their single molecule application in this thesis, we will describe the fluorescence properties of Green Fluorescent Proteins, of cyanine dyes and of Alexa dyes. Immobilization methods and detection techniques for single molecule fluorescence investigations will be considered. The Nucleotide Excision Repair process, subject of our single molecule study, will be described, followed by a description of the confocal fluorescence microscope used and an outline of the thesis.

## 1.2 Single Molecule Fluorescence Detection

### Fluorescence

Before switching to single molecule fluorescence we start with a general description of the fluorescence process. In Figure 1.2.1 the fluorescence process is represented schematically in an energy level diagram. When a molecule absorbs a photon of light, it is excited from the ground state ( $S_0$ ) to a vibrational level of the singlet excited state ( $S_1$ ). The absorption is very rapid and takes about 1 femtosecond ( $10^{-15}$  s). Following excitation, the molecule decays in about  $10^{-12}$  s. to the lowest vibrational level of the excited state through internal conversion while losing energy as heat. The molecule stays at the lowest excited state level during a relatively long time, usually 1-10 nanoseconds, which is called the fluorescence lifetime ( $\tau$ ). When the molecule returns to the ground state ( $S_0$ ) by emitting a fluorescence photon, the energy of this photon will be lower than the excitation energy. Hence the fluorescence wavelength will be longer than the excitation wavelength.

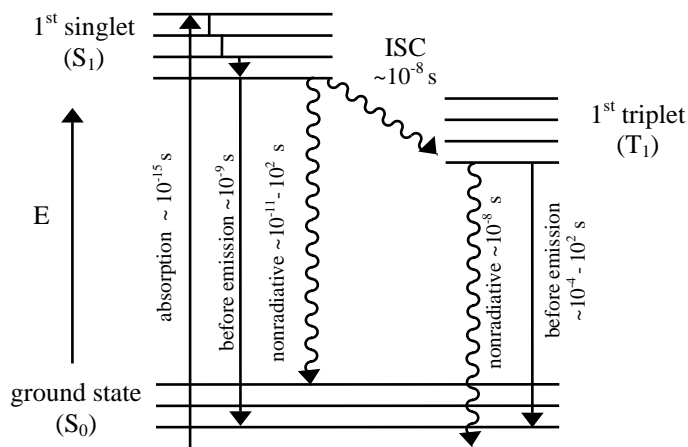


**Fig.1.2.1.** Energy level diagram representing schematically the excitation and emission process. ISC is intersystem crossing from singlet to triplet state (1,2).

Because of the long duration of the excited state lifetime, there is a considerable chance for loss of energy through a number of other processes than direct emission of fluorescence. First, excitation energy may be lost by internal conversion and dissipate as heat. Second, deexcitation also may occur because of collision or complex formation with solute molecules capable of quenching. Oxygen is known as a common quencher of an excited singlet state. Third, intersystem crossing may occur, in which an excited singlet is converted into an excited triplet state ( $T_1$ ). The triplet state lifetime can be extremely long, often seconds or longer. During this time quenching or internal conversion occurs rather

than emission of a photon of light. All of these three processes compete with fluorescence emission to depopulate the excited singlet state.

### **Fluorescence resonance energy transfer**

A process that may occur between pairs of fluorescent molecules that are in close proximity is fluorescence resonance energy transfer (FRET). FRET is transfer of energy from an excited state ( $S_1$ ) donor molecule to a ground state ( $S_0$ ) acceptor molecule, leading to excitation of the acceptor ( $S_1$ ). After loss of vibrational energy, the acceptor molecule can return to the ground state by emitting a fluorescence photon. Only if the emission spectrum of the donor molecule sufficiently overlaps with the excitation spectrum of the acceptor molecule FRET may happen. Energy is transferred without the appearance of a photon and is the result of dipole-dipole interactions between the donor and acceptor.

The efficiency of FRET can be described as (2):

$$E = \frac{1}{\left[1 + \left(\frac{R}{R_0}\right)^6\right]} \quad (1.1)$$

where  $R$  is the distance between the fluorophores and  $R_0$  is the characteristic Förster distance for a given donor-acceptor pair.  $R_0$  is determined by the donor quantum yield in the absence of the acceptor, the relative orientation of the donor and acceptor transition dipoles, the refractive index of the medium and the spectral overlap between donor emission and acceptor excitation.

An important characteristic of FRET is that it occurs over distances comparable to the dimensions of biological macromolecules (~5 nm). Therefore FRET studies are particularly useful in the study of dynamics within biological systems.

### **Single molecule fluorescence**

Keeping in mind the above-mentioned processes associated with fluorescence, we can explain differences in fluorescence behavior observed from single fluorescent molecules. For illustration, examples of single molecule emission profiles, as observed with our confocal fluorescence microscope, are shown in Figure 1.2.2. The fluorescence was registered after positioning a single molecule in the focus of the microscope. The intensity of the fluorescence emission varies in time and is recorded in a so-called time trace. Next we will discuss the typical single molecule features that can be discerned.

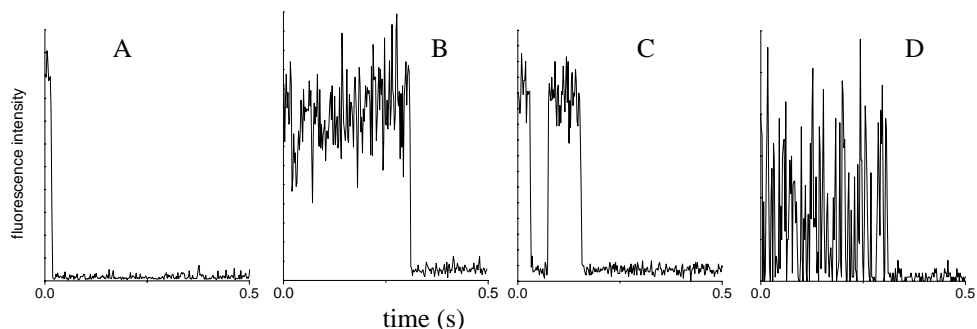


**Fig. 1.2.2.** Examples of single molecule fluorescence time traces as measured with confocal fluorescence microscopy from different fluorophores. The time traces are represented with a data bin time of 2 ms. For A, B, C and D see the text.

### Bleaching

Because of the high probability for quenching, fluorescent molecules will only emit a limited number of photons. Experimentally, the maximum amount of photons emitted by a single molecule has been found to be usually less than  $10^6$ . The time traces in Figure 1.2.2 all show periods of emission that stop suddenly. The abrupt *bleaching* is a behavior that is indicative for the emission by a single molecule. It is highly improbable that a time trace measured from a cluster of molecules displays a similar single bleaching step. Because of unsynchronized bleaching a gradual decrease in intensity is expected from a cluster. Figure 1.2.2.A and B indicate the difference in duration of emission as can be observed from individual molecules. The time periods that fluorescence can be detected from a single molecule are named *on-times*.

### Blinking

In Figure 1.2.2.C two periods of emission, with different *on-times*, are shown separated by a dark period. The *off-time* may be caused by a transition of the molecule from a singlet excited state to a triplet excited state. As long as the molecule stays in the triplet state, the molecule will not emit. A dark interval occurs from which the molecule, represented in this particular time trace, recovered by emitting photons again. Figure 1.2.2.D is a representation of single molecule fluorescence that is accompanied by strong fluctuations in intensity. This behavior may be attributed to fast conformational changes, as observed for single Green Fluorescent Protein (GFP) molecules (3). Also an isomerization process may be responsible for the fluctuating emission behavior, as has been reported for Cy5 dye (4). For Cy5 the existence of a fluorescent *trans*-state has been shown that changes into a non-fluorescent *cis*-state upon isomerization. In general, the occurrence of alternating bright and dark intervals during single

molecule emission is known as *blinking*. In the next paragraphs the use of GFP and Cy dyes in single molecule applications will be discussed further.

### Single pair FRET

To demonstrate the occurrence of FRET between a single donor and acceptor pair a typical example of a time trace measured with our confocal fluorescence microscope is shown in Figure 1.2.3.

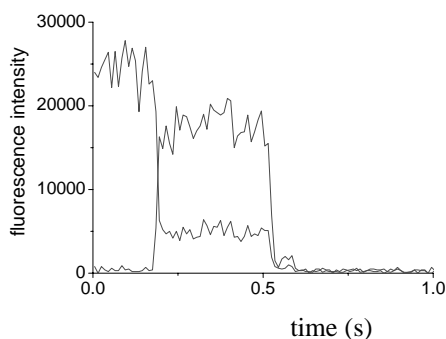


**Fig. 1.2.3.** Example of a single molecule time trace displaying FRET from a single donor Cy3.5 and acceptor Cy5 pair. Excitation wavelength was such that only the donor was excited. The red curve indicates the acceptor fluorescence and the green curve the donor fluorescence.

Figure 1.2.3 demonstrates the initial fluorescence of the acceptor molecule, although the acceptor is not directly excited by the applied excitation wavelength. At the same time there is hardly fluorescence from the donor. This means that probably energy transfer occurs. After about 200 ms the acceptor fluorescence suddenly drops and simultaneously the donor fluorescence increases. This is an indication that the acceptor is bleached resulting in fluorescence emission from the donor again.

## Fluorescent labels for single molecule detection

### Green Fluorescent Proteins

For fluorescent labeling of proteins, mutants of the autofluorescent Green Fluorescent Protein (GFP) have proven to be very useful. Originally, wild-type GFP was found in a small jellyfish in the Pacific Ocean. The chromophore of the 238 amino acid wild-type GFP was found to consist of only 3 amino acids, Ser65, Tyr66 and Gly67 (5). Later, the gene coding for the wild-type GFP, was discovered and cloned (6). The fluorophore was shown to be formed by an autocatalytic posttranslational cyclization reaction of the chromophore sequence (7). For chromophore formation and fluorescence emission proper folding of the

polypeptide was shown to be required. The chromophore sequence of GFP appeared to be part of a small  $\alpha$ -helix that is located in the center of an 11-stranded  $\beta$ -barrel (8). In Figure 1.2.4 the unique 3D-structure of GFP is shown.

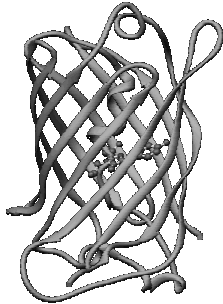


**Figure 1.2.4.** *Ribbon diagram of the three dimensional structure of GFP. The chromophore is shown as a ball and stick model (8).*

Hidden inside the unique barrel structure, the chromophore of GFP is protected against influences from the environment. Consequently, GFP appeared to be a very stable fluorophore. Hardly any effect was detected from fluorescence quenching agents like molecular oxygen (9). GFP fluorescence appeared hardly to be sensitive to temperature (10), pH (11,12), acid or base treatment (13), proteases (10) and detergents (14). Even a tolerance to fixatives like glutaraldehyde and formaldehyde was shown (11).

The postsynthetic formation of the fluorophore, without a need for any additional factors, made recombinant production of functional GFP possible (11,15). Introduction of the GFP gene into a host cell resulted in expression of recombinant GFP, spontaneously emitting fluorescence. For the same reason, GFP became a remarkably useful and valuable tool in cellular and molecular biology. By transfecting cells with GFP fusion genes, the possibility was offered to localize proteins and to study dynamics of cellular processes in intact cells, without a need for fixation. GFP has been successfully targeted to practically every major organelle of the cell (16). Surprisingly, in general the presence of the rather big GFP tag did not alter the normal function of the fusion partner.

### **Mutants of GFP**

Knowledge of the three-dimensional structure of GFP enabled investigators to design and develop mutant proteins with altered and improved spectral characteristics (8, 17-22). Mutagenesis yielded proteins that fluoresce from blue to yellowish green. From a different source, from coral, a red fluorescent protein was cloned. In the research described in this thesis we made use of two green fluorescent mutants, GFP(S65T) and EGFP, the cyan fluorescent ECFP and the yellow fluorescent EYFP mutant. In paragraph 2.1 their photophysical properties and excitation and emission spectra are shown. The photophysical properties of GFP mutants, like extinction coefficients and quantum yields, match well with

those from certain chemical dyes. Only the characteristics of the ECFP mutant are rather weak.

Combinations of mutant fluorescent proteins have mainly been used for *in vivo* experiments to simultaneously visualize multiple fusion proteins in cells (23,24). From *in vivo* (25) as well as from *in vitro* experiments the usefulness of GFP mutants in the study of protein dynamics and protein-protein interactions has been shown. In particular ECFP as a donor together with EYFP as an acceptor form a proper combination for application in fluorescence resonance energy transfer (FRET) experiments. A well-known GFP FRET application is the study of dynamic conformational changes in ECFP-calmodulin-M13 peptide-EYFP fusion proteins, so-called cameleons, upon binding of calcium ions (26,27).

### **Single molecule application of GFP**

Not only in cell biology and molecular biology, but also in single molecule studies GFP has shown its significance. Despite the known stability of the GFP fluorophore, GFP single molecule fluorescence appeared to be accompanied by strong intensity fluctuations, representing the typical GFP blinking behavior (3). Many single molecule investigations on the photophysical processes underlying the fluorescence of GFP have been performed (28-32). Yet these processes are not completely understood and are still subject of considerable interest.

*In vitro*, GFP was successfully applied in single molecule studies with total internal reflection microscopy on the functioning of the motor proteins myosin and kinesin (33,34). *In vivo*, single GFP molecules were imaged for the first time in living cells in a study on oligomerization and movement of the cell adhesion protein E-cadherin (35).

The usefulness of GFP donor and acceptor mutants in single molecule Fluorescence Resonant Energy Transfer (FRET) experiments has been demonstrated from the observation of dynamics in the above mentioned ECFP-EYFP labeled cameleon protein complexes (36).

Within the framework of our single molecule study on NER-complexes we are interested in dynamics of interactions between different proteins within a complex. For that purpose we prepared the donor ECFP labeled XPA protein and the acceptor EYFP labeled ERCC1/XPF complex. For correct interpretation of results it is important to know the single molecule quality of the applied fluorophores. Therefore we will show in paragraph 2.1 the single molecule characteristics of the GFP mutants that we used in our study, as measured with our confocal fluorescence microscope. The mutants included are GFP(S65T), EGFP, ECFP and EYFP.



## Chemical dyes

### Cyanine dyes

Sulfoindocyanine fluorescent dyes consist of two identical heterocyclic head groups bridged by unsaturated carbon chains. The negatively charged sulfonate groups make the dyes highly water soluble and thus very convenient in labeling of biomolecules (chemical structures of Cy3.5 and Cy5 are shown in paragraph 2.2). Because of the negative charge there is repulsion between the dye molecules, which results in less quenching and improved brightness. A series of fluorescent sulfocyanine dyes has been developed with fluorescence over a wide spectral range (500-750nm). The individual dyes are different in their heterocyclic head groups and the number of double bonds in the carbon chain bridges. The available cyanine dyes are named from Cy3 till Cy7. The number indicates the number of bridge carbon atoms that connect the two heterocyclic ring structures. The higher the number, the longer the wavelength of emission is. Cyanine dyes are attractive as fluorescent labels because of their brightness. They have high extinction coefficients (150,000 to 250,000) and quantum efficiencies of 0.15-0.27. They are insensitive for pH changes over a wide pH range. They are more photostable than most other fluorophores. A number of cyanine dyes, Cy5 and Cy7, absorb and emit above 600 nm, reducing problems with autofluorescence in cell biological applications. They are offered as reactive succinimidyl esters for labeling of aliphatic amino groups on proteins and amino-modified nucleic acids (37-39).

**Bulk applications** Cyanine dyes have been used for labeling of proteins (40) and DNA (41) for detection with different techniques. In flow cytometry, Cy5 has been applied frequently as an antibody label for immunophenotyping of blood cells (42,43). In cell biological applications with confocal fluorescence microscopy, combinations of Cy dyes are popular for simultaneous detection of different cellular components (44).

**Single molecule applications** Also in single molecule detection methods Cy dyes are popular. *In vivo*, in the cell membrane, the dimerization (45) of single Cy3-labeled protein molecules was followed as well as the lateral motion of Cy5-labeled lipid molecules (46).

*In vitro*, Cy5 was used as a fluorescent probe in single molecule DNA sizing with flow-cytometry (47). Characterization of Cy5 single molecule fluorescence was performed with fluorescence correlation spectroscopy (4). From this study it was concluded that a trans-cis isomerization process causes strong fluctuations in emission of Cy5. With wide-field microscopy also alternating bright and dark periods were observed as well as fast bleaching of Cy5 (48).

**FRET** Because their fluorescence covers a broad spectral range, combinations of Cy dyes have proven to be very useful in FRET studies. A single molecule FRET study has been reported from DNA molecules labeled with a combination of Cy3 as a donor and Cy5 as an acceptor (49). More frequently Cy5 has been used as an acceptor together with another type of dye as a donor, like Tetramethylrhodamine (TMR) (50-52), rhodamine 6G (49), rhodamine red (53) or Alexa 488 (54). In particular in the interpretation of FRET results it is important to take into consideration the fluorescence fluctuations of Cy5 (4). In a FRET situation, not every decrease in Cy5 acceptor emission may be caused by a larger separation from the donor.

In our single molecule study we used Cy3.5 and Cy5 as DNA labels. Because of the spectral properties their fluorescence can be well distinguished from EGFP and EYFP fluorescence. In paragraph 2.2 we show the single molecule characteristics of Cy3.5 and Cy5 as measured with confocal fluorescence microscopy. We demonstrate in paragraph 3.1.3 the usefulness of Cy3.5 and Cy5 as a FRET pair from single molecule experiments with four-way junction DNA. We combined Cy labeled DNA with EGFP and EYFP labeled NER-proteins for single molecule analysis of NER complexes (described in chapter 3, 4 and 5).

### **Alexa dyes**

Alexa dyes with different spectral characteristics were developed by modifying sulfonated aminocoumarin or rhodamine compounds (55,56). Because of their hydrophilicity Alexa dyes are convenient for labeling of biomolecules in a buffer environment (chemical structure of Alexa 488 is shown in paragraph 2.3). With the Cy dyes they share the insensitivity for pH, and the availability of a variety of colors. Alexa dyes are available in the whole range from Alexa 350 to Alexa 680, where the number indicates the approximate excitation maximum. At the moment the Alexa dyes were introduced they were announced as the best and brightest dyes ever. The extinction coefficients range from 19,000 for Alexa 350 to 239,000 for Alexa 647. The quantum efficiencies are higher than from Cy dyes. Their absorption spectra match well with principal output wavelengths of common excitation sources. Alexa dyes are offered as reactive succinimidyl esters for labeling of aliphatic amino groups on proteins and amino-modified nucleic acids, or as maleimide esters for labeling of thiol groups on cysteine containing proteins. Initially Alexa dyes were used mainly as protein labels, but now they are also available as DNA labels, conjugated to nucleotides as well as to oligomers.

**Bulk applications** In confocal fluorescence microscopy Alexa dyes have been used for simultaneous visualization of different cellular components. Immunofluorescence staining is very popular with Alexa dyes (57). In a study on Alexa 488-labeled calmodulin, Alexa 488 fluorescence intensity appeared to be indicative for conformational changes of the protein as a reaction on calcium

binding (58). FRET experiments have been performed with Alexa 488 as a donor in combination with rhodamine-X as an acceptor to study the trajectory of nucleosomal linker DNA (59). With fluorescence correlation spectroscopy FRET was measured between Alexa 488 and Cy5 (54).

**Single molecule applications** In spite of the superior photophysical properties in bulk, only a few literature reports appeared on single molecule applications with Alexa dyes. Conformational changes in an Alexa 488 labeled enzyme were studied by detection of fluorescence quenching on the single molecule level (60). Single particle tracking of Alexa 488 labeled protein molecules was performed to determine the trajectories of a single protein molecule inside the cell nucleus (61,62).

Because of their excellent photophysical properties, Alexa dyes would possibly be good candidates for use in our single molecule study on NER complexes. Therefore we studied the single molecule fluorescence characteristics of Alexa 488 dye bound to a DNA repair protein, the XRCC4 protein, with confocal fluorescence microscopy (described in paragraph 2.3). The confocal single molecule results indicate however that the fluorescence properties of Alexa 488 on the single molecule level are much less promising than expected.

### ***Comparison of GFP labeling and chemical labeling for single molecule applications***

1. GFP labeling is performed by fusion to the N- or C-terminus of a protein. If the N- or C-terminus is not essential for functionality, it is possible to connect GFP to a fusion partner without interference with its activity. Chemical modification usually is less specific and may cause inactivation of protein because of binding to or near the active site.
2. GFP labeling results in a well-defined labeling ratio of exactly one GFP molecule per polypeptide chain. With chemical labeling reactions a statistical mixture of proteins with differing numbers of fluorophores per molecule is obtained. For single molecule applications characterization of the mixture is required. Only if proteins contain a unique site for labeling, like a single cysteine residue, it is possible to achieve a 1:1 labeling ratio with chemical methods. Maleimide derivatives of dyes react selectively with cysteine thiol groups. Although cysteine amino acids are not very abundant in most proteins, it may be necessary to change their number or position within the protein with recombinant methods.
3. In chemical labeling procedures often organic solvents are required that may denature proteins. In contrast, labeling with GFP is performed in mild, biological conditions.

4. Like chemical dyes, GFP mutants are available with fluorescence over a wide spectral range. As well as chemical dyes, also certain combinations of GFP mutants form suitable FRET pairs.

## **Immobilization**

To be able to observe single molecules with scanning confocal fluorescence microscopy during a certain time some form of immobilization is required. It is important to immobilize the molecules of interest in the proper way, without affecting their biological and fluorescence properties. Also in other fields than single molecule research, proper immobilization of molecules is highly important. In particular in the development of microchips for array-based genetic diagnosis, the immobilization of DNA is an important issue. In this area mainly methods have been used based on adsorption, covalent binding, affinity binding or combinations of these methods. The same methods also have been applied in single molecule detection techniques. Covalent binding often is performed by amino-silanization of a surface, followed by activation and direct coupling of amino-modified DNA or proteins (63,64). Another possibility is to bind thiol-modified DNA to amino-silanized surfaces treated with crosslinkers (64) or to gold surfaces (65). With respect to affinity binding the biotin/streptavidin system is popular. Streptavidin may be covalently bound to silanized surfaces or to surfaces covered with biotinylated BSA (66). To prevent non-specific binding sometimes covalently bound biotinylated polyethyleneglycol is used as a spacer between streptavidin and the silanized surface (67). Protein immobilization can be accomplished by adsorption or by affinity binding to antibodies (68). Recombinantly produced histidine-tagged proteins may be affinity bound to nickel-treated surfaces (69).

**Single molecule aspects** In single molecule methods not only the preservation of functionality during immobilization is required, but also a homogeneous yet rather sparse distribution of molecules. The distribution should be such that molecules are located at sufficient distance to enable observation of individual molecules. It depends on the resolution of the applied technique what the maximum allowed density is. Diffraction limited methods, like confocal fluorescence microscopy and TIRF, require a lower density than higher resolution techniques, like NSOM.

All the above-mentioned immobilization methods usually result in a rather inhomogeneous distribution of molecules. Therefore in single molecule fluorescence microscopy additional procedures are used that allow more accurate control of the density. A commonly used procedure is to confine the molecules in the waterfilled pores of a polyacrylamide (PAA) or agarose gel matrix

(30,31,36,70). The concentration of the molecules of interest can be accurately controlled because they are included in the liquid gel mixture. During formation of the gel matrix the fluorescent molecules are trapped in the pores of the gel. Gel immobilization is however not possible with every type of biomolecule. In paragraph 3.2 we show that DNA molecules are not immobilized in gel matrices, but still show diffusional mobility. DNA molecules can be studied on the single molecule level after adsorption to a surface, as shown in paragraph 2.2 and 3.1.3. Protein molecules, on the other hand, like GFP molecules and GFP labeled NER proteins, are immobilized in gel matrices. In the next chapters of this thesis we will demonstrate that gel matrices are not only convenient for single molecule immobilization (chapter 2), but that they also offer the possibility to obtain quantitative results on protein-DNA binding (chapter 3, 4 and 5).

### 1.3 **Single Molecule Fluorescence Detection Methods**

For detection of single molecule fluorescence mainly three microscopic methods have been used, Total Internal Reflection Fluorescence Microscopy (TIRFM), Near Field Scanning Optical Microscopy (NSOM) and confocal fluorescence microscopy.

**TIRFM** Single molecule TIRFM has been performed in a prism-type (71) and an objective-type configuration (72). Illumination by total internal reflection produces an evanescent field just beyond the interface in the medium with a  $1/e$  penetration depth of about 150 nm. Because of the steep decline of the evanescent field with distance, only molecules residing very near to the interface will fluoresce brightly, resulting in a high ratio of fluorescence to background. With TIRFM a large area of a sample is illuminated allowing simultaneous detection of several molecules for instance with a CCD camera. This is an advantage of TIRFM over scanning techniques like confocal and NSOM. TIRFM is a non-scanning method with diffraction limited ( $\sim\lambda/2$ ) optical resolution and a time resolution limited by the frame rate of the CCD-camera, which is at present for single molecule detection around 10 ms per frame.

**NSOM** In NSOM a probe with an aperture of sub-wavelength dimension is used to illuminate the sample. The probe is held in close proximity, usually less than 10 nm, of the sample. An image is formed by scanning the probe and the sample with respect to each other. In this way the optical resolution is not limited by diffraction but completely determined by the size of the probe aperture, typically smaller than 100 nm. For localization purposes this is advantageous. Because of a small excitation volume and steep decline of the excitation field the relative contribution from background signal is low. By independently controlling the distance separation between the probe and the sample within 1 to 10 nm,

simultaneously a fluorescence and a topographic image can be generated. A drawback of NSOM is that the presence of the probe in close proximity of the sample may result in unwanted probe-sample interactions. Another problem is the difficulty to obtain high quality probes and the complexity of operating an NSOM instrument properly. Moreover, because NSOM is a surface technique there are restrictions to the types of samples that can be measured. So far only from dry samples satisfying results were obtained. In imaging mode, the time resolution of NSOM is determined by the speed of scanning. Time traces of individual molecules can be measured with a time resolution of a few microseconds. Applications of single molecule detection with NSOM involve imaging of single molecule labeled DNA (73) and single GFP molecules (74).

**Scanning confocal fluorescence microscopy** In the single molecule work described in this thesis we made use of a scanning confocal fluorescence microscope. In confocal microscopy the optical resolution is determined by the diffraction limit. This means a resolution of roughly half the excitation wavelength, like in TIRFM. Although in confocal fluorescence microscopy no details smaller than the diffraction limit can be resolved it is possible to determine the center of a fluorescence spot and hence the location of the fluorescent object with much higher precision by applying Gaussian fitting procedures. In paragraph 3.4 we show results from localization analysis of single molecule images measured with our confocal fluorescence microscope.

Fluorescence detection in our setup is performed with a small pinhole in front of the detector, which is confocally aligned with the focus of the excitation beam. In this way a sufficient reduction in background signal is obtained to enable detection of single molecule fluorescence. The time resolution in a scanning confocal fluorescence microscope is determined by the scan speed. This is similar to the situation in NSOM. Time traces can be measured with a similar time resolution as in NSOM. The time resolution can be larger in TIRFM. Compared to NSOM, the performance of confocal fluorescence microscopy is less complicated. There is also no interference from the presence of a probe. Many different types of samples can be examined with confocal fluorescence microscopy, dry samples as well as samples in buffer. Not only immobilized but also diffusing molecules can be studied (see paragraph 3.2). Although the possibility to image many molecules simultaneously is not offered by a scanning confocal fluorescence microscope, it still has many benefits as a convenient and versatile method for single molecule detection (75).

## 1.4 Confocal Fluorescence Microscope

For the single molecule experiments described in this thesis we made use of a home-built confocal fluorescence microscope. For construction high quality optics has been selected to reduce emission light losses as much as possible. In Figure 1.4.1 the confocal microscope setup is schematically represented.

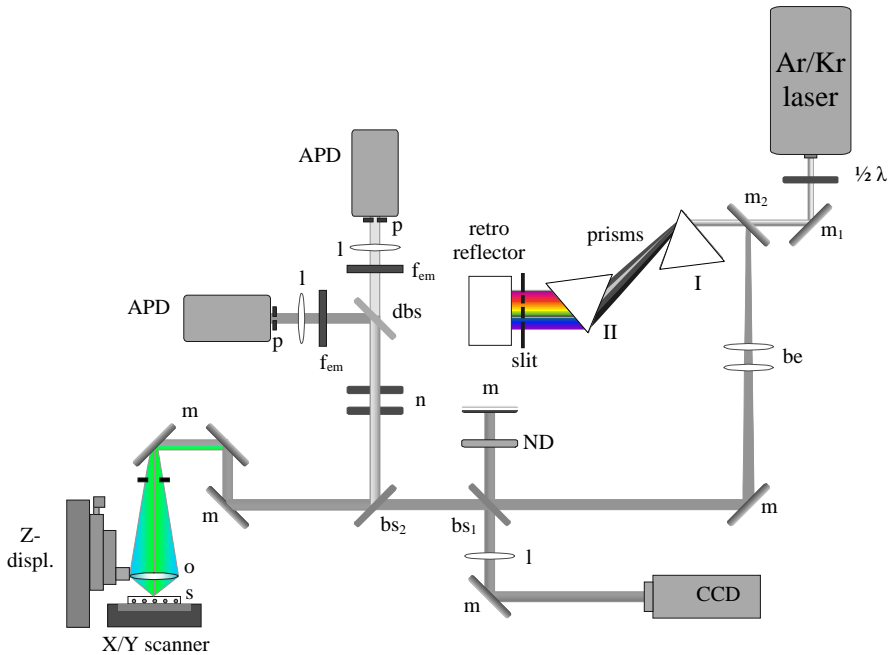


**Fig. 1.4.1.** *Confocal fluorescence microscope.* The essential parts of the setup are a prism combination for wavelength selection, a high numerical aperture objective, confocal pinholes in front of two APD detectors and an accurate X/Y scanning stage. *m* are mirrors, *be* is a beam expander, *l* are lenses, *ND* is a neutral density filter, *bs<sub>1</sub>* and *bs<sub>2</sub>* are high reflection/low transmission beam splitters, *o* is the objective, *s* is the sample, *n* are notch filters, *dbs* is a dichroic beam splitter, *f<sub>em</sub>* are emission filters and *p* are pinholes.

The light source for excitation is an Ar/Kr laser (Coherent, Innova 70). A  $\frac{1}{2} \lambda$ -plate provides p-polarized light to reduce reflection light losses upon passage through the prism setup for selection of excitation wavelengths. Mirror *m*<sub>1</sub> directs the light towards the upper part of the prism setup. The light does not hit mirror *m*<sub>2</sub> because it is positioned lower than the incoming beam. In prism I, with

Brewster angle orientation for both incoming and exiting beam, the light is dispersed. In prism II (in reverse position compared to prism I) the opposite is done, resulting in a parallel beam for all wavelengths. Both prisms are identical and prepared from flint F2 glass. The light enters the retro reflector in the upper part, is reflected downward and reflected backward to the prism setup. With a slit in front of the retro reflector, where the light is parallel, certain wavelengths can be selected for excitation. The selected wavelengths travel back through the lower part of both prisms and are recombined by prism I. Mirror  $m_2$  reflects the light through a beam expander in the direction of the sample, such that the entrance pupil of the objective is slightly overfilled. A water immersion objective (Zeiss, C-Apochromat 63X, 1.20 NA) focuses the excitation light in the sample. The objective is highly corrected for chromatic aberrations. Excitation is performed with linearly polarized light. The fluorescence signal is collected by the same objective and reflected by beam splitter  $bs_2$  (95%R/5%T) into the detection part of the setup. A dichroic beam splitter is used for spectral separation of the emitted wavelengths for detection with two avalanche photodiodes (APD's). In front of each APD a 25  $\mu\text{m}$  pinhole is present, confocally aligned with the diffraction limited focus in the sample. Emission filters are used for selection of the proper emission wavelengths. Reflected excitation wavelengths are suppressed by notch filters.  $Bs_1$  is a 95%R/5%T beam splitter, which directs part of the excitation light towards a CCD camera to examine if the incoming light beam is parallel.

The sample is scanned in two directions by a computer controlled piezoelectric scanning system, composed of an electronic position controller (E-500, Physik Instrumente, Waldbronn, Germany) and a scanning stage (P-740.20 50x50  $\mu\text{m}$ , Physik Instrumente, Waldbronn, Germany).

LabVIEW software (National Instruments, Austin, TX) is used to program and perform image acquisition. In addition to imaging by scanning, the setup also offers the possibility to exactly position the scanner so that a single molecule is in focus for a defined time. In this way, we recorded time traces of the fluorescence behavior of a single molecule with a time resolution of 100  $\mu\text{s}$  per data point.

### Optical resolution

The x/y resolution of our confocal microscope was determined by imaging the scattered light from a 6 nm gold bead during scanning. This resulted in a FWHM of 240 nm with a wavelength for illumination of 488 nm and a corresponding  $1/e^2$  diameter of 400 nm, as shown in Figure 1.4.2. This is in close correspondence with the value expected for diffraction-limited excitation.



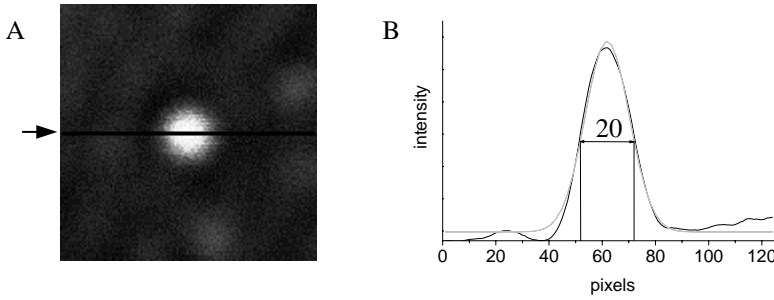


**Fig. 1.4.2.** Determination of  $x/y$  optical resolution. A. Scanning confocal image from signal scattered by a 6 nm gold bead upon excitation with 488 nm laser light. Image size is  $1.5 \times 1.5 \mu\text{m}$ ,  $128 \times 128$  pixels. B. Intensity profile at the position in the image (A) indicated by the arrow (black curve) together with the fitted Gauss curve (gray curve). The resulting FWHM is 20 pixels wide, which corresponds to 240 nm for a pixel size of 12 nm.

According to the Abbe criterion, the theoretically expected point-point  $x/y$  resolution of the microscope for plane wave excitation would be (81):

$$d_{\text{lateral}} = 0.61 \cdot \frac{\lambda}{NA} \quad (1.2)$$

where  $\lambda$  is the wavelength of light and  $NA$  is the numerical aperture of the objective. For our water immersion objective with a  $NA$  of 1.20 this corresponds to a resolution of 248 nm at a wavelength of 488 nm.

The  $z$ -resolution was determined by piezo scanning the same gold bead in the  $z$ -direction. This resulted in a FWHM in the axial direction of 1050 nm for a wavelength of 488 nm. In theory we would expect for an infinitesimal small pinhole and a fluorescent plane reflector an axial resolution of:

$$d_{\text{axial}} = \frac{0.67 \cdot \lambda}{n \cdot (1 - \cos \vartheta)} \quad (1.3)$$

where  $n$  is the refractive index of water (1.33) and  $\vartheta$  is half the maximum collection angle of the objective ( $64.2^\circ$  for an  $NA$  of 1.20). This corresponds to an axial resolution of 430 nm at a wavelength of 488 nm. The measured depth resolution of our microscope is worse, because we use a pinhole with a finite size of  $25 \mu\text{m}$ .

### Detection efficiency

For determination of the total number of photons emitted from a single molecule it is required to determine the detection efficiency of the setup. The detection efficiency of our system,  $\eta_D$  is given by:

$$\begin{aligned}\eta_D &= \eta_{NA} \cdot T_{obj} \cdot (R_m)^3 \cdot R_{bs2} \cdot T_{notch} \cdot T_{dbs} \cdot T_{f-em} \cdot \eta_{f-em} \cdot T_l \cdot \eta_{APD-\lambda} \\ &= 0.282 \cdot 0.74 \cdot (0.95)^3 \cdot 0.9 \cdot 0.8 \cdot T_{dbs} \cdot T_{f-em} \cdot \eta_{f-em} \cdot 0.92 \cdot \eta_{APD-\lambda} \\ &= 0.118 \cdot T_{dbs} \cdot T_{f-em} \cdot \eta_{f-em} \cdot \eta_{APD-\lambda}\end{aligned}\quad (1.4)$$

where  $\eta_{NA}$  designates the collection efficiency of the objective lens,  $T_{obj}$  the transmittance of the objective lens,  $R_m$  is the reflectance of the mirrors,  $R_{bs2}$  is the reflectance of beamsplitter<sub>2</sub>,  $T_{notch}$  is the transmittance of the notch filter,  $T_{f-em}$  is the transmittance of an emission filter,  $\eta_{f-em}$  is the fraction of the total emission spectrum transmitted by the emission filter,  $T_l$  is the transmittance of the lens in front of the APD and  $\eta_{APD-\lambda}$  is the quantum efficiency of the APD at the wavelength of detection.

### Theoretically expected count rates

The emission count rate that theoretically can be expected from fluorescent molecules can be calculated (82):

$$photons\ emitted/s = \frac{P}{E_{photon}} \cdot \sigma_{abs} \cdot \eta_{abs} \cdot Q \cdot k \quad (1.5)$$

where  $P$  is the excitation intensity in  $W \cdot cm^{-2}$ ,  $E_{photon}$  is the energy of one photon of excitation light in J,  $\sigma_{abs}$  is the absorption cross section in  $cm^2$  at  $\lambda_{max}$ ,  $\eta_{abs}$  is the absorption efficiency at the applied excitation wavelength,  $Q$  is the quantum yield and  $k$  is the absorption probability (including the orientation of the transition dipole moment). Excitation intensities in  $W \cdot cm^{-2}$  were calculated as an average intensity over a spot with a diameter determined at an intensity of  $1/e^2$ . During imaging individual molecules will experience the average intensity, during time trace measurement however the experienced intensity will be about 2.5 times higher, because then a molecule is positioned in the center of the focus. Hereafter the excitation mode for time trace measurements will be indicated as ‘peak power excitation’.

In our measurements with linearly polarized excitation the average absorption probability ( $k$ ) is  $1/3$  if a sufficiently large set of molecules with randomly oriented dipole orientations is considered (1, 82). For a single, freely rotating, fluorophore the absorption probability is also  $1/3$ .

The absorption cross section of a molecule at  $\lambda_{max}$  can be calculated as follows

$$\sigma_{abs} = \frac{\epsilon \cdot 10^3}{N \cdot \log(e)} = \frac{58,000 \cdot 10^3}{6 \cdot 10^{23} \cdot \log(e)} \quad (1.6)$$

To obtain the average expected count rate that can be detected from one molecule the emitted photons/s should be multiplied by the detection efficiency of the setup:

$$counts/s = \left( \frac{P}{E_{photon}} \cdot \sigma_{abs} \cdot \eta_{abs} \cdot Q \cdot k \right) \cdot \eta_D \quad (1.7)$$

It is important to realize that measured count rates for individual molecules may vary, because of the linearly polarized excitation in our microscope. Non-freely rotating molecules with different dipole orientations will be excited with different efficiencies. A bias towards measurement of time traces from only the brighter molecules may be the result.

### Relevant parameters for different fluorophores

In Table 1.4.1 the photophysical properties of the fluorescent labels applied in this single molecule study are listed. Also the detection efficiencies are indicated for measurement of the different fluorophores with our microscope. The indicated count rates are expected for an excitation intensity of  $1 \text{ kW} \cdot \text{cm}^{-2}$  at peak power excitation. All indicated values are based on bulk data without taking into account single molecule blinking properties.

dye	$\lambda_{exc}$ (nm)	$E_{photon}$ ( $\times 10^{-19} \text{ J}$ )	$\sigma_{abs}$ ( $\times 10^{-16} \text{ cm}^{-2}$ )	$\eta_{abs}$	Q	photons/s ( $\times 10^5$ )	$\eta_D$ (%)	cts/s ( $\times 10^4$ )
<b>GFP(S65T)</b>	488	4.1	2.1	1.0	0.60	2.5	3.3	0.8
<b>EGFP</b>			2.3		0.64			1.0
<b>ECFP</b>	457	4.35	1.0	0.7	0.40	0.54	2.0	0.11
<b>EYFP</b>	488	4.1	3.2	0.35	0.70	1.6	2.3	0.37
<b>Cy3.5</b>	568	3.5	5.8	0.7	0.15	1.4	3.7 <sup>†</sup>	0.53
<b>Cy5</b>	647	3.1	9.6	1.0	0.27	7.0	6.1	4.2
<b>Alexa 488</b>	488	4.1	3.0	0.75	0.48 <sup>*</sup>	2.2	3.3	0.72

**Table 1.4.1.** Relevant parameters for single molecule fluorescence microscopy of different fluorophores. <sup>\*</sup> averaged quantum yield from conjugations to different partners. <sup>†</sup> with D605/55 emission filter, <sup>‡</sup> with 565EFLP emission filter.

The characteristics of the emission filters used to prepare Table 1.4.1 are displayed in Table 1.4.2.

dye	emission filter	detected region (nm)	$\eta_{f-em}$
<b>GFP(S65T) EGFP</b>	HQ525/50	500-550	0.80
<b>ECFP</b>	D480/40	460-500	0.50
<b>EYFP</b>	HQ525/50	500-550	0.45
<b>Cy3.5</b>	D605/55 <sup>†</sup>	577-632	0.51
	565EFLP <sup>‡</sup>	>565	1.0
<b>Cy5</b>	HQ665LP	>665	0.82
<b>Alexa 488</b>	HQ525/50	500-550	0.80

**Table 1.4.2.** Emission filter characteristics.  $\eta_{f-em}$  is the fraction of the total emission spectrum transmitted by the emission filter

Purely from Table 1.4.1, disregarding single molecule fluorescence characteristics, far the highest detected count rates may be expected from Cy5. The detected count rates of Cy3.5 and (E)GFP will be 4-5 times lower.

### Background sources

In single molecule imaging it is important to have a background as low as possible. From background analysis in our confocal microscope we can conclude that most part of the background comes from the medium in which the molecules are present. The number of dark counts and counts from the environment are negligible. A gel medium yields about 5 times more background counts than water. If measurements are performed on a surface than it is beneficial to use quartz instead of glass. At 488 nm the contribution of quartz is more than 10 times less than from glass. With respect to water it is recommended to consider a possible Raman contribution from water. At 457 nm, 488 nm, 568 nm and 647 nm excitation, the 3400 cm<sup>-1</sup> Raman band of water corresponds respectively to 538nm, 585 nm, 704 nm and 829 nm. For optimal background suppression it is recommended to choose emission filters in such a way that contributions from Raman intensities of water are minimal. The bandpass filters applied in our measurements exclude the 3400 cm<sup>-1</sup> Raman water band.

## **Conclusions on single molecule aspects**

The average count rates to be expected from single fluorophores can be calculated with the photophysical properties obtained from bulk. However, the actual count rates observed from single molecules will be influenced by several factors:

- Intensity fluctuations occurring within the data collection interval will reduce the average detected count rate. The degree of blinking, with respect to frequency and intensity, will determine the extent of the decrease.
- In a situation with linearly polarized excitation, like in our confocal microscope, the dipole orientation of the fluorophore will determine largely the efficiency of excitation. Molecules that are oriented with their dipoles perpendicular to the polarization direction of the excitation beam will not be visible. It means that count rates may be expected from individual fluorophores with fixed dipoles between zero and 100%. The maximum is even 3 times higher than the average count rates given in Table 1.4.1. Rotational jumps may appear as alternating dark and bright periods in single molecule emission time traces.
- Changes in the environment of a fluorophore may result in spectral diffusion, spectral jumps or changes in quantum efficiencies. Fluctuating fluorescence intensities will be the result.
- Obviously, it is important in single molecule studies to take care that fluorophore dynamics is distinguished from dynamics that are characteristic for the biological system of interest.

Nevertheless, single molecule fluorescence methods are powerful in the study of complicated biological systems, like NER. By selecting proper fluorophores for identification of different components in a sample it is possible to selectively obtain information from only the relevant molecules. In the next paragraph the application of single molecule fluorescence microscopy in the study of NER complexes will be described.

### **1.5 Nucleotide Excision Repair**

We will demonstrate the value of confocal fluorescence microscopy in single molecule research from a study of protein-DNA complexes that are involved in Nucleotide Excision Repair (NER) (76,77). In living organisms many different DNA repair systems take care of the preservation of the integrity of the genome. In NER mainly damages are removed that significantly distort the DNA double-helix conformation. Examples of such damages are T-T dimers that are produced in the DNA of our skin cells by the UV-component of sunlight. The importance of properly functioning repair systems is illustrated from the occurrence of severe

inherited diseases caused by a NER defect like Xeroderma Pigmentosum (XP). For instance, patients that have a deficiency in the XPA protein only, are very sensitive for sunlight, show skin abnormalities, have a high risk for skin cancer and show sometimes neurological defects too.

From biochemical methods a lot of knowledge has been gained on the functioning of NER. So far however, the complicated mechanism, in which about 30 proteins participate, is not completely resolved. The NER process is believed to comprise the following basic steps: damage recognition, lesion demarcation, dual incision around the lesion, release of a 24-32 nucleotide damage-containing DNA fragment, gap-filling DNA synthesis and ligation. Typical for NER is the removal of a damage as part of a larger piece of DNA. Damage recognition is supposed to be performed by the XPC/hHR23B complex and/or by a combined action of the XPA and RPA protein (78,79). For subsequent DNA unwinding the presence of the XPC/hHR23B, TFIIH, XPA, RPA and XPG protein is required. The XPB and XPD subunits of TFIIH display DNA-unwinding activities and mediate the ATP-dependent melting of the DNA around a damaged site. The XPG and ERCC1/XPF endonucleases have been shown to be responsible for cleavage of the DNA at respectively the 3'-side and 5'-side of a damage. The RPA protein plays a role in proper positioning of the nucleases on the DNA (80). After release of a 24-32 nucleotide DNA fragment containing the damage, gap-filling DNA synthesis is performed by a joint action of number of proteins, including the RPA protein and DNA polymerase.

## ***NER and single molecule fluorescence***

Although the different components involved in NER are quite well known, the detailed performance of every individual step is not yet fully understood. In the context of NER there are still many questions that are extremely difficult to answer from bulk methods. Some of these questions are:

- what is *the order* in which NER proteins assemble over the damaged DNA?
- what is the *exact location* of different proteins in a NER complex?
- what is the *residence time* of the proteins within a complex?
- what proteins *associate and interact* at a certain stage during NER?
- what are the *dynamics of protein interactions*?

In order to address some of the questions raised above we started a *Single Molecule* study with *Scanning Confocal Fluorescence Microscopy* on *NER complexes*.

The cartoon in Figure 1.5.1 gives a simplified impression of the complexity and dimensions of a possible structure at the incision stage of NER (80).

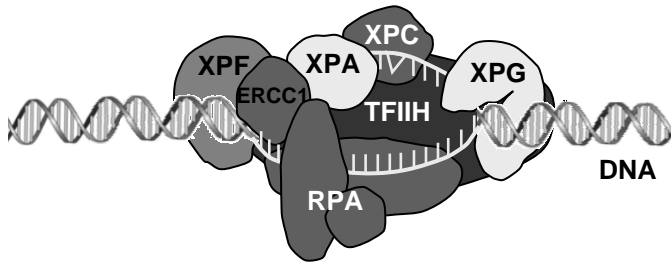


**Fig. 1.5.1.** Schematic drawing representing the possible composition of a NER complex at the stage of incision. A triangle indicates a damage.

From Figure 1.5.1 the size of a NER complex can be estimated. If we consider the length of the 24-32 nucleotide piece of DNA (~10 nm) together with the size of the assembled proteins (a diameter of few nm each) it is clear that a NER complex is much smaller than the size of the diffraction limited focus in confocal fluorescence microscopy. It is clear that the different proteins within NER complexes must be located at very close proximity to fulfill their job at the site of a damage. Therefore also single molecule FRET experiments will be useful to reveal information on distances between proteins in a complex as well as on dynamics of interactions. In this respect the application of a CFP donor in combination with a YFP acceptor is attractive.

The following issues were part of our *single molecule approach*:

- **recombinant fusion** of GFP mutants to different NER proteins for identification of individual components within a NER complex.
- **complex formation** by combining GFP-labeled NER proteins with Cy3.5-labeled DNA.
- **simultaneous imaging** of the fluorescence of GFP-labeled NER-proteins and Cy3.5 labeled DNA with scanning confocal fluorescence microscopy.
- **analysis** of the resulting images for the presence of *colocalized intensities* as an indication of protein-DNA binding.
- **quantification** of the degree of binding of NER proteins to different DNA substrates.
- **investigation of the localization accuracy** of fluorescently labeled molecules in confocal images by applying Gaussian fitting procedures.

## 1.6 Outline of this thesis

In the course of this thesis the emphasis shifts from just single molecule observation, through characterization, to application with biological relevance. In chapter 2, not only the possibility to observe single fluorescent molecules with Confocal Fluorescence Microscopy will be demonstrated but also the fluorescence properties of different fluorophores will be characterized. With most optimal imaging in mind the advantages and drawbacks will be pointed out with respect to fluorescence intensities and stability. Chapter 3 will be about the structure, dynamics and diffusion of DNA molecules, the interaction of NER proteins with DNA substrates and the localization of individual fluorescent molecules. In chapter 4 and 5, the significance of single molecule Confocal Fluorescence Microscopy will be shown from a study on NER complexes. Finally in chapter 6, a general discussion and future prospects are given based on the results described in this thesis.

## 1.7 References

1. van Holde, K.E., Johnson, W.C., and Ho, P.S. (1998) *Principles of Physical Biochemistry*. Prentice-Hall, Inc., New Jersey.
2. Lakowicz, J.R. (1999) *Principles of fluorescence spectroscopy*. Kluwer Academic/Plenum Publishers, New York.
3. Dickson, R.M., Cubitt, A.B., Tsien, R.Y., and Moerner W.E. (1997) On/off blinking and switching behaviour of single molecules of green fluorescent protein. *Nature*, 388, 355-358
4. Widengren, J., and Schwille, P. (2000) Characterization of photoinduced isomerization and back-isomerization of the cyanine dye Cy5 by fluorescence correlation spectroscopy. *J. Phys. Chem.*, **104**, 6416-6428
5. Shimomura, O., Johnson, F.H., and Saiga, Y. (1962) Extraction, purification, and properties of aequorin, a bioluminescent protein from the luminous hydromedusa, *Aequorea*. *J. Cell Comp. Physiol.*, **59**, 223-239
6. Prasher, D.C., Eckenrode, V.K., Ward, W.W., Prendergast, F.G., and Cormier, M.J. (1992) Primary structure of the *Aequorea victoria* green-fluorescent protein. *Gene*, **111**, 229-233
7. Cody, C.W., Prasher, D.C., Westler, W.M., Prendergast, F.G., and Ward, W.W. (1993) Chemical structure of the hexapeptide chromophore of the *Aequorea* green-fluorescent protein. *Biochemistry*, **32**, 1212-1218
8. Ormö, M., Cubitt, A.B., Kallio, K., Gross, L.A., Tsien, R.Y., and Remington, S.J. (1996) Crystal structure of the *Aequorea victoria* green fluorescent protein. *Science*, **273**, 1392-1395
9. Rao, B., Kemple, M., and Prendergast, F. (1980) Proton nuclear magnetic resonance and fluorescence spectroscopic studies of segmental mobility in aequorin and a green fluorescent protein from *Aequorea forskalea*. *Biophys. J.*, **32**, 630-632



10. Bokman, S.H., and Ward, W.W. (1981) Renaturation of *Aequorea* green-fluorescent protein. *Biochem. Biophys. Res. Commun.*, **101**, 1372-1380
11. Chalfie, M., Tu, Y., Euskirchen, G., Ward, W.W., and Prasher, D.C. (1994) Green fluorescent protein as a marker for gene expression. *Science*, **263**, 802-805
12. Cramer, A., Whitehorn, E.A., Tate, E., and Stemmer, W.P.C. (1996) Improved green fluorescent protein by molecular evolution using DNA shuffling. *Nature Biotech.*, **14**, 315-319
13. Ward, W.W., and Bokman, S.H. (1982) Reversible denaturation of *Aequorea* green-fluorescent protein: Physical separation and characterization of the renatured protein. *Biochemistry*, **21**, 4535-4540
14. González, D., Sawyer, A., and Ward, W.W. (1997) Spectral perturbations of mutants of recombinant *Aequorea victoria* green fluorescent protein (GFP). *Photochem. Photobiol.*, **65**, 21S
15. Inouye, S., and Tsuji, F.I. (1994a) *Aequorea* green fluorescent protein: Expression of the gene and fluorescent characteristics of the recombinant protein. *FEBS Lett.*, **341**, 277-280
16. van Roessel, P., and Brand, A.H. (2002) Imaging into the future: visualizing gene expression and protein interactions with fluorescent proteins. *Nat. Cell Biol.*, **4**, E15-20
17. Cubitt, A.B., Heim, R., Adams, S.R., Boyd, A.E., Gross, L.A., and Tsien, R.Y. (1995) Understanding, improving and using green fluorescent proteins. *Trends Biochem. Sci.*, **20**, 448-455
18. Cormack, B.P., Valdivia, R.H., and Falkow, S. (1996) FACS-optimized mutants of the green fluorescent protein (GFP). *Gene*, **173**, 33-38
19. Tsien, R.Y. (1998) The green fluorescent protein. *Ann. Rev. Biochem.*, **67**, 509-544
20. Cubitt, A.B., Woollenweber, L.A., and Heim, R. (1999) Understanding, structure-function relationships in the *Aequorea victoria* green fluorescent protein. *Meth. Cell Biol.*, **58**, 19-30
21. Ward, W.W. (1998) Biochemical and physical properties of green fluorescent proteins. In Chalfie, M. and Kain, S. (eds.), *Green fluorescent protein: properties, applications, and protocols*. Wiley-Liss, 45-75
22. Heim, R., and Tsien, R.Y. (1996) Engineering green fluorescent protein for improved brightness, longer wavelengths and fluorescence resonance energy transfer. *Curr. Biol.*, **6**, 178-182
23. Rizzuto, R., Brini, M., De Giorgi, F., Rossi, R., Heim, R., Tsien, R.Y., and Pozzan, T. (1996) Double labelling of subcellular structures with organelle-targeted GFP mutants *in vivo*. *Curr. Biol.*, **6**, 183-188
24. Ellenberg, J., Lippincott-Schwartz and Presley, J.F. (1999) Dual-colour imaging with GFP variants. *Trends Cell. Biol.*, **9**, 52-56
25. Day, R.N., Periasamy, A., and Schaufele, F. (2001) Fluorescence resonance energy transfer microscopy of localized protein interactions in the living cell nucleus. *Methods*, **25**, 4-18
26. Miyawaki, A., Llopis, J., Heim, R., McCaffery M., Adams, J.A., Ikura, M., and Tsien, Y. (1997) Fluorescent indicators for Ca<sup>2+</sup> based on green fluorescent proteins and calmodulin. *Nature*, **388**, 882-887

27. Miyawaki, A., Griesbeck, O., Heim, R., and Tsien, R.Y. (1999) Dynamic and quantitative  $\text{Ca}^{2+}$  measurements using improved cameleons. *Proc. Natl. Acad. Sci. USA*, **96**, 2135-2140
28. Pierce, D.W., Hom-Booher, N., and Vale, R.D. (1997) Imaging individual green fluorescent proteins. *Nature*, **388**, 338
29. Pierce, D.W., and Vale, R.D. (1999) Single-molecule fluorescence detection of green fluorescent protein and application to single-protein dynamics. *Meth. Cell Biol.*, **58**, 49-73
30. Peterman, E.J.G., Brasselet, S., and Moerner, W.E. (1999) The fluorescence dynamics of single molecules of green fluorescent protein. *J. Phys. Chem. A*, **103**, 10553-1056
31. Moerner, W.E., Peterman, E.J.G., Brasselet, S., Kummer, S., and Dickson, R.M. (1999) Optical methods for exploring dynamics of single copies of green fluorescent protein. *Cytometry*, **36**, 232-238
32. Garcia-Parajo, M.F., Segers-Nolten, G.M.J., Veerman, J.-A., Greve, J., and van Hulst, N.F. (2000) Real-time light-driven dynamics of the fluorescence emission in single green fluorescent protein molecules. *Proc. Natl. Acad. Sci.*, **97**, 7237-7242
33. Iwane, A.H., Funatsu, T., Harada, Y., Tokunaga, M., Ohara, O., Morimoto, S., Yanagida, T. (1997) Single molecular assay of individual ATP turnover by a myosin-GFP fusion protein expressed in vitro *FEBS Lett.*, **407**, 235-238
34. Vale, R.D., Funatsu, T., Pierce, D.W., Romberg, L., Harada, Y., and Yanagida, T. (1996) Direct observation of single kinesin molecules moving along microtubules. *Nature*, **380**, 451-453.
35. Iino, R., Koyama, I., and Kusumi, A. (2001) Single molecule imaging of green fluorescent proteins in living cells: E-cadherin forms oligomers on the free cell surface. *Biophys J.*, **80**, 2667-2677
36. Brasselet, S., Peterman, E.J.G., Miyawaki, A., and Moerner, W.E. (2000) Single-molecule fluorescence resonant energy transfer in calcium concentration dependent cameleon. *J. Phys. Chem B*, **104**, 3676-3682
37. Mujumdar, S.R., Mujumdar, R.B., Grant, C.M., and Waggoner, A.S. (1996) Cyanine-labeling reagents: sulfobenzindocyanine succinimidyl esters. *Bioconj. Chem.*, **7**, 356-362
38. Mujumdar, R.B., Ernst, L.A., Mujumdar, S.R., Lewis, C.J., and Waggoner, A.S. (1993) Cyanine dye labeling reagents: sulfoindocyanine succinimidyl esters. *Bioconj. Chem.*, **4**, 105-111
39. <http://www4.amershambiosciences.com>
40. Gruber, H.J., Hahn, C.D., Kada, G.K., Riener, C.K., Harms, G.S., Ahrer, W., Dax, T.G., and Knaus, H-G. (2000) Anomalous fluorescence enhancement of Cy3 and Cy3.5 versus anomalous fluorescence loss of Cy5 and Cy7 upon covalent linking to IgG and noncovalent binding to avidin. *Bioconj. Chem.*, **11**, 696-704
41. Randolph, J.B., and Waggoner A.S. (1997) Stability, specificity and fluorescence brightness of multiply-labeled fluorescent DNA probes. *Nucl. Acids Res.*, **25**, 2923-2929
42. Roederer, M., De Rosa, S., Gerstein, R., Anderson, M., Bigos, M., Stovel, R., Nozaki, T., Parks, D., Herzenberg, L., and Herzenberg, L. (1997) 8 color, 10-parameter flow cytometry to elucidate complex leukocyte heterogeneity. *Cytometry*, **29**, 328-339

43. Tibbe, A.G., de Grooth, B.G., Greve, J., Rao, C., Dolan G.J., and Terstappen, L.W. (2002) Cell analysis system based on compact disk technology. *Cytometry*, **47**, 173-182
44. Sargent, P.B. (1994) Double-label immunofluorescence with the laser scanning confocal microscope using cyanine dyes. *Neuroimage*, **1**, 288-295.
45. Sako, Y., Minoguchi, S., and Yanagida, T. (2000) Single-molecule imaging of EGFR signalling on the surface of living cells. *Nat Cell Biol.*, **2**, 168-172.
46. Schütz, G.J., Kada, G., Patushenko, V.P., and Schindler, H. (2000) Properties of lipid microdomains in a muscle cell membrane visualized by single molecule microscopy. *EMBO J.*, **19**, 892-901
47. Agronskaia, A., Schins, J.M., de Grooth, B.G., and Greve, J. (1999) Two-color fluorescence in flow cytometry DNA sizing: identification of single-molecule fluorescent probes. *Anal. Chem.*, **71**, 4684-4689
48. van Sark, W.G.J.H.M., Frederix, P.L.T.M., van den Heuvel, D.J., Asselbergs, M.A.H., Senf, I., and Gerritsen, H.C. (2000) Fast imaging of single molecules and nanoparticles by wide-field microscopy and spectrally resolved confocal microscopy. *Single Molecules*, **4**, 291-298
49. Dietrich, A., Buschmann, V., Müller, C., and Sauer, M. (2002) Fluorescence resonance energy transfer (FRET) and competing processes in donor-acceptor substituted DNA strands: a comparative study of ensemble and single-molecule data. *Rev. Mol. Biotech.*, **82**, 211-231
50. Grunwell, J.R., Glass, J.L., Lacoste, T.D., Deniz, A.A., Chemla, D.S., and Schultz, P.G. (2001) Monitoring the conformational fluctuations of DNA hairpins using single-pair fluorescence resonance energy transfer. *J. Am. Chem. Soc.*, **123**, 4295-4303
51. Schütz, G.J., Trabesinger, W., and Schmidt, T. (1998) Direct observation of ligand colocalization on individual receptor molecules. *Biophys. J.*, **74**, 2223-2226
52. Ha, T., Ting, A.Y., Liang, J., Caldwell, W.B., Deniz, A.A., Chemla, D.S., Schultz, P.G., and Weiss, S. (1999) Single-molecule fluorescence spectroscopy of enzyme conformational dynamics and cleavage mechanism. *Proc. Natl. Acad. Sci. USA*, **96**, 893-898
53. Suzuki, Y., Tani, T., Sutoh, K., and Kamimura, S. (2002) Imaging of the fluorescence spectrum of a single fluorescent molecule by prism-based spectroscopy. *FEBS Letters*, **512**, 235-239
54. Widengren, J., Schweinberger, E., Berger, S., and Seidel, C.A.M. (2001) Two new concepts to measure fluorescence resonance energy transfer via fluorescence correlation spectroscopy: theory and experimental realization. *J. Phys. Chem.*, **105**, 6851-6866
55. Panchuk-Voloshina, N., Haugland, R.P., Bishop-Stewart, J., Bhalgat, M.K., Millard, P.J., Mao, F., Leung, W-Y., and Haugland, R.P. (1999) Alexa dyes, a series of new fluorescent dyes that yield exceptionally bright, photostable conjugates. *J. Histochem. Cytochem.*, **47**, 1179-1188
56. <http://www.probes.com>
57. Kumar, R.K., Chapple, C.C., and Hunter, N. (1999) Improved double immunofluorescence for confocal laser scanning microscopy. *J. Histochem. Cytochem.*, **47**, 1213-1217

58. Nguyen, T., Rosenzweig, Z. (2002) Calcium ion fluorescence detection using liposomes containing Alexa-labeled calmodulin. *Anal. Bioanal. Chem.*, **374**, 69-74
59. Tóth, K., Brun, N., and Langkowski J. (2001) Trajectory of nucleosomal linker DNA studied by fluorescence resonance energy transfer. *Biochemistry*, **40**, 6921-6928
60. Rajagopalan, P.T.R., Zhang, Z., McCourt, L., Dwyer M., Benkovic, S.J., and Hammes, G.G. (2002) Interaction of dihydrofolate reductase with methotrexate: ensemble and single-molecule kinetics. *Proc. Natl. Acad. Sci. USA*, **99**, 13481-13486
61. Kues, T., Peters, R., and Kubitscheck U. (2001) Visualization and tracking of single protein molecules in the cell nucleus. *Biophys. J.*, **80**, 2954-2967
62. Kues, T., Dickmanns, A., Lührmann, R., Peters, R., and Kubitscheck, U. (2001) High intranuclear mobility and dynamic clustering of the splicing factor U1 snRNP observed by single particle tracking. *Proc. Natl. Acad. Sci. USA*, **98**, 12021-12026
63. Weetall, H.H., and Lee, M.J. (1989) Antibodies immobilized on organic supports. *Appl. Biochem. Biotech.*, **22**, 311-330
64. Adessi, C., Matton, G., Ayala, G., Turcatti, G., Mermod, J.-J., Mayer, P., and Kawashima, E. (2000) Solid phase DNA amplification: characterisation of primer attachment and amplification mechanisms. *Nucl. Acids Res.*, **28**, e87
65. Hegner, M., Wagner, P. and Semenza, G. (1993) Immobilizing DNA on gold via thiol modification for atomic force microscopy imaging in buffer solutions. *FEBS Lett.*, **336**, 452-456
66. Pirrung, M.C., and Huang, C.Y. (1996) A general method for the spatially defined immobilization of biomolecules on glass surfaces using "caged" biotin. *Bioconjug Chem.*, **7**, 317-321.
67. Merkel, R., Nassoy, P., Leung, A., Ritchie, K., and Evans, E. (1999) Energy landscapes of receptor-ligand bonds explored with dynamic force spectroscopy. *Nature*, **397**, 50-53
68. Peluso, P., Wilson, D.S., Do, D., Tran, H., Venkatasubbaiah, M. et al. (2003) Optimizing antibody immobilization strategies for the construction of protein microarrays. *Anal Biochem.*, **312**, 113-124
69. Thomson, N.H., Smith, B.L., Almqvist, N., Schmitt, L., Kashlev, M., Kool, E.T., and Hansma, P.K. (1999) Oriented, active Escherichia coli RNA polymerase: an atomic force microscope study. *Biophys J.*, **76**, 1024-1033
70. Kubitscheck, U., Kückmann, O., Kues, T., and Peters, R. (2000) Imaging and tracking of single GFP molecules in solution. *Biophys. J.*, **78**, 2170-2179
71. Funatsu, T., Harada, Y., Tokunaga, M., Saito, K., and Yanagida, T. (1995) Imaging of single fluorescent molecules and individual ATP turnovers by single myosin molecules in aqueous solution. *Nature*, **374**, 555-559
72. Tokunaga, M., Aoki, T., Hiroshima, M., Kitamura, K., and Yanagida, T. (1997) Subpiconewton intermolecular force microscopy. *Biochem. Biophys. Res. Commun.*, **231**, 566-569
73. Ha, T., Enderle, T., Ogletree, D.F., Chemla, D.S., Selvin, P.R., and Weiss, S. (1996) Probing the interaction between two single molecules: fluorescence resonance energy transfer between a single donor and a single acceptor. *Proc Natl Acad Sci U S A.*, **93**, 6264-6268
74. Garcia-Parajo, M.F., Veerman, J.-A., Segers-Nolten, G.M.J., de Grooth, B.G., Greve, J, and van Hulst, N.F. (1999) Visualising individual green fluorescent proteins with a near field optical microscope. *Cytometry*, **36**, 239-246

75. Nie, S., Chiu, D.T., and Zare, R.N. (1994) Probing individual molecules with confocal fluorescence microscopy. *Science*, **266**, 1018-1021
76. de Laat, W.L., Jaspers, N.G.J., and Hoeijmakers, J.H.J. (1999) Molecular mechanism of nucleotide excision repair. *Genes Dev.*, **13**, 768-785
77. Hoeijmakers, J.H.J. (2001) Genome maintenance mechanisms for preventing cancer. *Nature*, **411**, 366-374
78. Sugasawa, K., Ng, J.M.Y., Masutani, C., Iwai, S., van der Spek, P.J., Eker, A.P.M., Hanaoka, F., Bootsma, D., and Hoeijmakers, J.H.J. (1998) Xeroderma pigmentosum group C protein complex is the initiator of global genome nucleotide excision repair. *Mol. Cell*, **2**, 223-232
79. Sugasawa, K., Okamoto, T., Shimizu, Y., Masutani, C., Iwai, S., and Hanaoka, F. (2001) A multistep damage recognition mechanism for global genomic nucleotide excision repair. *Genes & Dev.*, **15**, 507-521
80. de Laat W.L., Appeldoorn, E., Sugasawa, K., Weterings, E., Jaspers, N.G., and Hoeijmakers, J.H. (1998) DNA-binding polarity of human replication protein A positions nucleases in nucleotide excision repair. *Genes Dev.*, **12**, 2598-2609
81. Freeman, M.H. (1990) *Optics, 10nd ed.*, Butterworth, London
82. Cantor, C.A., and Schimmel, P.R. (1980) *Biophysical chemistry. Part II: Techniques for the study of biological structure and function.* Freeman and Company.



# 2

## CHARACTERIZATION of FLUOROPHORES used in SINGLE MOLECULE FLUORESCENCE MICROSCOPY

*Within the context of this thesis several fluorophores have been used for the identification of different individual molecules present in a sample. For correct interpretation of single molecule results it is important to characterize the fluorescence behavior of the fluorophores. In this chapter the single molecule fluorescence characteristics, like on-times, fluorescence intensity and blinking behavior, of different fluorophores will be described as measured with scanning confocal fluorescence microscopy. The consequences for their application in single molecule imaging will be discussed.*

## 2.1 Green Fluorescent Protein Mutants

### GFP(S65T), EGFP, ECFP and EYFP

In paragraph 1.2 general characteristics of GFP mutants have been described. Here we focus on the GFP(S65T), EGFP, ECFP and EYFP mutants that we used in our single molecule experiments.

The S65T mutant of GFP only contains a single mutation inside the chromophore, compared to wild-type GFP. GFP(S65T) is described as a 4-6 times brighter fluorophore than wt-GFP with a 4 times faster chromophore formation. In the EGFP mutant there is, besides the S65T mutation, also a F64L mutation, resulting in 35 times brighter fluorescence than wt-GFP. The excitation and emission spectra are identical for GFP(S65T) and EGFP(1-8).

The cyan fluorescent mutant of GFP (ECFP) contains a S65A and a Y66W mutation inside the chromophore as well as 4 mutations in other amino acids of the protein. The mutations in the chromophore are responsible for a shift in excitation and emission wavelength compared to wt-GFP and GFP(S65T).

The yellow fluorescent mutant of GFP (EYFP) contains a S65G mutation inside the chromophore and 3 mutations elsewhere in the protein. The S65G mutation in the chromophore is responsible for a shift in excitation and emission wavelength compared to wt-GFP and GFP(S65T). The mutations outside the chromophore region in ECFP and EYFP result in improved bacterial expression, brightness and protein folding (1-8).

In Table 2.1.1 the photophysical properties of GFP(S65T), EGFP, ECFP and EYFP in bulk are summarized (1-8). The product of  $\epsilon$  and  $Q$  gives an indication for the relative effectiveness of the fluorophores in fluorescence applications at identical excitation conditions.

	<b>GFP (S65T)</b>	<b>EGFP</b>	<b>ECFP</b>	<b>EYFP</b>
$\lambda_{abs}^{max}$ (nm)	489	489	434	513
$\lambda_{em}^{max}$ (nm)	509	509	477	527
$\epsilon$ at $\lambda_{abs}^{max}$ ( $M^{-1}.cm^{-1}$ )	56,000	61,000	26,000	84,000
$Q$	0.64	0.60	0.40	0.70
$\epsilon \times Q$	35,840	36,600	10,400	58,800

**Table 2.1.1.** Photophysical properties of GFP(S65T), EGFP, ECFP and EYFP.  $\epsilon$  is the extinction coefficient and  $Q$  is the quantum yield.



Although EGFP has been reported as a much brighter mutant than GFP(65T), this is not evident from the photophysical properties. Neither extinction coefficients nor quantum yields are much different. Probably here brightness should not be interpreted in photophysical sense, but in a molecular biology sense. Then brightness may be connected with a more efficient transcription and translation, more efficient protein folding and improved codon usage. Consequently cells expressing ‘brighter’ GFP fusion products will have a brighter appearance in fluorescence microscopy (7).

The ECFP mutant has relatively weak photophysical properties, the extinction coefficient as well as the quantum yield are lower than for the other mutants. EYFP on the other hand has fluorescence properties even better than the GFP variants.

In Figure 2.1.1 the excitation and emission spectra are shown of (E)GFP, ECFP and EYFP. Because of similar spectral properties, GFP(S65T) and EGFP are indicated together as (E)GFP.

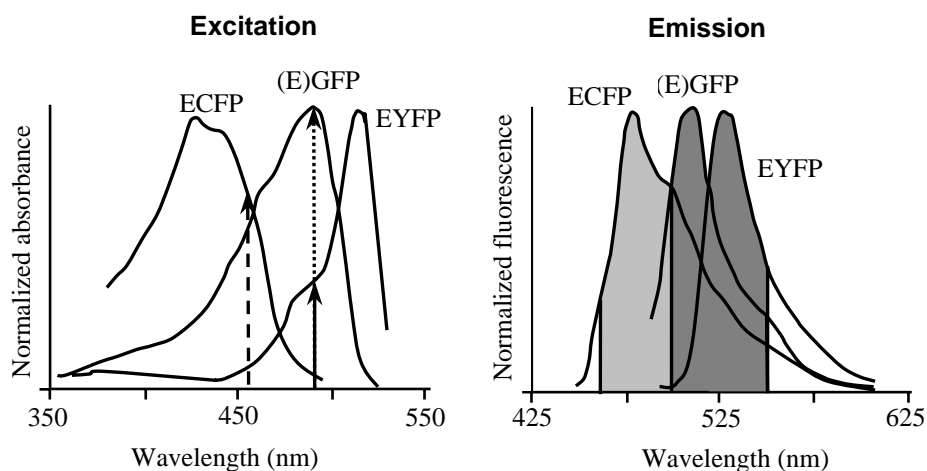


**Fig. 2.1.1.** Excitation and emission spectra of (E)GFP, ECFP and EYFP. The arrows indicate the wavelengths of the 457 nm and 488 nm laser lines that will be used for excitation. The shaded areas show the wavelength regions that are detected with different emission filters applied in our confocal microscope. The D480/40 band-pass filter for detection of ECFP is indicated in light gray, the HQ525/50 band-pass filter is in dark gray.

From the excitation spectrum of (E)GFP we can conclude that the 488 nm line produced by an Ar-Kr laser excites (E)GFP in the absorption maximum (excitation efficiency  $\eta_{\text{abs}}$  is 1.0). We also used the 488 nm line for excitation of EYFP. Compared to excitation in the absorption maximum, the excitation

efficiency at 488 nm is 0.35. For excitation of ECFP we used the 457 nm Ar-Kr line that excites ECFP with an efficiency of 0.7.

In paragraph 1.4-Table 1.4.1 the most relevant parameters in our GFP measurements have been summarized. The expected fluorescence count rates for each GFP mutant, based on bulk data, are also indicated.

In our single molecule fluorescence characterization study we included the green mutants of GFP, GFP(S65T) and EGFP (see paragraph 1.2). The possible effect of protein fusion on the fluorescence properties of EGFP was investigated on the EGFP labeled XPA protein. In chapter 4 and 5 single molecule results will be shown from EGFP-XPA binding to fluorescently labeled DNA substrates. For the study of dynamics of interactions between different proteins, FRET (described in paragraph 1.2) is a suitable tool (6,9-13). For that purpose ECFP-XPA and ERCC1-EYFP/XPF were produced. The XPA protein and the ERCC1/XPF complex probably interact during Nucleotide Excision Repair (described in paragraph 1.5). Single molecule confocal results of ECFP and EYFP detection will be shown.

To be able to observe single molecules with scanning confocal fluorescence microscopy during a certain time some form of immobilization is required (see also chapter 3). To achieve optimal imaging results it is important to use an immobilization method that maximally preserves the fluorescence properties of the fluorophores. A convenient method for immobilization of proteins, like GFP molecules, is trapping in the pores of a gel matrix (6,14-17). In our search for proper immobilization methods we compared the fluorescence characteristics of GFP(S65T), EGFP and EGFP-XPA molecules in polyacrylamide and agarose matrices.

### **2.1.1 Materials and Methods**

#### **GFP(S65T) and EGFP**

The recombinant proteins GFP(S65T) and EGFP were purchased from Clontech (Palo Alto, CA, USA).

#### **EGFP-XPA and ECFP-XPA**

EGFP-XPA and ECFP-XPA were produced and purified as described in paragraph 4.2 at the Department of Cell Biology & Genetics, Erasmus MC, Rotterdam, the Netherlands (18). Briefly, recombinant protein expression in *E. coli* was induced by IPTG, after which the collected cells were lysed. For purification of the clarified cell extract successively a Heparin-Sepharose, a Phosphocellulose and a Ni-NTA column were used. Protein fractions at each

stage during production and purification were analyzed by standard SDS-PAGE, followed by Coomassie brilliant blue staining and immunoblotting.

### **ERCC1-EYFP/XPF**

ERCC1-EYFP/XPF complex was produced and purified at the Department of Cell Biology & Genetics, Erasmus MC, Rotterdam, the Netherlands.

ERCC1-EYFP/XPF was produced after co-infection of Sf21 insect cells with ERCC1-EYFP-His<sub>6</sub>HA- and XPF-containing baculovirus expression constructs. The cDNA coding for ERCC1-EYFP-His<sub>6</sub>HA and XPF were each cloned in separate pFastbacI vectors (BAC-to-BAC Baculovirus Expression System, GIBCO BRL). The resulting pFastbacI- ERCC-EYFP-His<sub>6</sub>HA and pFastbacI-XPF plasmids were transfected separately into DH10Bac cells to allow transposition with the bacmid. The recombinant bacmids were transfected into Sf21 insect cells to produce the primary virus. The primary virus was amplified according to the instruction manual (BAC-to-BAC system, GIBCO BRL) after which a large amount of Sf21 insect cells were co-infected with virBac-ERCC1-EYFP-His<sub>6</sub>HA and virBAC-XPF. During expression the produced ERCC1-EYFP-His<sub>6</sub>HA and XPF reconstitute to ERCC1-EYFP-His<sub>6</sub>HA/XPF complexes. Isolation and purification of expressed ERCC1-EYFP-His<sub>6</sub>HA/XPF protein implied lysis of the insect cells, Ni-NTA purification, size exclusion via gel filtration on Superdex 200 and concentration on a Heparin column (19).

### **Sample preparation for confocal microscopy**

For single molecule confocal measurements, GFP(S65T) and EGFP molecules were diluted to concentrations of typically  $5 \times 10^{-10}$  M in 15 % (w/v) acrylamide/ 0.75 % (w/v) bis-acrylamide gels or 1 % (w/v) low melting point agarose gels in PBS, pH 7.35 at 30° C. The EGFP-XPA, ECFP-XPA and ERCC1-EYFP-His<sub>6</sub>HA /XPF were diluted to about  $5 \times 10^{-10}$  M in 1 % agarose only. Three microliters of the gel mixtures were sandwiched between two extensively cleaned glass cover slips, diameter 24 mm.

### **Scanning confocal fluorescence microscopy**

For single molecule characterization the confocal microscope was used as described in paragraph 1.4. The measurement configuration was as shown in Figure 2.1.1.

## **2.1.2 Results**

### **Production and purification of EGFP-XPA and ECFP-XPA**

In paragraph 4.3 the results are shown for the production and purification of EGFP-XPA protein. For ECFP-XPA similar results were obtained.

### Production and purification of ERCC1-EYFP/XPF

ERCC1-EYFP/XPF was purified from Sf21 insect cells harboring virBac-ERCC1-EYFP/XPF and virBAC-XPF. As shown in Figure 2.1.2 a protein migrating at the expected position for the EYFP-tagged ERCC1 in SDS-PAGE was visible (arrow 1). Also a protein band appeared at the position of the XPF protein (arrow 2).

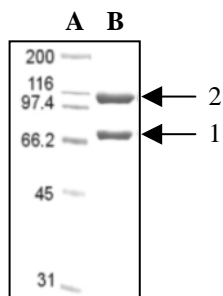


**Fig. 2.1.2.** Coomassie stain of ERCC1-EYFP-His<sub>6</sub>HA/XPF purification. Purification of the protein complexes is determined after loading fractions of the final purification step on SDS-PAGE and staining with Coomassie brilliant blue. A, Standard molecular weight pre-stained markers (Gibco BRL), molecular size is indicated in kDa. B, elution fraction of final Heparin column. Arrow 1 indicates the ERCC1-EYFP-His<sub>6</sub>HA fusion protein, running at about 69 kDa, arrow 2 points at the position of the XPF protein, running at about 115 kDa.

Immunoblot analysis, using ERCC1 and XPF specific antibodies, confirmed that indeed the desired products were obtained (data not shown). The elution fractions of the last purification step contained predominantly intact ERCC1-EYFP and XPF polypeptides. The final concentration of pure protein was about 0.9  $\mu$ M.

### Confocal single molecule detection of GFP fluorescence

#### Imaging

In Figure 2.1.3 sequential confocal images are shown from GFP(S65T) molecules immobilized in a 15% polyacrylamide matrix. In Fig. 2.1.3A six individual molecules can be observed. From this image it is clear that GFP(S65T) molecules are not very stable emitters, the single molecule spots show an inhomogeneous distribution of intensities. Within one spot dark periods can be observed, which is a representation of the blinking of a GFP molecule (14,16,17,20,21). Two molecules can be seen that switch off during the first scan demonstrating the one-step bleaching behavior, characteristic for a single molecule. From the second (B) and third image (C) we conclude that some molecules bleach much faster than others. From EGFP and EGFP-XPA molecules similar images were obtained.

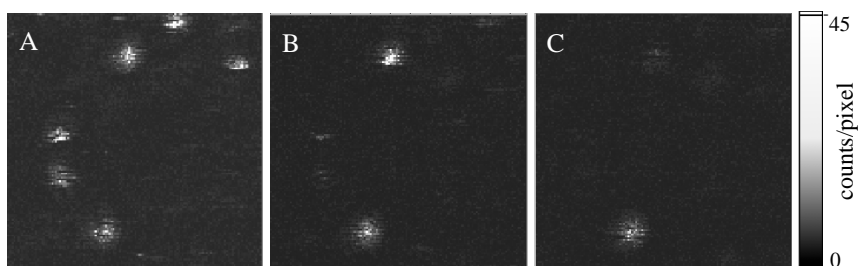


**Fig. 2.1.3.** Sequential images of single molecules of GFP(S65T) immobilized at a concentration of  $5 \times 10^{-10}$  M in PAA gel. Image size is  $5 \times 5 \mu\text{m}^2$ ,  $128 \times 128$  pixels, dwell time is 0.5 ms/pixel. Average excitation intensity was  $12 \text{ kW.cm}^{-2}$ . All images have been scaled on a maximum intensity of 45 counts.

### Time traces

The characteristic blinking of GFP molecules is even more evident from time traces representing the fluorescence behavior in time. In this procedure one single molecule is positioned in the center of the focus and upon continuous illumination the emitted photons are recorded during a defined time. Because of Gaussian intensity distribution the actual power experienced by a molecule in the center of the focus is about 2.5 times higher than the measured average power.

In Figure 2.1.4 examples of GFP(S65T) time traces are shown with a data bin of 20 ms. Time trace A has been recorded with an average excitation intensity of  $6 \text{ kW.cm}^{-2}$ , time trace B with an average excitation intensity of  $0.75 \text{ kW.cm}^{-2}$ . These time traces are representative for the irregular fluorescence behavior that we generally observed from GFP molecules.

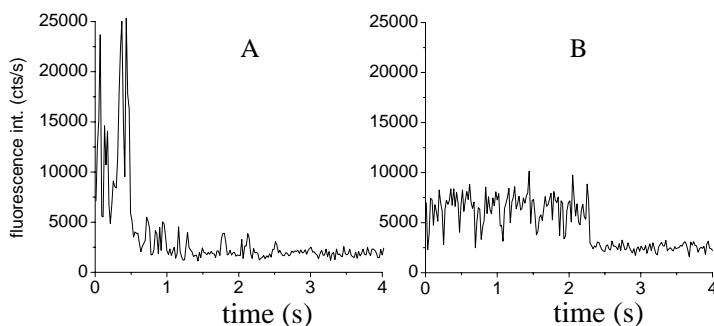


**Fig. 2.1.4.** Time traces of individual GFP(S65T) molecules immobilized in PAA gel. A, average excitation intensity of  $6 \text{ kW.cm}^{-2}$ ; B, average excitation intensity of  $0.75 \text{ kW.cm}^{-2}$ . Data bin is 20 ms.

In both time traces the one-step bleaching behavior typical for a single molecule can be observed. It is clear that GFP molecules stay longer in an emissive state at lower excitation intensities. Obviously the fluorescence count rate decreases with decreasing excitation intensity. The integrated fluorescence intensity in the low intensity measurement is  $4.4 \times 10^5$  photons, while the total intensity is only  $1.9 \times 10^5$  photons in the higher intensity measurement. To visualize the position of molecules a time trace measurement is always preceded by a scan to produce an image. At higher excitation intensities relatively a larger part of the available photons will be emitted during scanning. To be able to record the fluorescence from individual GFP molecules as long as possible it is favorable to use low intensities for excitation.

The strong fluctuations in fluorescence intensity from one single molecule are demonstrated more clearly in Figure 2.1.5. In Figure 2.1.5.A a time trace of an EGFP molecule is shown after data binning with 20 ms intervals. Upon continuous illumination the molecule was emitting during about 0.2 s, then it suddenly stopped fluorescing. In Figure 2.1.5.B, the same time trace is represented with a smaller bin time of 2 ms. Much shorter emission events are disclosed now. From the analysis of 46 time traces of individual EGFP molecules immobilized in a 15 % PAA gel we obtained an average on-time of  $170 \pm 17$  ms when an integration time of 20 ms was applied. If we however analyzed the same set of 46 time traces with a data bin of only 2 ms, we obtained an average on-time of only  $14.4 \pm 1.7$  ms. This means that the high time-resolution acquisition and analysis of data available in our confocal system, offers the possibility to reveal photodynamics of single fluorescent molecules on a very small timescale.

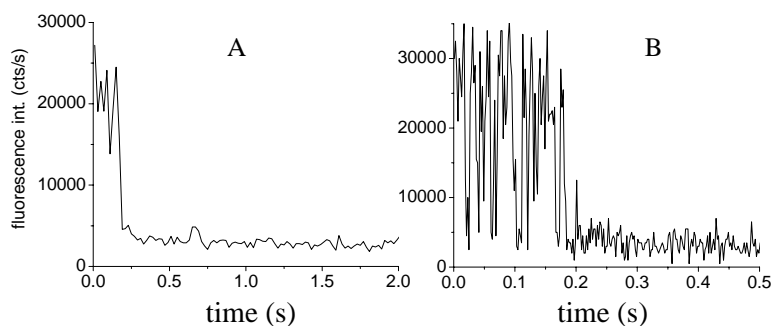


**Fig. 2.1.5.** Representation of one time trace of an individual EGFP molecule immobilized in 15% PAA analyzed with different integration times. A. Data bin 20 ms. B. Data bin 2 ms. Average excitation intensity was  $6 \text{ kW.cm}^{-2}$ .

From Poisson statistics only we would expect less fluctuations than observed for EGFP in Figure 2.1.5.B. From Figure 2.1.6 it follows that the probability to measure events below 20 counts (corresponding to 10,000 counts/s during one 20 ms bin) is 0.006 for an average signal of 40 counts (corresponding to 20,000 counts/s during one 20 ms bin). For the EGFP on-time of about 200 ms containing 100 data points, this would be equal to only 1 event at most. The EGFP time trace however shows about 20% of low-level events. From this we can conclude that the irregular EGFP fluorescence as observed in the time trace is not in the first place a result of statistical fluctuations. Additional off-events are caused by the well-known blinking of EGFP.

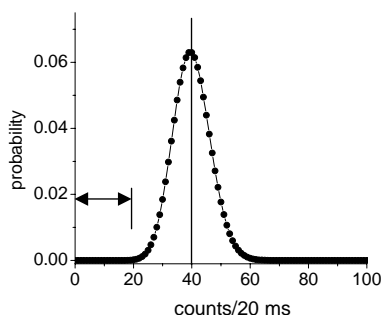


**Fig. 2.1.6.** *Poisson distribution for an average signal of 40 counts. The cumulative probability to observe events below 20 counts is  $3.6 \times 10^{-4}$ . Relative to the probability at the average of 40 counts this is 0.6%.*

## Comparison of GFP fluorescence within different matrices

### On-times

In view of single molecule applications in which biological processes are studied, it is important to know what observation time is offered by the GFP label. To investigate if on-times are influenced by the immobilization procedure and type of matrix, we decided to compare GFP(S65T) and EGFP molecules within polyacrylamide and agarose gels. The results are shown in Table 2.1.2. In the previous paragraph we have shown that the result of on-time analysis is highly dependent on the applied data binning. Therefore the on-time data mentioned should be interpreted as apparent on-times as obtained with the indicated data binning.

Table 2.1.2 shows that there is no significant difference in on-times of GFP molecules upon immobilization in either matrix. Also the mutants GFP(S65T) and EGFP behave in a similar way, with an average excitation intensity of  $6 \text{ kW} \cdot \text{cm}^{-2}$  the average on-times are below 100 ms. A way to increase the observation time is

by lowering the excitation intensity. At an average intensity of  $0.75 \text{ kW.cm}^{-2}$  the molecules stay 2 to 3 times longer in an emitting state.

matrix	av. exc. int. $\text{kW.cm}^{-2}$	GFP (S65T) on-time (s)	N	EGFP on-time (s)	N	EGFP-XPA on-time (s)	N
1% agarose	0.75	-		$0.182 \pm 0.018$	22	$0.176 \pm 0.014$	31
	6	$0.051 \pm 0.006$	22	$0.086 \pm 0.004$	24	-	
15% PAA	0.75	-		$0.266 \pm 0.007$	21	-	
	6	$0.091 \pm 0.010$	28	$0.069 \pm 0.008$	22	-	

**Table 2.1.2.** Comparison of on-times of GFP(S65T), EGFP and EGFP-XPA molecules after immobilization in 1% agarose or 15% PAA at an excitation intensity of  $0.75 \text{ kW.cm}^{-2}$  and  $6 \text{ kW.cm}^{-2}$ . Result of analysis of time traces of individual GFP molecules with a 10 ms data bin. N is the number of molecules analyzed. Analysis was performed only on time traces of molecules that were in an emitting state at  $t_0$ . Time interval analyzed was from 0-5 s. On-time distributions were plotted in histograms. By fitting each histogram with a mono-exponential decay function the average on-times were extracted.

In literature also longer GFP on-times were reported at lower excitation intensities (14). From our results we may conclude that the on-times of GFP molecules are not affected by the immobilization method. This is in agreement with literature data (14). Apparently immobilization in polyacrylamide, where the GFP molecules are present in the acrylamide mixture during the quite aggressive polymerization reaction, is not harmful with respect to the fluorescence properties of the GFP molecules.

We also determined on-times from EGFP labeled XPA molecules, to investigate if fusion to another protein influences the duration of the on-times. It appeared that there is no effect on average on-times of EGFP because of the presence of the XPA protein. Upon excitation with  $0.75 \text{ kW.cm}^{-2}$  at 488 nm and immobilization of EGFP-XPA molecules in 1% agarose, on-times are determined of 176 ms, similar as found for free EGFP under the same conditions.

### Blinking

The on-time data were further analyzed for the number of times that a molecule switches on and off during the 5 s measurement time interval, a representation of the so-called blinking behavior of molecules. The results are listed in Table 2.1.3. These results show that individual GFP molecules display a strong blinking behavior, indicated by the high number of on-times per time trace, which is rather independent of excitation intensity and matrix. The fraction of GFP(S65T)



molecules showing multiple blinking appears to be lower than for EGFP and EGFP-XPA. The amount of data is however not sufficient to conclude that this is a real difference between the GFP(S65T) and EGFP mutant.

Matrix	Average exc. power (kW.cm <sup>-2</sup> )	GFP (S65T)		EGFP		EGFP-XPA	
		N <sub>on</sub>	Fr <sub>N&gt;1</sub> (%)	N <sub>on</sub>	Fr <sub>N&gt;1</sub> (%)	N <sub>on</sub>	Fr <sub>N&gt;1</sub> (%)
1% agarose	0.75	-	-	3.3	73	4.2	81
	6	4.0	50	3.7	87	-	-
15% PAA	0.75	-	-	2.1	70	-	-
	6	3.0	64	3.2	77	-	-

**Table 2.1.3.** Comparison of blinking behavior of GFP(S65T), EGFP and EGFP-XPA molecules after immobilization in 1% agarose or 15% PAA at 0.75 kW.cm<sup>-2</sup> and 6 kW.cm<sup>-2</sup> 488 nm excitation. The average number of on-times per 5 s time trace (N<sub>on</sub>) and the fraction of molecules with multiple blinking (Fr<sub>N>1</sub>) are presented. Data bin was 10 ms. The number of molecules analyzed is the same as in Table 2.1.2.

### Fluorescence intensity

Also the fluorescence intensities and the total number of photons collected from an individual GFP(S65T), EGFP or EGFP-XPA molecule were not significantly different in either matrix.

The number of photons that we collected from a single GFP molecule was typically between  $6 \times 10^4$  and  $5 \times 10^5$  with a count rate of  $1\text{--}5 \times 10^5$  photons/s and a signal to background ratio between 5 and 10. From equation 1.5 (paragraph 1.4) an expected count rate of  $1.5 \times 10^6$  photons/s is obtained for GFP at 6 kW.cm<sup>-2</sup> with peak power excitation. The lower measured average count rates may be attributed to the strong blinking behavior of GFP molecules during emission. Moreover we did not observe a stronger fluorescence from EGFP than from GFP(S65T) on the single molecule level.

These results do not provide a reason to express a preference for either gel material. However for biological applications agarose gels are preferred, because the preparation involves more mild conditions in which the protein molecules are not exposed to unnatural conditions.

### Confocal single molecule detection of ECFP fluorescence

In Figure 2.1.7, a confocal image is shown from ECFP-XPA molecules immobilized in a 1% agarose matrix.

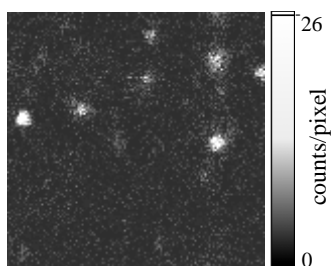


**Fig. 2.1.7.** Scanning confocal image of ECFP-XPA molecules immobilized in 1% agarose. Image size is  $6.2 \times 6.2 \mu\text{m}^2$ ,  $128 \times 128$  pixels, dwell time is 0.5 ms/pixel. Average excitation intensity was  $1.2 \text{ kW}\cdot\text{cm}^{-2}$ .

The ECFP-XPA preparation was not sufficiently pure to fully characterize the single molecule fluorescence of individual ECFP molecules. Protein aggregation resulted in spots with much higher intensities than expected from single molecules. Time traces measured from aggregates rather showed a gradual than a stepwise decrease in intensity, as shown in Figure 2.1.8.A. The time trace in Figure 2.1.8.B shows a stepwise bleaching behavior.

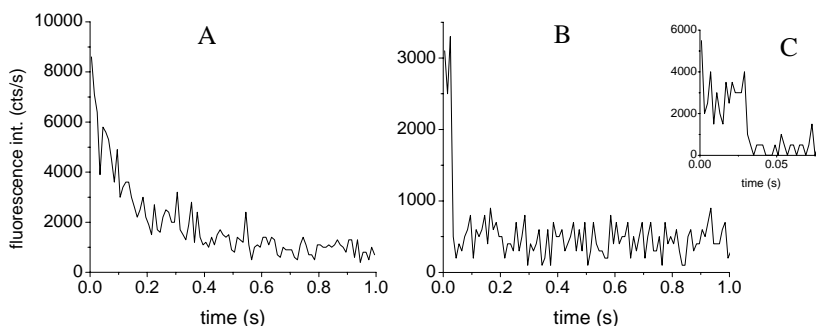


**Fig. 2.1.8.** Time traces of ECFP-XPA molecules immobilized in a 1% agarose matrix. The average excitation intensity was  $1.2 \text{ kW}\cdot\text{cm}^{-2}$ . A and B: data bin is 10 ms. C: same time trace as B with data bin of 2 ms.

The average count rate that theoretically can be expected from a single ECFP molecule was calculated at an average excitation intensity of  $1.2 \text{ kW}\cdot\text{cm}^{-2}$  (according to equation 1.5-paragraph 1.4). From a single ECFP molecule we would expect a count rate of  $6.5 \times 10^4$  photons/s at peak power excitation. In the ECFP measurement configuration we have a detection efficiency of 2.0% and hence  $1.3 \times 10^3$  counts/s can be expected per single ECFP molecule.

The average count rate during the on-time in Figure 2.1.8.B is about  $2.5 \times 10^3$  cts/s. The measured count rate in this particular time trace is higher than expected for one molecule. In the interpretation however of one individual time trace the influence of dipole orientation should be considered. In time trace measurement there may be a bias towards selection of only bright spots, representing molecules with a more favorable dipole orientation. From a molecule with an optimally oriented dipole we may observe a three times higher count rate than from a population of molecules with random dipole orientation. To determine if the particular time trace of Figure 2.1.8.B represents the fluorescence behavior of one or more molecules we applied a smaller integration time of only 2 ms. Then the successive bleaching of two molecules was revealed, as shown in Figure 2.1.8.C.

### Confocal single molecule detection of EYFP fluorescence

In Figure 2.1.9, a confocal image is shown from ERCC1-EYFP/XPF molecules immobilized in a 1% agarose matrix.

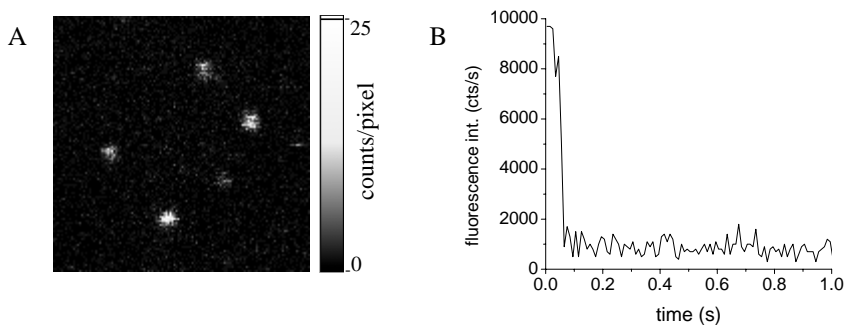


**Fig. 2.1.9.** Confocal fluorescence detection of ERCC1-EYFP/XPF. A. Scanning confocal image of ERCC1-EYFP/XPF molecules immobilized in 1% agarose. Image size is  $6.2 \times 6.2 \mu\text{m}^2$ ,  $128 \times 128$  pixels, dwell time is 0.5 ms/pixel. B. Example of an ERCC1-EYFP/XPF time trace represented with a data bin of 10 ms. The average excitation intensity was  $5 \text{ kW.cm}^{-2}$ .

The confocal image of Figure 2.1.9.A demonstrates that we can image the EYFP label present as ERCC1-EYFP/XPF. Figure 2.1.9.B shows an example of a single molecule time trace of ERCC1-EYFP/XPF with one step bleaching.

The theoretically expected count rate from a single EYFP molecule was calculated at an average excitation intensity of  $5 \text{ kW.cm}^{-2}$  (according to equation 1.5-paragraph 1.4). From a single EYFP molecule a count rate of  $8.0 \times 10^5$  photons/s is expected at peak power excitation. In the EYFP measurement configuration the detection efficiency is 2.3%. Therefore we may detect  $1.8 \times 10^4$  counts/s per single EYFP molecule. The intensity in the time trace of Figure

2.1.9.B is about half of the expected intensity. An unfavorable dipole orientation may result in a lower count rate from an individual EYFP molecule. Upon application of smaller integration times only one bleaching step was observed, indicating that this time trace represents the fluorescence behavior of a single EYFP molecule.

### **2.1.3 Discussion and Conclusions**

Our results demonstrate that it is well possible to apply GFP mutants in single molecule investigations with confocal fluorescence microscopy. It is however important to realize that GFP molecules do not behave as stable emitters. In confocal images and time traces from individual GFP molecules both blinking and bleaching is observed. In general we can conclude that the fluorescence behavior of individual GFP(S65T) and EGFP is similar. From the EGFP-XPA results we conclude that recombinant fusion to the XPA protein does not influence the fluorescence properties of EGFP. Considering single molecule studies on the NER system this is a relevant observation.

We did not observe a difference in on-times, blinking behavior and fluorescence intensities of GFP molecules after immobilization in different matrices. This is in agreement with literature data (14). The on-times measured at different excitation intensities are smaller than those reported from TIRFM experiments at similar conditions (14). The higher time-resolution in our analysis reveals photodynamics of single GFP molecules on a smaller timescale. Our confocal results are in good correspondence with single molecule GFP results that were obtained with NSOM (21).

The emission count rates observed for GFP molecules were lower than expected from their photophysical properties. Here again the strong blinking plays a role. Fast blinking, occurring during the integration time of the measurement, will result in lower average count rates. Unlike the name suggests, the EGFP, enhanced green fluorescent protein, did not show stronger fluorescence than GFP(S65T) on the single molecule level. Yet this is in agreement with the almost equal photophysical properties known for both mutants.

The ECFP results are in agreement with the weak photophysical properties of this mutant. The fluorescence detection of ECFP can be improved by about 20% by using a He-Cd laser with a wavelength of 442 nm for excitation. So far our results on ECFP should be considered as preliminary. The issue of protein purification and impurity requires further study.

Like the other GFP mutants also EYFP shows single molecule blinking and bleaching features. The emission count rate observed from individual EYFP molecules is shown to be in the range of the expected count rate. Selection of 514.5 nm excitation will result in a 5 times higher fluorescence intensity.

In general, low excitation intensities result in a longer time span of emission and higher total numbers of photons from GFP molecules. We conclude, because of the strong blinking behavior, that GFP mutants are suitable but not ideal fluorophores for single molecule studies on biological systems. With respect to application in our single molecule NER study, still GFP labeling offers considerable advantages. In general NER proteins, being very different in size and amino acid composition, are not easily labeled with chemical methods without interference with their biological function. Single molecule labeling with methods other than GFP will usually require mutagenesis to generate proteins with only one cysteine residue.

## 2.1.4 References

1. Cubitt, A.B., Heim, R., Adams, S.R., Boyd, A.E., Gross, L.A., and Tsien, R.Y. (1995) Understanding, improving and using green fluorescent proteins. *Trends Biochem. Sci.*, **20**, 448-455
2. Cormack, B.P., Valdivia, R.H., and Falkow, S. (1996) FACS-optimized mutants of the green fluorescent protein (GFP). *Gene*, **173**,33–38
3. Tsien, R.Y. (1998) The green fluorescent protein. *Ann. Rev. Biochem.*, **67**, 509-544
4. Cubitt, A.B., Woollenweber, L.A., and Heim, R. (1999) Understanding, structure-function relationships in the *Aequoria victoria* green fluorescent protein. *Meth. Cell Biol.*, **58**,19-30
5. Ormö, M., Cubitt, A.B., Kallio, K., Gross, L.A., Tsien, R.Y., and Remington, S.J. (1996) Crystal structure of the *Aequoria Victoria* green fluorescent protein. *Scienc*, **273**,1392–1395
6. Brasselet, S., Peterman, E.J.G., Miyawaki, A., and Moerner, W.E. (2000) Single-molecule fluorescence resonant energy transfer in calcium concentration dependent cameleon. *J. Phys. Chem B*, **104**, 3676-3682
7. Ward, W.W. (1998) Biochemical and physical properties of green fluorescent proteins. In Chalfie, M. and Kain, S. (eds.), *Green fluorescent protein: properties, applications, and protocols*. Wiley-Liss, 45-75
8. Patterson, G., Day, R.N., and Piston, D. (2001) Fluorescent protein spectra. *J. cell Sci.*, **114**, 837-838
9. Heim, R., and Tsien, R.Y. (1996) Engineering green fluorescent protein for improved brightness, longer wavelengths and fluorescence resonance energy transfer. *Curr. Biol.*, **6**, 178-182
10. Miyawaki, A., Llopis, J., Heim, R., McCaffery M., Adams, J.A., Ikura, M., and Tsien, Y. (1997) Fluorescent indicators for Ca<sup>2+</sup> based on green fluorescent proteins and calmodulin. *Nature*, **388**, 882-887

11. Miyawaki, A., Griesbeck, O., Heim, R., and Tsien, R.Y. (1999) Dynamic and quantitative  $\text{Ca}^{2+}$  measurements using improved cameleons. *Proc. Natl. Acad. Sci. USA*, **96**, 2135-2140
12. Pollok, B.A., and Heim, R. (1999) Using GFP in FRET-based applications. *Trends in Cell Biol.*, **9**, 57-60
13. Mitra, R.D., Silva, C., and Youvan, D.C. (1996) Fluorescence resonance energy transfer between blue-emitting and red-shifted excitation derivatives of the green fluorescent protein. *Gene*, **173**, 13-17
14. Peterman, E.J.G., Brasselet, S., and Moerner, W.E. (1999) The fluorescence dynamics of single molecules of green fluorescent protein. *J. Phys. Chem. A*, **103**, 10553-1056
15. Kubitschek, U., Kückmann, O., Kues, T., and Peters, R. (2000) Imaging and tracking of single GFP molecules in solution. *Biophys. J.*, **78**, 2170-2179
16. Moerner, W.E., Peterman, E.J.G., Brasselet, S., Kummer, S., and Dickson, R.M. (1999) Optical methods for exploring dynamics of single copies of green fluorescent protein. *Cytometry*, **36**, 232-238
17. Dickson, R.M., Cubitt, A.B., Tsien, R.Y., and Moerner W.E. (1997) On/off blinking and switching behaviour of single molecules of green fluorescent protein. *Nature*, **388**, 355-358
18. Segers-Nolten, G.M.J., Wyman, C., Wijgers, N., Vermeulen, W., Lenferink, A.T.M., Hoeijmakers, J.H.J., Greve, J., and Otto, C. (2002) Scanning confocal fluorescence microscopy for single molecule analysis of nucleotide excision repair complexes. *Nucl. Acids Res.*, **30**, 4720-4727
19. Enzlin, J.H., and Schärer, O.D. (2002) The active site of the DNA repair endonuclease XPF-ERCC1 forms a highly conserved nuclease motif. *EMBO J.*, **21**, 2045-2053
20. Garcia-Parajo, M.F., Veerman, J.-A., Segers-Nolten, G.M.J., de Grooth, B.G., Greve, J., and van Hulst, N.F. (1999) Visualising individual green fluorescent proteins with a near field optical microscope. *Cytometry*, **36**, 239-246
21. Garcia-Parajo, M.F., Segers-Nolten, G.M.J., Veerman, J.-A., Greve, J., and van Hulst, N.F. (2000) Real-time light-driven dynamics of the fluorescence emission in single green fluorescent protein molecules. *Proc. Natl. Acad. Sci.*, **97**, 7237-7242

## 2.2 Cyanine dyes

### Cy3.5 and Cy5

In paragraph 1.2 we described general aspects of cyanine labels. Here we characterized the single molecule fluorescence properties of the cyanine dyes Cy3.5 and Cy5, because of their application as DNA labels in our NER-protein/DNA binding studies (chapter 4 and 5). The combination of Cy3.5 and Cy5 was selected for future use as a FRET pair. Single Cy3.5 and Cy5 fluorophores were covalently bound to DNA oligomers.

The chemical structure of Cy3.5 and Cy5 is shown in Figure 2.2.1 (1,2). Cy3.5 and Cy5 both are represented as mono-functional succinimidyl (NHS) esters. The presence of the NHS-group is convenient for conjugation to biomolecules containing aliphatic amino groups. The molecular mass of the Cy3.5-NHS ester is 1102.4 and of the Cy5-NHS ester 791.99.

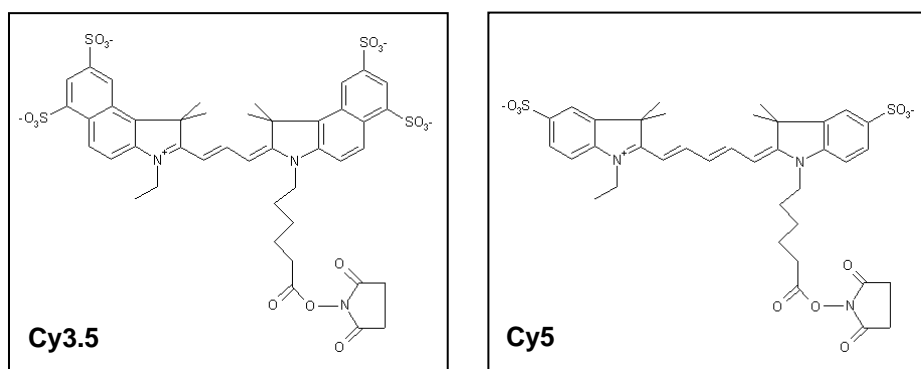


**Fig. 2.2.1.** Chemical structure of monofunctional Cy3.5- and Cy5-succinimidyl ester.

In Table 2.2.1 the photophysical properties of Cy3.5 and Cy5 are summarized (1,2). The product of  $\epsilon$  and  $Q$  is given as an indication for their relative fluorescence brightness. At identical excitation conditions we may expect from Cy5 a 3 times higher fluorescence intensity than from Cy3.5.

	Cy3.5	Cy5
$\lambda_{abs}^{max}$ (nm)	581	649
$\lambda_{em}^{max}$ (nm)	596	670
$\epsilon$ at $\lambda_{abs}^{max}$ ( $M^{-1}.cm^{-1}$ )	150,000	250,000
Q	0.15	0.27
$\epsilon \times Q$	22,500	67,500

**Table 2.2.1.** Photophysical properties of Cy3.5 and Cy5 as determined in bulk.  $\epsilon$  is the extinction coefficient,  $Q$  is the quantum yield.

In paragraph 1.4-Table 1.4.1 the most relevant parameters in our Cy3.5 and Cy5 measurements have been summarized. The expected count rates for each fluorophore are indicated too. Purely on the basis of bulk data we may expect to detect a more than 4 times higher count rate from Cy5 than from Cy3.5.

The measured absorption and emission spectra of Cy3.5 and Cy5 dye are shown in Figure 2.2.2.

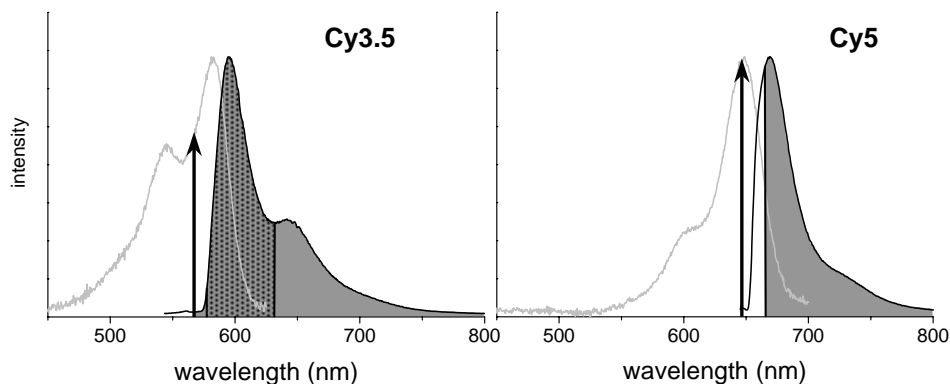


**Fig. 2.2.2.** Absorption and emission spectra of Cy3.5 and Cy5. The arrows indicate the wavelengths of the 568 nm and 647 nm laser lines that will be used for excitation. The shaded areas show the wavelength regions that are detected with different emission filters applied in our confocal microscope. For detection of Cy3.5 the D605/55 band pass filter is shown in gray, the 565EFLP long pass filter in dotted gray. For Cy5 detection the HQ665LP emission filter is indicated in gray.

From the absorption spectrum it can be concluded that the 568 nm line produced by an Ar-Kr laser has the proper wavelength for excitation of Cy3.5. Compared to excitation in the maximum the excitation efficiency at 568 nm is 72%. The



excitation spectrum of Cy5 shows that the 647 nm Ar-Kr line excites Cy5 in the excitation maximum.

The fluorescence of individual Cy3.5 and Cy5 molecules, covalently attached to DNA molecules by a carbon linker, was characterized with respect to on-times, blinking behavior and fluorescence intensities at different excitation powers. The dye molecules are supposed to be freely rotating over the carbon-linker on a timescale smaller than our measurement integration time. Because of the dependence on data binning (see paragraph 2.1.2), unless otherwise indicated, all time trace analysis was performed at a 10 ms data bin.

## **2.2.1 Materials and Methods**

### **Cy3.5 and Cy5 labeled DNA oligomers**

5'-Cy3.5 and 5'-Cy5 labeled 90 nucleotide oligomers were purchased (DNA Technology A/S, Aarhus, Denmark). The cyanines are coupled to the 5'OH of the last nucleotide via a 3-carbon linker.

### **Sample preparation for confocal microscopy**

Immobilization of Cy-labeled DNA oligomers was achieved by adsorption on quartz. A 10  $\mu$ l volume of 1 M MgCl<sub>2</sub> solution in water was applied to a carefully cleaned 25 mm diameter cover slip. After about 30 s the slide was rinsed with water and dried. For immobilization of Cy3.5-oligomers 10  $\mu$ l of a  $2 \times 10^{-9}$  M solution of Cy3.5 labeled DNA in water was applied to the cover slip. Another 25 mm diameter quartz cover slip was placed on top. During confocal scanning the sample was oriented with the Mg-treated slide at the top, such that molecules adhered to this slide will be measured.

For immobilization of Cy5-oligomers 10  $\mu$ l of a  $1.3 \times 10^{-8}$  M solution of Cy5 labeled DNA in water was used.

Sample preparation for confocal microscopy in the presence of an oxygen scavenging system was performed in the same way, only the Cy-labeled DNA was in 25 mM Hepes, 100 mM NaCl, pH 7.9. After adsorption for about 30 s about 0.3 ml of oxygen scavenging solution was added. Excess solution was drained off before another 25 mm diameter quartz cover slip was placed on top.

The composition of the oxygen scavenging mixture was: 216  $\mu$ g/ml glucose oxidase, 4.5 mg/ml glucose, 36  $\mu$ g/ml catalase and 0.5%  $\beta$ -mercapto-ethanol in 25 mM Hepes, 100 mM NaCl, pH 7.9 (3).

### **Scanning confocal fluorescence microscopy**

The confocal microscope, described in paragraph 1.4, was used. The measurement configuration was as shown in Figure 2.2.2.

## 2.2.2 Results

### Confocal single molecule detection of Cy3.5 and Cy5 fluorescence

In Figure 2.2.3 confocal images are shown from the fluorescence of Cy3.5-labeled 90-mers and Cy5-labeled 90-mers immobilized on quartz.

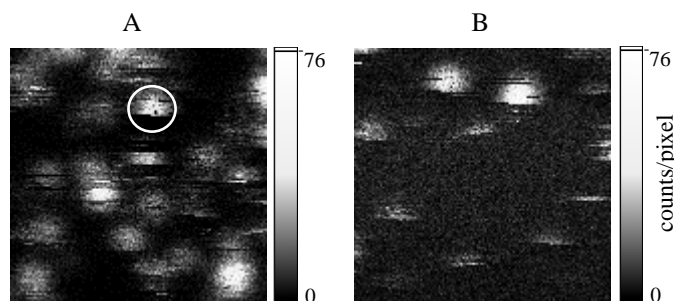


**Fig. 2.2.3.** Scanning confocal image of Cy-labeled -90mers adhered to quartz. A. Cy3.5; B Cy5. Image size is  $3.1 \times 3.1 \mu\text{m}^2$ ,  $128 \times 128$  pixels, dwell time is 0.5 ms/pixel. The average excitation intensity was  $5 \text{ kW}\cdot\text{cm}^{-2}$  for Cy3.5 and  $4 \text{ kW}\cdot\text{cm}^{-2}$  for Cy5.

A number of typical single molecule features are observed in both images. In the Cy3.5 image an incomplete spot is present at the circled position, while the Cy5 image only contains incomplete spots. This is an indication of sudden bleaching of individual molecules during scanning. It is unlikely that several molecules within a cluster bleach at exactly the same moment. From the different appearance of both images we can conclude that Cy5 molecules bleach faster than Cy3.5 molecules at almost equal excitation intensities. Also the number of molecules per image is much lower for Cy5 than for Cy3.5, although the Cy5 samples are prepared by applying even 6.5 times more molecules compared to the Cy3.5 samples. We must assume that a significant fraction of the Cy5 molecules have bleached before they can be recognized as a single molecule in the images. The intensity of the fluorescence spots in the images is not homogeneous. The alternating bright and dark periods are a representation of blinking. Blinking is characterized by frequent short-lived periods in which the fluorescence appears to be photobleached but rapidly recovers.

In Figure 2.2.4 some typical time traces are shown of single Cy3.5 and Cy5 molecules excited with different average excitation intensities. Both Cy3.5 and Cy5 display longer on-times and lower count rates at low excitation intensity. It is remarkable that the on-times of Cy5 are shorter than those of Cy3.5 at similar excitation conditions.

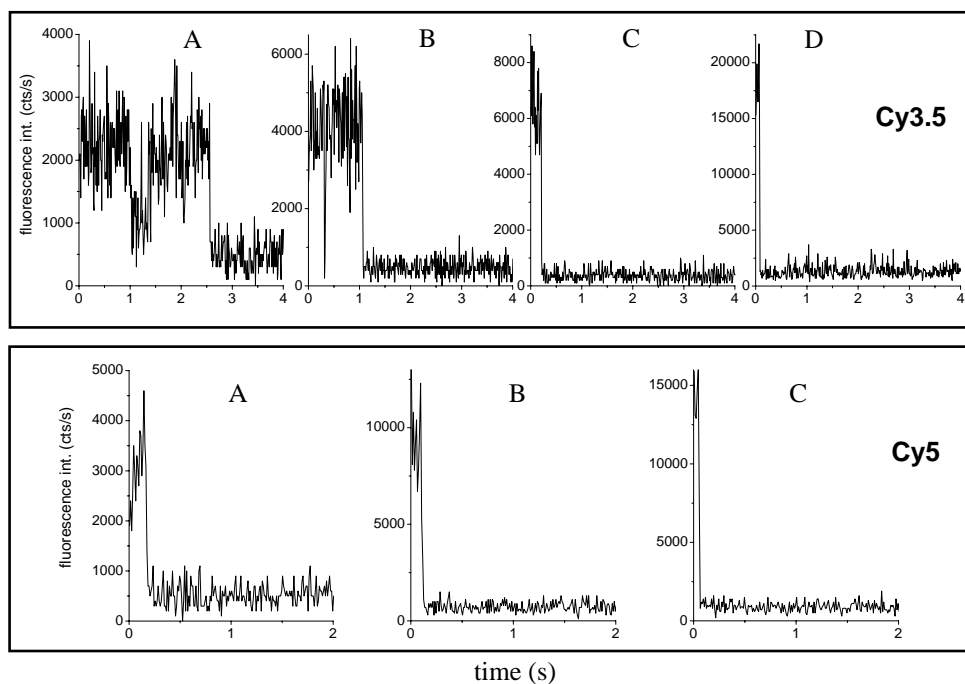


**Fig. 2.2.4.** Time traces of individual Cy dye molecules excited with different average excitation intensities. Upper panel: Cy3.5. A. 0.4; B. 1.2; C. 2.5; D. 5  $\text{kW}\cdot\text{cm}^{-2}$ . Lower panel Cy5. A. 0.35; B. 1; C. 2  $\text{kW}\cdot\text{cm}^{-2}$ .

### ***Analysis of Cy3.5 and Cy5 single molecule fluorescence***

The single molecule fluorescence behavior of Cy3.5 and Cy5 was characterized at different average excitation powers by analyzing images and time traces. In Table 2.2.2 the on-times and collected photons per molecule have been summarized. On-time data should be interpreted as apparent on-times at the indicated data binning.

**Cy3.5**

Exc. intensity (kW.cm <sup>-2</sup> )	N	on-time (s)	Image ph/molecule (×10 <sup>3</sup> )	Time trace ph/molecule (×10 <sup>4</sup> )	Total ph/molecule (×10 <sup>4</sup> )
0.4	56	0.816 ± 0.066	1.9 ± 1.1	11.4 ± 13.5	11.6 ± 13.6
1.2	57	0.337 ± 0.016	4.9 ± 3.4	5.8 ± 4.6	6.3 ± 4.7
2.5	61	0.211 ± 0.010	4.0 ± 1.5	7.0 ± 7.9	7.4 ± 7.9
5	74	0.166 ± 0.010	8.0 ± 2.2	5.5 ± 5.4	6.3 ± 5.5

**Cy5**

0.35	40	0.218 ± 0.028	1.9 ± 1.1	2.2 ± 2.3	2.4 ± 2.3
1	64	0.102 ± 0.007	3.2 ± 2.6	1.3 ± 1.8	1.6 ± 1.9
2	43	0.099 ± 0.006	3.5 ± 1.7	1.6 ± 2.5	1.9 ± 2.6

**Table 2.2.2.** On-times and collected photons for individual Cy3.5 and Cy5 molecules at different average excitation intensities. On-time analysis was performed on time traces with a data bin of 10 ms. Time interval analyzed was from 0-5 s. On-time distributions were plotted in histograms. By fitting each histogram with a mono-exponential decay function the average on-times were extracted. The photons collected from individual molecules in images were obtained by integration of the intensities per spot. Background intensity was subtracted. Images were scanned with an integration time of 0.5 ms/pixel, 128×128 pixels, 6.2×6.2 μm<sup>2</sup>. The number of photons collected in time traces was obtained by integration of the total intensity during on-times. The average background intensity was subtracted. The applied data bin in time traces during analysis was 10 ms. By adding the number of photons of a spot in an image and the number of photons in the corresponding time trace the total intensity per molecule was calculated.

**Total number of photons**

For obvious reasons Table 2.2.2 shows that the number of photons per Cy3.5 and Cy5 molecule collected in an image decreases at lower excitation intensities.

*Conclusions from Table 2.2.2 for Cy3.5:*

The number of photons per molecule collected in a time trace is for Cy3.5 not significantly different at excitation intensities between 1.2 and 5 kW.cm<sup>-2</sup>. In average 10 times more photons are collected in the time traces than in the images. Because of the rather low intensity in the images also the total number of photons does not change a lot with excitation power. Only at very low powers, 0.4 kW.cm<sup>-2</sup>, the total number of photons that can be obtained is higher.

*Conclusions from Table 2.2.2 for Cy5:*

The number of photons per molecule collected in a time trace does not depend significantly for average excitation intensities of 1 and 2 kW.cm<sup>-2</sup>. About 4 times more photons are collected in the time traces than in the images. Consequently also the total number of photons does not change a lot with excitation intensity.

Only at the lowest intensity of  $0.35 \text{ kW}\cdot\text{cm}^{-2}$ , the total number of photons that can be obtained is somewhat higher. Probably at low excitation power, the emission of Cy5 is more stable.

### On-times

Table 2.2.2 shows that a decrease of the excitation intensity can significantly increase the duration of the time-period that a molecule stays in an emissive state. It is clear however that the average on-times of Cy5 molecules are much shorter than those of Cy3.5 molecules at comparable excitation intensities. The on-time results are also represented in a graphical way in Figure 2.2.5.

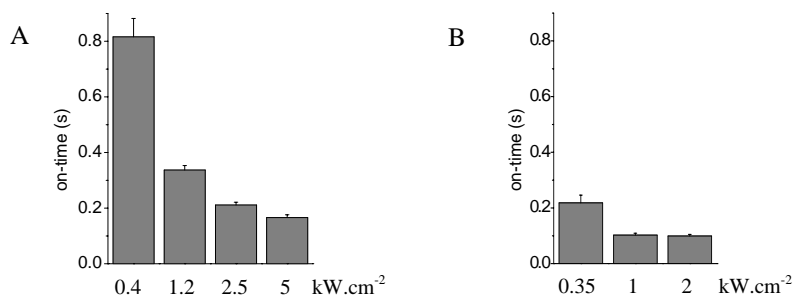


**Fig. 2.2.5.** Average on-times of individual Cy dye molecules at different average excitation intensities. A. Cy3.5. B. Cy5.

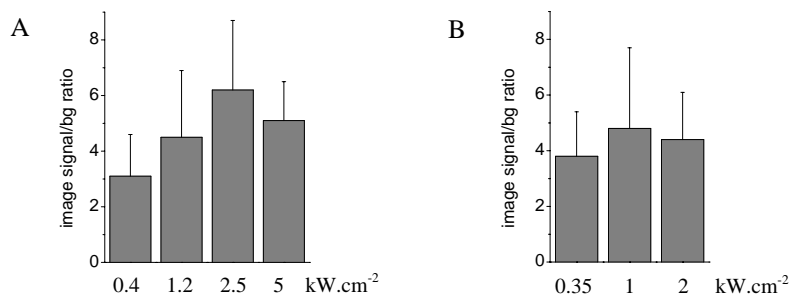


**Fig. 2.2.6.** Signal/background ratio of individual Cy dye spots in images at different excitation intensities. A. Cy3.5. B. Cy5. The ratio was calculated by dividing the total intensity in a fluorescence spot by the total intensity in a background area with the same size as the fluorescence spot.

In imaging it is evident that longer on-times will result in more complete spots. Therefore from Cy5 less frequently complete spots will be obtained than from Cy3.5 at equal excitation conditions, which is in agreement with the observation in the images. Low intensity excitation will be advantageous for the purpose of

localization analysis, although the signal to background ratios slightly decrease at lower excitation intensities.

### Blinking

The on-time data were further analyzed for the number of times that a molecule switches on and off during the 5 s measurement time interval, a representation of the so-called blinking behavior of molecules. In interpretation of the data it is important to consider that the result is dependent on the applied data bin. On-off switching on a timescale smaller than the applied time resolution will not be revealed. The results are represented in Figure 2.2.7 and 2.2.8.

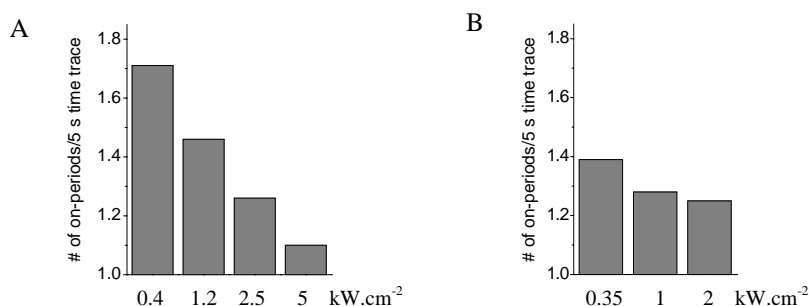


**Fig. 2.2.7.** Average number of on-periods per 5 s time trace at different excitation intensities. A. Cy3.5. B. Cy5.

From Figure 2.2.7 it is clear that individual Cy3.5 molecules switch more frequently on and off during emission, in particular at low excitation intensities. Cy5 molecules are blinking only slightly more at lower excitation intensities.

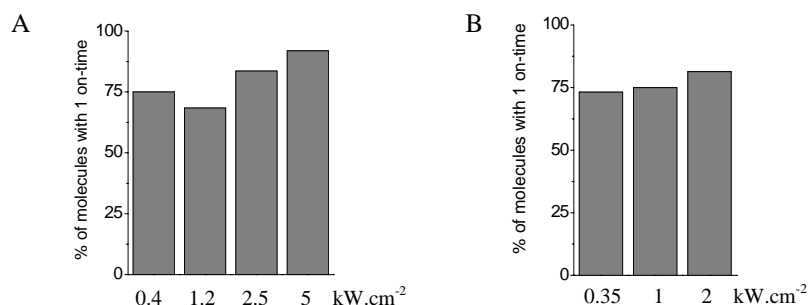


**Fig. 2.2.8.** Fraction of Cy dye molecules with one on-time. A. Cy3.5. B. Cy5.

From Figure 2.2.7 and 2.2.8 we can conclude that at low excitation intensities, although blinking is slightly increased, the majority of Cy3.5 and Cy5 molecules emits during one relatively long period.

## Count rates

The average count rates that theoretically can be expected from single Cy3.5 and Cy5 molecules at peak power excitation were calculated and compared with the measured count rates (according to equation 1.5-paragraph 1.4).

In Table 2.2.3 the results are shown for different excitation powers.

### Cy3.5

Exc. intensity (kW.cm <sup>-2</sup> )	N	Theoretical av. count rate (photons/s×10 <sup>5</sup> )	Measured av. count rate (photons/s×10 <sup>5</sup> )
0.4	56	0.6	1.4 ± 1.7
1.2	57	1.8	1.9 ± 1.4
2.5	61	3.6	3.5 ± 3.7
5	74	7.2	3.8 ± 3.3

### Cy5

0.35	40	2.45	1.1 ± 1.1
1	64	7.0	1.6 ± 1.9
2	43	14.0	1.9 ± 2.6

**Table 2.2.3.** Comparison of measured count rates with theoretically expected count rates of Cy3.5 and Cy5 molecules at peak power excitation.

Table 2.2.3 shows that the measured count rates and the theoretically expected count rates for Cy3.5 are in quite good agreement. For Cy5 however the measured count rates are much lower than the theoretical values. It is likely that large fluctuations in emission rate, occurring on a time scale smaller than our measurement integration time, are responsible for the lower measured count rates for Cy5. These fluctuations have been shown to be caused by photoinduced isomerization of Cy5, for Cy3.5 isomerization has not been reported. The rate of interchange between the emitting trans-state and non-emitting cis-state was found to be in the sub-milliseconds range and proportional to the excitation rate (6,7). In line with this observation our data show a larger difference between theoretical and measured values with an increase in excitation intensity. Fluorescence intensity fluctuations may also be caused by singlet-triplet transitions. However, at the excitation intensities that we used, the population of triplet states is supposed to be negligible (6,7).

All together we can conclude that the single molecule fluorescence characteristics of Cy5 as observed with confocal fluorescence microscopy are much weaker than expected from the photophysical properties determined in bulk.

## ***Influence of oxygen scavenging on single molecule fluorescence properties of Cy dyes***

In the previous paragraph we showed that the fluorescence duration of Cy3.5, and in particular Cy5, is limited. However for application in single molecule fluorescence studies on biological systems it is important to be able to follow a process for a sufficient amount of time. In literature the sensitivity of Cy5 to photobleaching by oxygen radicals has been reported (4,5) To increase the observation time it was recommended to use an oxygen scavenging system together with Cy5. The purpose of oxygen scavenging is to remove oxygen from the system and thereby prevent (excited state) oxidation of the components. We investigated if the use of an oxygen scavenging system could prolong the single molecule observation times of Cy3.5 and Cy5. Here we used the glucose oxidase/catalase scavenging system (3).

### **Cy3.5 and Cy5**

The single molecule fluorescence behavior of Cy3.5 in the presence of oxygen scavenger was characterized at an average excitation intensity of  $2.5 \text{ kW.cm}^{-2}$  by analyzing images and time traces. For Cy5 the excitation intensity was  $2 \text{ kW.cm}^{-2}$ . In Figure 2.2.9 some typical examples of Cy3.5 and Cy5 time traces are shown. From these time traces it is evident that much longer on-times are obtained when oxygen is removed.

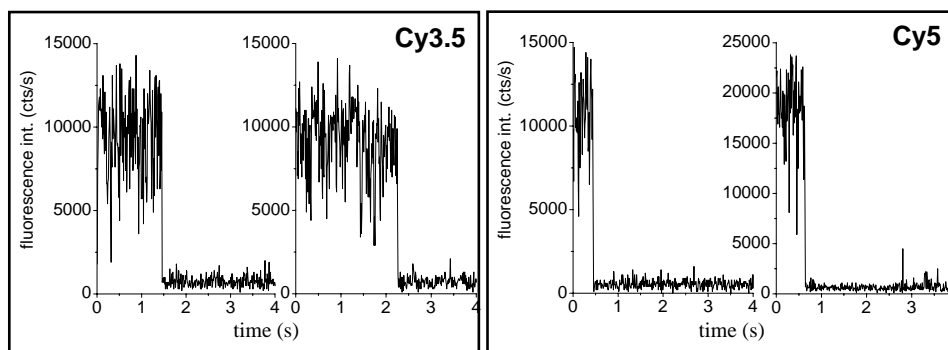


**Fig. 2.2.9.** Time traces of individual Cy3.5 and Cy5 molecules in the presence of oxygen scavenger. Cy3.5 was excited with  $2.5 \text{ kW.cm}^{-2}$ , Cy5 with  $2 \text{ kW.cm}^{-2}$ .

In Table 2.2.4 the on-times and collected photons per Cy3.5 molecule, with oxygen scavenger present, are summarized and compared with data from Cy3.5 and Cy5 molecules in the absence of oxygen scavenger (see Table 2.2.2.).



**Cy3.5**

	N	on-time (s)	Image ph/molecule ( $\times 10^3$ )	Time trace ph/molecule ( $\times 10^4$ )	Total ph/molecule ( $\times 10^4$ )
+ oxygen scavenger	45	$2.633 \pm 0.320$	$3.3 \pm 1.1$	$33.4 \pm 34.8$	$33.7 \pm 34.9$
- oxygen scavenger	61	$0.211 \pm 0.010$	$4.0 \pm 1.5$	$7.0 \pm 7.9$	$7.4 \pm 7.9$

**Cy5**

+ oxygen scavenger	40	$0.338 \pm 0.032$	$4.0 \pm 1.5$	$12.7 \pm 18.9$	$13.1 \pm 19.0$
- oxygen scavenger	43	$0.099 \pm 0.006$	$3.5 \pm 1.7$	$1.6 \pm 2.5$	$1.9 \pm 2.6$

**Table 2.2.4.** Effect of oxygen scavenging on on-times and collected photons of individual Cy3.5 and Cy5 molecules. For Cy3.5 the excitation intensity was  $2.5 \text{ kW.cm}^{-2}$ , for Cy5  $2 \text{ kW.cm}^{-2}$ . A time interval was analyzed from 0-5 s. On-time analysis was performed as described in the legend of Table 2.2.2.

*Conclusions from Table 2.2.4 for Cy3.5:*

From the data in Table 2.2.4 it follows that Cy3.5 molecules remain in an emissive state about 12 times longer when oxygen is scavenged.

The number of photons obtained per single Cy3.5 molecule in an image stays the same. The amount of collected photons in time traces, and consequently also the total number of photons per molecule, is about 4.5 times higher with oxygen scavenger present. For imaging this means that higher excitation intensities will be allowed without immediately bleaching the fluorescence, resulting in improved signal to background ratios. For localization studies this will definitely be beneficial.

*Conclusions from Table 2.2.4 for Cy5:*

The data in Table 2.2.4 show that oxygen scavenging has a positive effect on the fluorescence properties of Cy5 molecules. The effect is not as dramatic as for Cy3.5, but under otherwise identical conditions, Cy5 molecules stay about 4 times longer in an emissive state when oxygen is removed. A 30-fold increase in photostability was reported for Cy5 (4) and a smaller effect for Cy3. The effect of oxygen on the emission properties of Cy3.5 has not been reported previously. Our measurements indicate a significant effect for Cy5, but an even stronger effect for Cy3.5. The numbers of photons obtained per single Cy5 molecule in an image is not much different under both conditions. The total amount of photons collected per molecule, is about 7 times higher with oxygen scavenger present. At identical

scanning conditions, Cy5 images will contain more complete single molecule spots in the absence of oxygen than with oxygen present. Longer observation of single Cy5 molecules will be allowed at oxygen depleted conditions.

### **Comparison of Cy dye and GFP single molecule fluorescence behavior**

In general there is a striking difference in fluorescence behavior of GFP single molecules and Cy molecules. In paragraph 2.1.2 the very instable fluorescence of GFP molecules was already notified. This observation was corroborated by images and time traces (Fig.2.1.3-5) as well as by the results from on-time analysis (Table 2.1.3). In Fig.2.2.13 a time trace of an EGFP molecule and a Cy3.5 molecule are shown together.

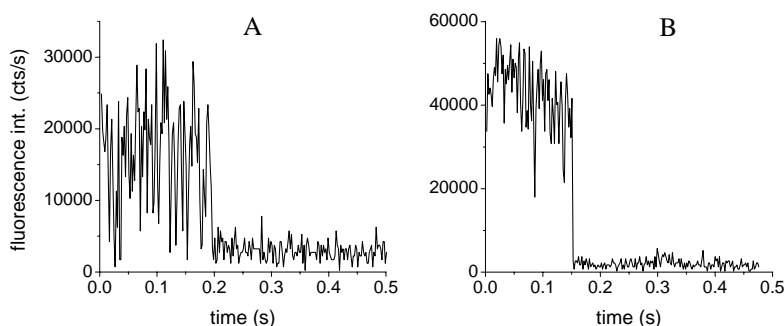


**Fig. 2.2.13.** Comparison of fluorescence behavior of an individual EGFP molecule (A) immobilized in 15% PAA gel and an individual Cy3.5 molecule immobilized by adsorption onto quartz. Average excitation power was  $6 \text{ kW.cm}^{-2}$  at 488 nm for EGFP and  $5 \text{ kW.cm}^{-2}$  at 568 nm for Cy3.5. Time traces are represented with a data bin of 2 ms.

Although in both profiles the on-periods are of almost equal length, it is evident that the fluorescence of Cy3.5 is much more stable than from EGFP. This effect has been reported before by in literature (8,9). From Poisson statistics only we would expect less fluctuations than observed for EGFP in Figure 2.2.13.A. The probability to measure events below 10 counts (corresponding to 5,000 counts/s during one 2 ms bin) is about 0.03 for an average signal of 30 counts (corresponding to 15,000 counts/s during one 2 ms bin). The EGFP time trace however shows about 10% of low-level events. In contrast, the Cy3.5 time trace in Figure 2.2.13.B shows hardly any low-level events, which may be expected from Poisson statistics for an average of 80 counts. From this it is concluded that the fluctuations in time traces of GFP single molecules are dominated by molecular dynamics and not by Poisson statistics of the photon emission. In spite of the very general use of GFP as a label no definitive conclusions have been drawn with respect to the nature of the molecular dynamics.

### **2.2.3 Discussion and Conclusions**

The photophysical properties determined in bulk from Cy3.5 and Cy5 indicate that Cy5 is a stronger fluorophore than Cy3.5. In literature no reports are available on single molecule characterization of Cy dyes, although in particular Cy5 has been used widely in single molecule applications (10-17). Nevertheless, our single molecule data demonstrate clearly that Cy3.5 is more photostable than Cy5. At similar excitation powers on-times are longer for Cy3.5 than for Cy5. The average number of photons collected per Cy3.5 molecule also is higher than for a Cy5 molecule. The deviation of the measured count rates from theoretical values is much larger for Cy5 than for Cy3.5. Because of photoisomerization Cy5 molecules are supposed to be in the non-fluorescent cis-state during 50% of the time (6,7). This may explain the low number of molecules visible. So far isomerization has not been reported for Cy3.5.

From the results in the presence of oxygen scavengers, we can conclude that not only Cy5, but also Cy3.5 is sensitive for photobleaching by oxygen radicals. The photophysical properties of Cy5 as well as from Cy3.5 improved considerably when oxygen was removed. In particular on-times and number of collected photons are important aspects in single molecule fluorescence investigations. To study dynamic aspects of a biological process it is necessary to follow the process during a certain time. At least during the time of observation the emission of the applied fluorescent labels should not stop. In this respect the use of oxygen scavengers will be useful. Nevertheless it is necessary to be aware of the composition of the oxygen scavenging system. Here we used a combination of two proteins, glucose oxidase and catalase. A drawback of this system may be the addition of extra proteins in a reaction mixture. For example in the study of specific protein-DNA interactions it may be undesirable to include proteins in the reaction other than the proteins of interest. Another disadvantage may be that glucose oxidase itself fluoresces when excited at 488 nm. At this wavelength we observed single molecule glucose oxidase fluorescence. For that reason we conclude that the glucose oxidase/catalase system is only useful in combination with fluorescent dyes that are excited in the yellow and red wavelength region. Other oxygen scavengers should be used in combination with dyes that require 488 nm excitation. For GFP no effect of oxygen removal has been observed.

In general we can conclude that both Cy3.5 and Cy5 are suitable fluorophores for single molecule investigations. Removal of oxygen considerably improves the photophysical properties of both fluorophores. With Cy3.5 oxygen scavenging is recommended, for Cy5 applications it is absolutely required. Another possibility is to work in an oxygen-free environment.

In particular for simultaneous detection of biomolecules labeled with different fluorophores, for example EGFP labeled XPA together with Cy3.5 labeled DNA, it is important to have sufficient notion of the fluorescence characteristics of both fluorophores. Fluorescence intensities and photostability differ a lot for different types of fluorescent molecules upon excitation with similar powers at their optimal wavelengths. Upon excitation of EGFP with 488 nm and excitation of Cy3.5 with 568 nm at equal powers the on-times for Cy3.5 will be twice as long as for EGFP with much less blinking.

## 2.2.4 References

1. Mujumdar, S.R., Mujumdar, R.B., Grant, C.M., and Waggoner, A.S. (1996) Cyanine-labeling reagents: sulfobenzindocyanine succinimidyl esters. *Bioconj. Chem.*, **7**, 356-362
2. <http://www1.amershambiosciences.com>
3. Harada, Y., Sakurada, K., Aoki, T., Thomas, D.D., and Yanakida, T. (1990) Mechanical coupling in actomyosin energy transduction studied by *in vitro* movement assay. *J. Mol. Biol.*, **216**, 49-68
4. Ha, T. (2001) Single-molecule fluorescence resonance energy transfer. *Methods*, **25**, 78-86
5. Grunwell, J.R., Glass, J.L., Lacoste, T.D., Deniz, A.A., Chemla, D.S., and Schultz, P.G. (2001) Monitoring the conformational fluctuations of DNA hairpins using single-pair fluorescence resonance energy transfer. *J. Am. Chem. Soc.*, **123**, 4295-4303
6. Widengren, J., Schweinberger, E., Berger, S., and Seidel, C.A.M. (2001) Two new concepts to measure fluorescence resonance energy transfer via fluorescence correlation spectroscopy: theory and experimental realization. *J. Phys. Chem.*, **105**, 6851-6866
7. Widengren, J., and Schwille, P. (2000) Characterization of photoinduced isomerization and back-isomerization of the cyanine dye Cy5 by fluorescence correlation spectroscopy. *J. Phys. Chem.*, **104**, 6416-6428
8. Pierce, D.W., Hom-Booher, N., and Vale, R.D. (1997) Imaging individual green fluorescent proteins. *Nature*, **388**, 338
9. Pierce, D.W., and Vale, R.D. (1999) Single-molecule fluorescence detection of green fluorescent protein and application to single-protein dynamics. *Meth. Cell Biol.*, **58**, 49-73
10. Schütz, G.J., Kada, G., Pastushenko, V.P., and Schindler, H. (2000) Properties of lipid microdomains in a muscle cell membrane visualized by single molecule microscopy. *EMBO J.*, **19**, 892-901
11. Tinnefeld, P., Buschmann, V., Herten, D-P., Han, K-T., Sauer, M. (2000) Confocal fluorescence lifetime imaging microscopy (FLIM) at the single molecule level. *Single Molecules*, **3**, 215-223
12. Schütz, G.J., Trabesinger, W., and Schmidt, T. (1998) Direct observation of ligand colocalization on individual receptor molecules. *Biophys. J.*, **74**, 2223-2226

13. Suzuki, Y., Tani, T., Sutoh, K., and Kamimura, S. (2002) Imaging of the fluorescence spectrum of a single fluorescent molecule by prism-based spectroscopy. *FEBS Letters*, **512**, 235-239
14. Osborne, M.A., Barnes, C.L., Balasubramanian, and Klenerman, D. (2001) Probing DNA surface attachment and local environment using single molecule spectroscopy. *J. Phys. Chem. B.*, **105**, 3120-3126
15. Ha, T., Ting, A.Y., Liang, J., Caldwell, W.B., Deniz, A.A., Chemla, D.S., Schultz, P.G., and Weiss, S. (1999) Single-molecule fluorescence spectroscopy of enzyme conformational dynamics and cleavage mechanism. *Proc. Natl. Acad. Sci. USA*, **96**, 893-898
16. Dietrich, A., Buschmann, V., Müller, C., and Sauer, M. (2002) Fluorescence resonance energy transfer (FRET) and competing processes in donor-acceptor substituted DNA strands: a comparative study of ensemble and single-molecule data. *Rev. Mol. Biotech.* , **82**, 211-231
17. van Sark, W.G.J.H.M., Frederix, P.L.T.M., van den Heuvel, D.J., Asselbergs, M.A.H., Senf, I., and Gerritsen, H.C. (2000) Fast imaging of single molecules and nanoparticles by wide-field microscopy and spectrally resolved confocal microscopy. *Single Molecules*, **4**, 291-298

## 2.3 Alexa dyes

In paragraph 1.2 we described general characteristics of Alexa dyes. Here we investigated the single molecule fluorescence properties of Alexa 488 conjugated to the XRCC4 protein, that is involved in Double Strand Break repair (1). DNA double strand breaks can be produced by ionizing radiation or oxidative agents. The XRCC4 protein occurs in dimer form and has been genetically modified in such a way that there is only a single cystein residue per monomer. The molecular mass is 39 kD per monomer. In Figure 2.3.1 the structure of an XRCC4 dimer is shown.

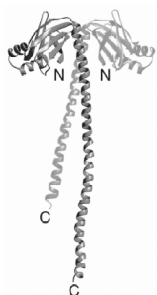


**Fig. 2.3.1.** *Ribbon diagram of the structure of an XRCC4 dimer. Each XRCC4 monomer consists of a head domain, composed of an  $\alpha$ -helix and  $\beta$ -sheet part, and a 12 nm long  $\alpha$ -helical stalk (2).*

Alexa Fluor 488 maleimide is used to label the cystein residues (Cys93) located in the head parts of the XRCC4 protein (2).

### Alexa 488

The chemical structure of Alexa 488 is shown in Figure 2.3.2 as a maleimide derivative. Thiol reactive maleimides are used for labeling of cystein sulfhydryl groups of proteins. The molecular mass of the Alexa 488-maleimide is 720.66 (3,4).

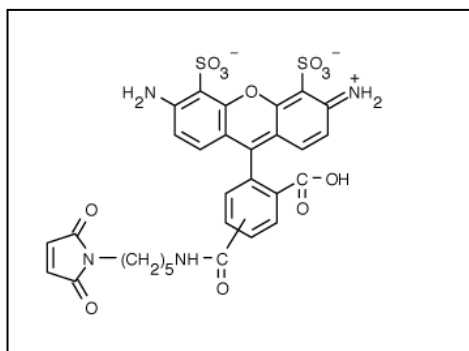


**Fig. 2.3.2.** *Chemical structure of Alexa 488-maleimide.*

In Table 2.3.1 the photophysical properties of Alexa 488 in bulk are summarized (3,4). The product of  $\epsilon$  and  $Q$  gives an indication for the effectiveness of Alexa 488 in fluorescence applications.

	<b>Alexa 488</b>
$\lambda_{abs}^{max}$ (nm)	495
$\lambda_{em}^{max}$ (nm)	519
$\epsilon$ at $\lambda_{abs}^{max}$ ( $M^{-1}.cm^{-1}$ )	78,000
$Q$	0.36-0.60*
$\epsilon \times Q$	28,080-46,800

**Table 2.3.1.** Photophysical properties of Alexa 488.  $\epsilon$  is the extinction coefficient and  $Q$  is the quantum yield. \* the quantum yield depends on the conjugation partner.

In paragraph 1.4-Table 1.4.1 the most relevant parameters in our Alexa 488 measurements have been summarized. The expected count rates are indicated too. Purely on the basis of bulk data we may expect to detect a count rate for Alexa 488 similar to (E)GFP.

The excitation and emission spectrum of Alexa 488 is shown in Figure 2.3.3 (3,4).

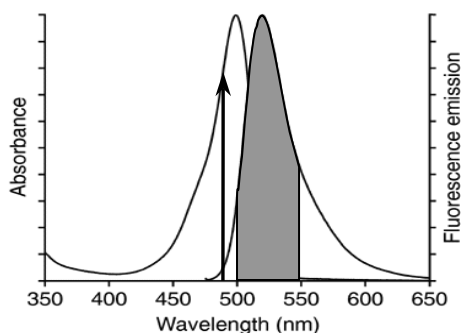


**Fig. 2.3.3.** Excitation and emission spectrum of Alexa 488, pH 8. The arrow indicates the wavelength of the 488 nm laser line that will be used for excitation. The shaded area shows the wavelength region that is detected with the HQ525/50 band pass filter.

From the excitation spectrum it can be concluded that the 488 nm line from an Ar-Kr laser has the proper wavelength for excitation of Alexa 488. Compared to excitation in the maximum the excitation efficiency at 488 nm is 75%.

### 2.3.1 Materials and Methods

#### XRCC4 protein production and labeling with Alexa 488

The labeled protein was kindly provided by M. Modesti (Genetics, Rotterdam, the Netherlands) (2). The Alexa 488 labeled XRCC4 protein was stored in buffer containing 20 mM Hepes, 300 mM KCl, 0.5 mM EDTA, 2 mM DTT, 10% glycerol, pH 7.2. About 90% of the preparation was estimated to contain 1 Alexa 488 fluorophore per monomer.

#### Sample preparation for confocal microscopy

For single molecule confocal measurements, the Alexa 488-XRCC4 was diluted to concentrations of about  $5 \times 10^{-10}$  M in 1 % (w/v) low melting point agarose in 20 mM Hepes, 300 mM KCl, 0.5 mM EDTA, pH 7.2. at 30° C. 5 microliters of this mixture was sandwiched between two extensively cleaned quartz cover slips, diameter 25 mm.

#### Scanning confocal fluorescence microscopy

For measurements on the Alexa 488-XRCC4 protein the confocal microscope, described in section 1.4, was used. Measurement configuration was as shown in Figure 2.3.3.

### 2.3.2 Results

#### Confocal single molecule detection of Alexa 488 fluorescence

In Figure 2.3.4 a confocal image is shown of single fluorescing Alexa 488-XRCC4 protein molecules immobilized in 1% agarose.

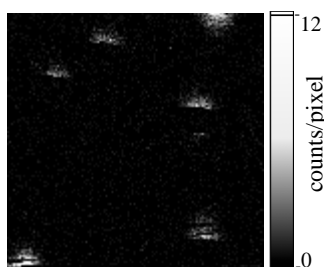


**Fig. 2.3.4.** Scanning confocal image of Alexa 488-XRCC4 protein immobilized in 1% agarose. Image size is  $3.1 \times 3.1 \mu\text{m}^2$ ,  $128 \times 128$  pixels, dwell time is 0.5 ms/pixel. Average excitation intensity was  $6 \text{ kW.cm}^{-2}$ .



In the Alexa 488-XRCC4 image typical single molecule bleaching and blinking can be observed. At the applied average excitation intensity of  $6 \text{ kW}\cdot\text{cm}^{-2}$  only fractions of single molecule spots are visible in the images. Also the emission intensity per molecule is rather low. On the single molecule level the photophysical properties of Alexa 488 molecules seem to be less favorable than suggested by the specifications measured in bulk.

In Figure 2.3.5 some typical examples of Alexa 488-XRCC4 time traces are shown. From these time traces it is apparent that the on-times of Alexa 488 molecules are very short. At first glance they are similar to the Cy5 on-times (Figure 2.2.4). At low excitation intensity Alexa 488 molecules exhibit longer on-times and lower count rates, a similar behavior as observed for Cy dyes and GFP molecules. The time trace in Figure 2.3.5.A displays a two-step bleaching behavior, probably because of successive bleaching of two Alexa 488 molecules present on one XRCC4 dimer.

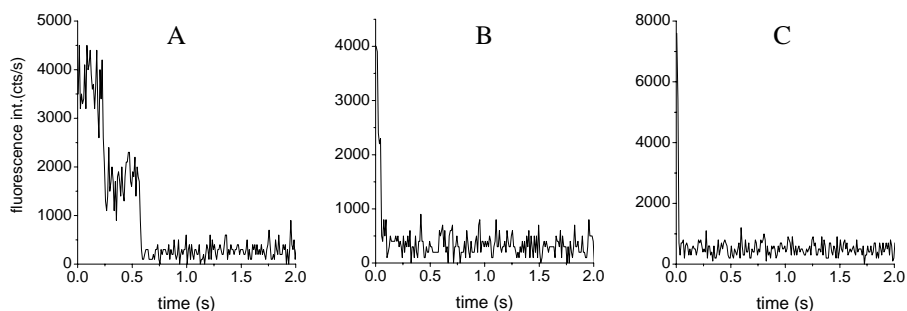


**Fig. 2.3.5.** Time traces of individual Alexa 488-XRCC4 molecules excited with different average excitation intensities. A.  $0.45$ ; B.  $3$ ; C.  $6 \text{ kW}\cdot\text{cm}^{-2}$ .

### **Analysis of Alexa 488 single molecule fluorescence**

The single molecule fluorescence behavior of Alexa 488 was characterized at different excitation intensities by analyzing images and time traces. In Table 2.3.2 the on-times and collected photons per Alexa 488 molecule at different excitation intensities are summarized. Because of too fast bleaching only a limited number of molecules could be measured with an excitation intensity of  $6 \text{ kW}\cdot\text{cm}^{-2}$ .

Exc. int. (kW.cm <sup>-2</sup> )	N	on-time (s)	Total ph/molecule (×10 <sup>4</sup> )
0.45	41	0.335 ± 0.022	3.7 ± 3.9
3	40	0.132 ± 0.014	1.3 ± 1.3
6	10	0.033 ± 0.020 <sup>a</sup>	0.8 ± 0.9

**Table 2.3.2.** On-times and collected photons of individual Alexa 488 molecules at different average excitation intensities. On-time analysis was performed as described in the legend of Table 2.2.2. Only time traces were included with a single bleaching step. In calculation of the total number of photons per molecule, photons emitted while imaging were neglected, because these intensities do not contribute significantly to the total intensity (see also Tables 2.2.2, 2.2.4, 2.2.6 and 2.2.7). <sup>a</sup>not extracted from fit, just averaged because of low number of measurements.

The number of photons collected from Alexa 488 molecules is very low and comparable to Cy5 molecules without oxygen scavenging (Table 2.2.2) at similar excitation intensities. As for the Cy dyes also for imaging of Alexa 488 single molecules lower excitation intensities are favorable.

### On-times

Table 2.3.2 shows that the on-times of Alexa 488 are very short. This could be due to an extreme sensitivity of Alexa 488 for photobleaching by oxygen radicals. In literature however only a small effect of oxygen removal on photostability of Alexa 488 was mentioned (5) and so far we did not check this. The on-times of Alexa 488 are comparable to those of Cy5 without oxygen scavenging at similar excitation intensities. The duration of Alexa 488 on-times can be significantly increased by a decrease in excitation intensity. The on-time results are also represented in a graphical way in Figure 2.3.6 together with blinking data.

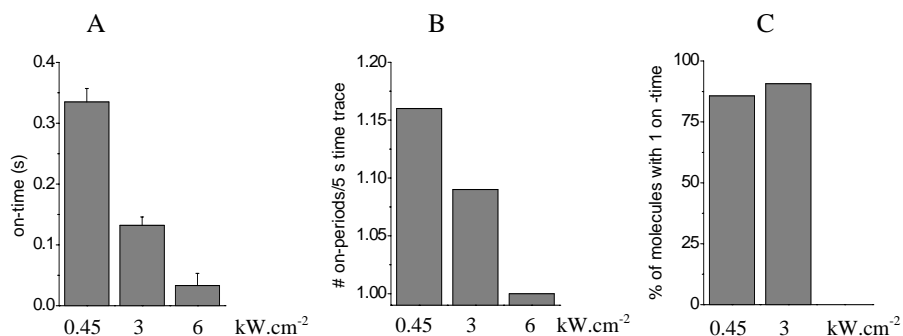


**Fig. 2.3.6.** On-time analysis of single Alexa 488 labeled XRCC4 molecules at different average excitation powers.

From Figure 2.3.6 we can conclude that on-times of Alexa 488 are significantly longer at low excitation intensities. The largest part of the Alexa 488 molecules emits during one on-period (Figure 2.3.6.C).

### Count rates

The theoretically expected average count rates from Alexa 488 molecules at peak power excitation were calculated (according to equation 1.5-paragraph 1.4) and compared with the measured count rates. The result is shown in Table 2.3.3.

Exc. intensity (kW.cm <sup>-2</sup> )	N	Theoretical av. count rate (photons/s×10 <sup>5</sup> )	Measured av. count rate (photons/s×10 <sup>5</sup> )
0.45	41	1.0	1.1 ± 1.2
3	40	6.6	1.0 ± 1.0
6	10	13.2	2.4 ± 2.7

**Table 2.3.3.** Comparison of theoretically expected count rates of Alexa 488 molecules with measured count rates. Only time traces were included with a single bleaching step.

The measured count rates are lower than the theoretical values. Only at the lowest excitation intensity of 0.45 kW.cm<sup>-2</sup> the measured count rate is equal to the expected one.

### Two-step bleaching

Besides longer emission periods, at lower excitation power more frequently a two-step bleaching feature can be observed (Fig. 2.3.5.A). As mentioned in Materials and Methods Alexa 488 is conjugated to the XRCC4 protein that is in a dimer configuration (2). From those protein molecules in which both monomers are labeled, a two-step bleaching behavior may be expected. To get an impression about the fraction of molecules that is double-labeled, the time traces were analyzed for the presence of a two-step bleaching characteristic. The results are presented in Figure 2.3.7.

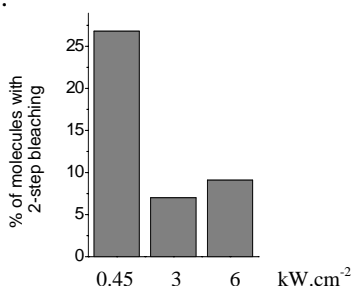


**Fig. 2.3.7.** Fraction of Alexa 488-XRCC4 molecules showing two-step bleaching behavior. Results obtained from time trace measurements at different average excitation intensities.

Figure 2.3.7 shows that upon excitation with low intensity from about 25% of the molecules a two-step bleaching can be observed. If 90% of the XRCC4 dimers were provided with 2 fluorophores then probably during prior imaging from about 65% of the molecules one of the fluorophores bleached. Dependent on the proximity of both fluorophores in double-labeled XRCC4 dimers quenching also may occur. Anyway low excitation intensities are required for the observation of the two-step bleaching.

### **2.3.3 Discussion and Conclusions**

The favorable bulk photophysical properties together with the exciting experiences of investigators with Alexa dyes in cell biological studies (6-13) gave rise to optimistic expectations for single molecule applications. Our conclusion so far is that Alexa 488 behaves poorly in single molecule experiments. The appearance of hardly any single molecule reports on Alexa dyes in literature until now is at least remarkable (14). Further investigations are required to determine if proper conditions can be found for the use of Alexa 488 in single molecule experiments.

### **2.3.4 References**

1. Hoeijmakers, J.H.J. (2001) Genome maintenance mechanisms for preventing cancer. *Nature*, **411**, 366-374
2. Junop, M.S., Modesti, M., Guarné, A., Ghirlando, R., Gellert, M., and Yang, W. (2000) Crystal structure of the Xrcc4 DNA repair protein and implications for end joining. *EMBO J.*, **19**, 5962-5970
3. Panchuk-Voloshina, N., Haugland, R.P., Bishop-Stewart, J., Bhalgat, M.K., Millard, P.J., Mao, F., Leung, W-Y., and Haugland, R.P. (1999) Alexa dyes, a series of new fluorescent dyes that yield exceptionally bright, photostable conjugates. *J. Histochem. Cytochem.*, **47**, 1179-1188
4. <http://www.probes.com>
5. Ha, T. (2001) Single-molecule fluorescence resonance energy transfer. *Methods*, **25**, 78-86
6. Kumar, R.K., Chapple, C.C., and Hunter, N. (1999) Improved double immunofluorescence for confocal laser scanning microscopy. *J. Histochem. Cytochem.*, **47**, 1213-1217
7. Huang, S., Hayes, S.J., and Serwer P. (2001) Fluorescence microscopy of single viral capsids. *J. Struct. Biol.*, **135**, 270-280
8. Kues, T., Dickmanns, A., Lührmann, R., Peters, R., and Kubitscheck, U. (2001) High intranuclear mobility and dynamic clustering of the splicing factor U1 snRNP observed by single particle tracking. *Proc. Natl. Acad. Sci. USA*, **98**, 12021-12026

9. Rusinova, E., Tretyachenko-Ladokhina, V., Vele, O.E., Senear, D.F., and Ross, J.B.A. (2002) Alexa and Oregon Green dyes as fluorescence anisotropy probes for measuring protein-protein and protein-nucleic acid interactions. *Anal. Biochem.*, **308**, 18-25
10. Nguyen, T., and Rosenzweig, Z. (2002) Calcium ion fluorescence detection using liposomes containing Alexa-labeled calmodulin. *Anal. Bioanal. Chem.*, **374**, 69-74
11. Peccia, J., and Hernandez, M. (2002) Rapid immunoassays for detection of UV-induced cyclobutane pyrimidine dimers in whole bacterial cells. *Appl. Environm. Microbiol.*, **68**, 2542-2549
12. Tóth, K., Brun, N., and Langkowski J. (2001) Trajectory of nucleosomal linker DNA studied by fluorescence resonance energy transfer. *Biochemistry*, **40**, 6921-6928
13. Kues, T., Peters, R., and Kubitscheck U. (2001) Visualization and tracking of single protein molecules in the cell nucleus. *Biophys. J.*, **80**, 2954-2967
14. Rajagopalan, P.T.R., Zhang, Z., McCourt, L., Dwyer M., Benkovic, S.J., and Hammes, G.G. (2002) Interaction of dihydrofolate reductase with methotrexate: ensemble and single-molecule kinetics. *Proc. Natl. Acad. Sci. USA*, **99**, 13481-13486



# 3

## STRUCTURE, DYNAMICS and INTERACTION of SINGLE DNA and PROTEIN MOLECULES

*One of our aims in this confocal study is to determine the exact position of a molecule within a confocal image, and even within a complex of molecules. Moreover we are interested in the dynamics of interactions that take place between different individual molecules. For this purpose it is important to image single fluorescent molecules at optimal scanning conditions. This implies that the molecule should stay in focus at least during the time of observation. Therefore it is important to immobilize the molecules of interest in the proper way. In this chapter we will show confocal single molecule results from surface immobilized DNA molecules, from diffusing DNA molecules in an agarose matrix and from DNA molecules immobilized in agarose by protein binding. Finally results will be shown of a method to determine accurately the position of individual fluorescent molecules within confocal images.*

### 3.1 General introduction

Immobilization of molecules with a homogeneous distribution has been an issue of interest ever since single molecule investigations were initiated. Surface adsorption, although not very well controllable with respect to the resulting surface density, is a proper technique for immobilization of DNA molecules.

The advantages of immobilization in gel matrices for single molecule fluorescence detection, like the availability of a sample with a controlled, homogeneous distribution of molecules, have been mentioned in paragraph 1.2. With respect to the gel type, agarose gels are preferred over polyacrylamide gels. When polyacrylamide gels are used, the molecules of interest are already present during polymerization of the gel. The polymerization reaction is a quite aggressive process that may be harmful with respect to functionality. It is also not excluded that, in particular with proteins, crosslinking occurs to the matrix that may affect the properties of the molecules. Immobilization in agarose is a more mild method, where molecules will be trapped during formation of a gel network through cooling of the agarose mixture. To what extent the mobility of the molecules of interest is restricted within a certain type of gel depends largely on their 3D-conformation. For instance protein and DNA molecules with equal molecular mass have a completely different 3D-structure. Protein molecules usually have a more globular shape, while DNA molecules are more elongated. In paragraph 2.1 we already showed results from GFP mutants and GFP-XPA fusion protein immobilized in polyacrylamide and agarose gels. DNA molecules however did not immobilize in these gel matrices.

When fluorescently labeled protein and DNA molecules both are present in an agarose matrix, we expect to observe immobilized protein molecules in an environment of diffusing DNA molecules. If however the protein molecules have an affinity for binding to the DNA, immobilization of DNA in the agarose matrix will occur. Together with the protein also the bound DNA will be trapped in the pores of the gel. With our scanning confocal microscope we can excite different fluorophores simultaneously at their characteristic excitation wavelengths. In a single scan multiple emission bands from different fluorescent molecules can be detected at the same time. If protein and DNA molecules are labeled with different fluorophores we can detect protein-DNA complexes within the gel from the colocalization of the fluorescence signals within one diffraction-limited spot.

To localize individual fluorescent molecules within a confocal image with higher precision than the diffraction limited resolution, we used a method based on Gaussian fitting and simulation of noise.



In paragraph 3.1.3 we show confocal fluorescence results from DNA molecules immobilized by adsorption onto quartz, displaying single molecule FRET (see paragraph 1.2). In paragraph 3.2 we demonstrate that DNA molecules, different in size and conformation, only diffuse within agarose gels. Because of the relevance for later single molecule investigations on DNA binding by NER proteins within agarose gels (see paragraph 3.3 and chapter 4 and 5), the diffusional properties of the different DNA molecules were characterized. In paragraph 3.3 results are shown of DNA immobilization in an agarose gel as a result of binding by NER proteins. In paragraph 3.4 we show results from localization analysis on fluorescence spots in confocal images obtained with Gaussian fitting procedures.

### 3.1.1 Structure of 4-way junction DNA from single molecule FRET

In Figure 3.1.1 the measured absorption and emission spectra of Cy3.5 and Cy5 are shown. From this figure it is clear that there is a considerable overlap between the emission spectrum of Cy3.5 and the absorption spectrum of Cy5. The spectral overlap suggests that Cy3.5 and Cy5 are good candidates as a FRET pair. Cy3.5 can function as the donor and Cy5 as the acceptor.

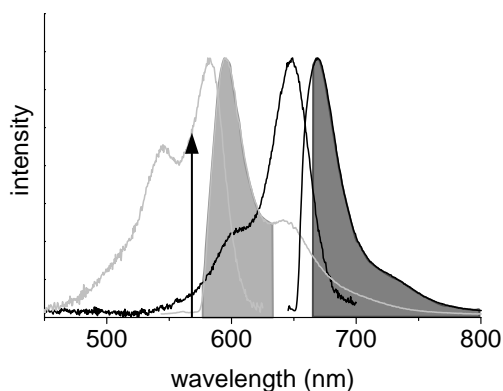


**Fig.3.1.1.** Absorption and emission spectra measured from Cy3.5 and Cy5 labeled DNA. The gray spectra are from Cy3.5, the black spectra are from Cy5. The arrow indicates the excitation wavelength used for FRET. The light gray area indicates the wavelength region detected with the D605/55 band pass filter for detection of Cy3.5 emission, the dark gray area indicates the wavelength region detected with the HQ665LP emission filter for detection of Cy5 emission.

### 4-Way junction DNA

The 4-way junction DNA, also known as the Holliday junction, is supposed to be an important intermediate DNA structure in genetic recombination events. Earlier studies have suggested that the conformation of the junction depends on the salt concentration present. At low salt concentrations an extended unstacked conformation has been proposed, while at high salt concentrations the junction folds into a stacked X structure. These conclusions have been drawn from gel electrophoresis experiments (6) as well as from ensemble FRET experiments (7,8). It is highly dependent on the base sequence at the junction, which two arms move towards each other. From the so-called junction 3 (7,8) it has been demonstrated that the X and R arms move towards each other upon addition of magnesium ions. The positive charges are supposed to shield the high concentration of negative charges present at the junction resulting in less repulsion between the arms. In Figure 3.1.2 the base sequence at the junction and a schematic representation of the junction is shown.

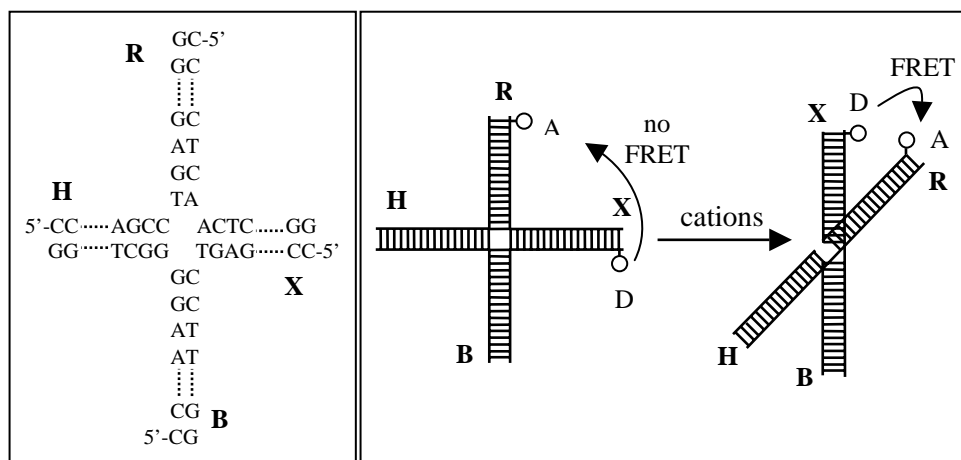


**Fig. 3.1.2.** Schematic representation of the base sequence and structure of 4-way junction DNA. In the left panel the base sequence at the junction is shown for junction 3. In the right panel the effect of cation addition is represented. In the absence of extra cations the junction is unable to fold and remains in an extended conformation (left). In the presence of added cations the junction is folded into an X-structure undergoing a 60° rotation. If two successive arms that move towards each other have been labeled with a proper FRET donor and acceptor pair, FRET is likely to occur. The dotted lines in the left panel represent 11 base pairs in the particular 4-way junction DNA used in our study.

Not only enzymes involved in recombination but also linker histones and the XPA protein (9), involved in Nucleotide Excision Repair, have been shown to bind to 4-way junction DNA. For the purpose of single molecule investigations on binding of XPA to DNA we prepared a 4-way junction DNA, identical to

junction 3, labeled with Cy3.5 at the 5'-end of the X-arm and Cy5 at the 5'-end of the R-arm. The presence of the fluorescent labels not only gives us the opportunity to assess binding of the XPA protein to the 4-way junction DNA, but also accompanying changes in DNA conformation can be determined by FRET measurements. To this aim we first studied the single molecule fluorescence properties of Cy3.5 and Cy5 double-labeled 4-way junction DNA, immobilized on quartz by adsorption, in the absence of protein.

The DNA was prepared from four oligomers of 34 nucleotides length, resulting in a junction with arms of 17 base pairs each. The arm length is equivalent to about 5.6 nm per arm. In a planar conformation the distance between the ends of successive arms will be about 8 nm. In the presence of cations we expect to observe FRET between the Cy3.5 donor and Cy5 acceptor molecule.

### Expected single molecule observations

For the purpose of FRET measurements on Cy3.5 and Cy5 labeled DNA, excitation is performed with only 568 nm, which is the wavelength for excitation of the donor Cy3.5 molecule. In the donor channel we expect to detect only Cy3.5 emission. If no FRET occurs we expect to detect in the acceptor channel some emission from Cy5, which is excited at 568 nm with about 10% of the excitation efficiency at 647 nm, together with cross talk from Cy3.5 emission into this channel. The emission spectrum of Cy3.5 indicates that 20% of Cy3.5 emission will be detected in the acceptor channel, having wavelengths longer than 665 nm.

In a situation of only colocalization of Cy3.5 and Cy5, without FRET, the expected photon intensity in the Cy3.5 detection channel upon 568 nm excitation with power P will be equal to (equation 1.5-paragraph 1.4):

$$0.8 \cdot \sigma_{abs-Cy3.5} \cdot \eta_{abs-cy3.5} \cdot Q_{Cy3.5} \cdot \frac{P}{E_{photon}} \cdot \frac{1}{3}$$

With  $\sigma_{abs-Cy3.5}$  is  $5.8 \cdot 10^{-16} \text{ cm}^2$ ,  $\eta_{abs-Cy3.5}$  is 0.7 and  $Q_{Cy3.5}$  is 0.15 (see paragraph 1.4) this results in:

$$0.162 \cdot 10^{-16} \cdot \frac{P}{E_{photon}}$$

The total photon intensity in the Cy5 channel from direct excitation of Cy5 plus cross talk from Cy3.5 emission will be:

$$\left( \frac{P}{E_{photon}} \cdot \sigma_{abs-Cy5} \cdot \eta_{abs-Cy5} \cdot Q_{Cy5} + 0.2 \cdot \frac{P}{E_{photon}} \cdot \sigma_{abs-Cy3.5} \cdot \eta_{abs-Cy3.5} \cdot Q_{Cy3.5} \right) \cdot \frac{1}{3}$$

With  $\sigma_{abs-Cy5}$  is  $9.6 \cdot 10^{-16} \text{ cm}^2$ ,  $\eta_{abs-Cy5}$  is 0.10 and  $Q_{Cy5}$  is 0.27 (see paragraph 1.4) this results in:

$$0.126 \cdot 10^{-16} \cdot \frac{P}{E_{photon}}$$

This means for a situation without FRET that the ratio between the photon intensities in the Cy3.5 channel and the Cy5 channel is  $0.162/0.126 = 1.28$ . The total photon intensity in the Cy5 channel will be composed for about 30% of cross talk from Cy3.5 emission and for about 70% of emission from Cy5.

To be able to detect donor and acceptor emission separately the setup is equipped with a 635 nm dichroic beam splitter. Together with the other optical components present in the detection path this results in a detection efficiency of 3.3% in the donor channel and of 5.5% in the acceptor channel. Consequently the detected counts in the donor channel will be about 0.8 times the intensity in the acceptor channel in a situation where no FRET occurs upon excitation with only 568 nm. In a FRET situation the intensity in the acceptor channel will increase at the expense of the intensity in the donor channel. From DNA molecules labeled only with Cy3.5 donor or from which the Cy5 label has bleached, the photon intensity in the acceptor channel will be equal to the expected 20% cross talk. The intensity detected in counts will be about 2.5 times higher in the donor channel than in the acceptor channel. If only the acceptor Cy5 molecule is present a 10 times lower count rate is expected in the acceptor channel upon excitation with 568 nm compared to excitation with the same power at 647 nm.

### 3.1.2 Materials and Methods

#### Construction of 4-way junction DNA

4-way DNA junctions were assembled from one 34-mer 5'-labeled with Cy3.5, one 34-mer 5'-labeled with Cy5 and two unlabeled 34-mers (Isogen Bioscience BV, Maarsen, the Netherlands). The Cy labels have been connected to the DNA by a 7-12 atom carbon-linker. The sequence of the unlabeled 34-mers was: 5'-CCTCCGTCCTAGCAAGGGGCTGCTACCGGAAGGG and 5'-CCCTTCGG TAGCAGCCTGAGCGGTGGTTGAAGG. The Cy3.5-labeled oligo had a 5'-CCGACTGCAGTTGAGTCCTTGCTAGGACGGAGG sequence and the Cy5-labeled oligo a 5'-CCTTCAACCACCGCTCAACTCAACTGCAGTCTGG sequence (8). Equimolar amounts of each 34-mer were hybridized in buffer containing 25 mM HEPES, 100 mM NaCl, pH 7.5, with and without 2 mM MgCl<sub>2</sub>. Hybridization was performed by heating the reaction mixture to 70 °C for 3 min. followed by slow cooling to room temperature over several hours. Formation of 4-way junctions was checked by electrophoresis on an 8% non-denaturing

polyacrylamide gel. The 4-way junction DNA was used without further purification.

### **Visualization of PAA-gel electrophoresis result**

Before staining with ethidium bromide the gel was imaged with a home-built fluorescence gel imager. As a light source a NOVAFLEX fiber optic illuminator (World Precision Instruments) producing white light was used. For selection of a certain wavelength region for excitation, filters were placed in the light path. Behind the excitation filter the light entered the darkroom attached to an UVIKON transilluminator. The gel was positioned on the transilluminator glass plate during illumination. On top of the darkroom emission filters were placed for detection of fluorescence in a particular wavelength region. For detection of Cy3.5 an HQ560/55 excitation filter was used in combination with an HQ620/60 emission filter. For detection of Cy5 an HQ620/60 excitation filter was used in combination with an HQ665LP emission filter. Total DNA was detected after ethidium bromide staining. For this purpose the standard transilluminator configuration was used, with 302 nm excitation and emission detection around 590 nm. All filters were purchased from Chroma Technology Corporation, Brattleboro, VT.

### **Sample preparation for confocal microscopy**

Immobilization of Cy-labeled 4-way DNA junctions was achieved by adsorption. A 10  $\mu$ l volume of 1 M MgCl<sub>2</sub> solution in water was applied to a carefully cleaned 25 mm diameter quartz cover slip. After about 30 s the slide was rinsed with water and dried. For immobilization a 10  $\mu$ l aliquot of a 10<sup>-8</sup> M 4-way junction DNA solution in 25 mM Hepes, pH 7.5, 100 mM NaCl, 2 mM MgCl<sub>2</sub> buffer was applied to the cover slip. After the DNA was allowed to settle for a few minutes the cover slip with DNA was placed upside down on top of a special sample chamber filled with about 1 ml buffer (25 mM Hepes, pH 7.5, 100 mM NaCl, 2 mM MgCl<sub>2</sub>). Immobilization of 4-way junction DNA in the absence of Mg<sup>2+</sup> ions was performed without pretreatment of the cover slip with MgCl<sub>2</sub>. The sample chamber was equipped with an inlet and outlet tube to be able to exchange buffer. By replacing the contents of the chamber for buffer with a different MgCl<sub>2</sub> concentration, measurement conditions could be changed.

### **Scanning confocal fluorescence microscopy**

For confocal measurements on the Cy-labeled 4-way DNA junctions the microscope, described in paragraph 1.4, was used. For FRET measurements excitation was performed with 568 nm only and emission from both fluorophores was detected in two channels simultaneously. For spectral separation of Cy3.5 and Cy5 fluorescence a Q635LP dichroic beam splitter was used. All filters and dichroics were purchased (Chroma Technology Corporation, Brattleboro, VT).

### 3.1.3 Results

#### Preparation of 4-way junction DNA

In Figure 3.1.3. the result is shown of electrophoresis of the 4-way junction preparation on an 8% polyacrylamide gel. From this gel we can conclude that the preparation mainly consists of double-labeled 4-way junction DNA. A minor fraction consists of other products that run faster in the gel. In Figure 3.1.3.B. however there are similar bands present on top of the main oligo band too (lane 1). The appearance is similar to the additional bands in the 4-way junctions (lane 2 and 3). Perhaps some secondary structures occur within the Cy5-labeled 34-mers. The additional bands seem to contain only a Cy5 label (Figure 3.1.3.B), there is no intensity present at the same positions in Figure 3.1.3.C. It is likely that the 4-way junction preparation contains a small excess of Cy5-labeled oligomers. Because of these observations we may expect to observe not purely double-labeled DNA molecules but also a small fraction with only a Cy5 label. From a comparison of the gels in Figure 3.1.3.B, representing the Cy5 label, and Figure 3.1.3.C, representing the Cy3.5 label, we may conclude that only the 4-way junctions will contain both a Cy3.5 and a Cy5 label. There is hardly any difference between the patterns in lane 2 and 3, indicating that the presence or absence of  $Mg^{2+}$  ions does not influence the hybridization of the oligomers. Probably the 100 mM NaCl concentration provides sufficient cations that there is no extra effect of the rather low  $MgCl_2$  conc.

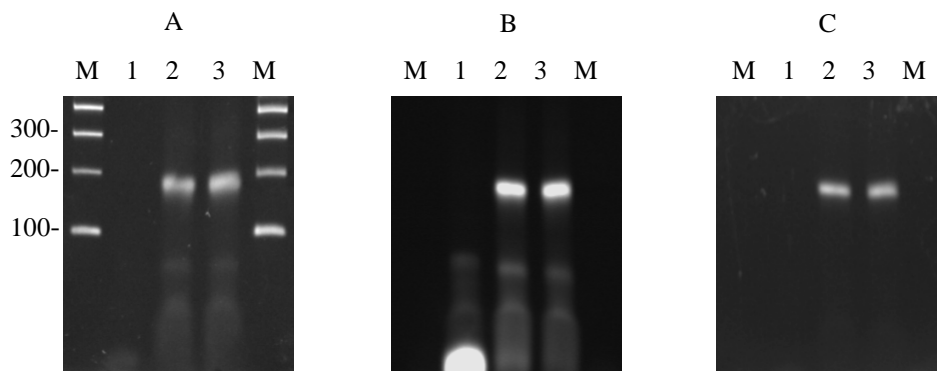


**Fig. 3.1.3.** Result of electrophoresis of 4-way junction preparation. Samples are run on an 8% non-denaturing polyacrylamide gel in 1X TBE buffer (0.09 M Tris-borate, 2 mM EDTA, pH 8.0). Panel A: ethidium bromide stained gel visualizing total DNA; panel B: unstained gel illuminated with red light (590-650 nm) in combination with emission detection at wavelengths longer than 665 nm visualizing the Cy5 label; panel C: unstained gel illuminated with yellow light (533-588 nm) in combination with emission detection at 590-650 nm visualizing the Cy3.5 label. Lane M: 100-bp ds-DNA marker; lane 1: Cy5-labeled 34-mer; lane 2: 4-way junction preparation without 2 mM  $MgCl_2$  and 3: 4-way junction preparation with 2 mM  $MgCl_2$ .

From the electrophoresis result the 4-way junction preparation is considered to be sufficiently pure for the intended purpose, which is the observation of single molecule fluorescence and in particular single molecule FRET.

### Confocal single molecule detection of surface immobilized 4-way junction DNA

In Figure 3.1.4.A simultaneously recorded scanning confocal fluorescence microscopy images are shown from donor and acceptor emission detection upon excitation of Cy3.5 and Cy5 labeled 4-way junction DNA with only 568 nm, which is the wavelength for excitation of the donor Cy3.5 molecule.

In both images spots of individual fluorescent 4-way junction DNA molecules can be recognized. The maximum fluorescence intensities of both images are similar, nevertheless quite large differences in intensities can be observed. At the positions indicated by circles, numbered from 1 to 3, colocalization of intensities can be seen.

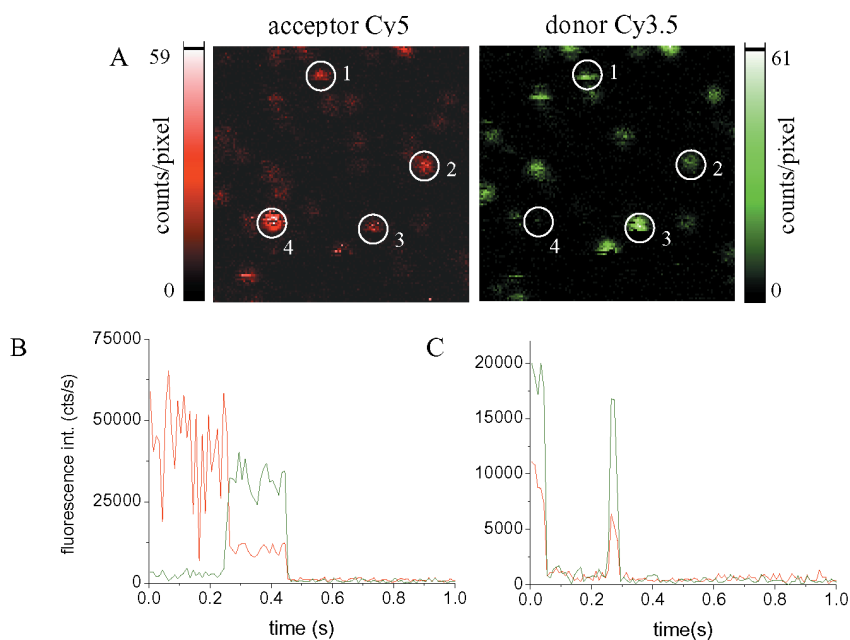


**Fig. 3.1.4.** Scanning confocal results from Cy3.5 and Cy5 labeled DNA molecules in the presence of 2 mM MgCl<sub>2</sub> immobilized on quartz. A. Images recorded simultaneously from emission detection of wavelengths longer than 665 nm (acceptor channel-left) and from detection in the 577-632 nm region (donor channel-right). Image size is 6.2×6.2 μm<sup>2</sup>, 128×128 pixels, dwell time 0.5 ms/pixel, excitation 19 kW.cm<sup>-2</sup> at 568 nm. The circled positions 1-3 indicate colocalized intensities. B. Time trace measured at the position of molecule 4. C. Time trace measured at the position of molecule 2. The signal detected in the Cy5 acceptor channel is indicated in red, the signal in the Cy3.5 donor channel is in green. Data bin time in the time traces is 10 ms.

From one pair of images alone however it is quite difficult to draw a definite conclusion concerning FRET. Successively measured images from the same area may give more information regarding FRET. Still at the position of molecule 4, the intensity in the acceptor channel is much higher than in the donor channel. At this position in the donor channel there is no intensity at all. This is a typical feature that can be expected if energy transfer occurs. To explore the FRET possibility in more detail a time trace was measured at the position of molecule 4. The time trace was registered simultaneously in the donor and acceptor detection channel. In the time trace represented in Figure 3.1.4.B the fluorescence behavior of molecule 4 can be observed. In Figure 3.1.4.C a time trace is shown measured at the position of molecule 2.

### **FRET time traces**

The time trace in Figure 3.1.4.B clearly demonstrates single molecule FRET as already predicted from the images in Figure 3.1.4.A. In a situation without FRET we would expect to detect in the donor channel about  $7.3 \times 10^4$  counts/s and in the acceptor channel about  $9.4 \times 10^4$  at the applied 568 nm excitation power. The first part of the time trace, a time period of 0.26 s, shows emission from the Cy5 acceptor only. During the same period there is hardly any intensity in the Cy3.5 donor channel. After 0.26 s there is a sudden drop in acceptor emission intensity accompanied by an abrupt increase in donor emission. It is highly probable that the drop in acceptor emission intensity is caused by bleaching of the Cy5 acceptor molecule. At the moment that the acceptor bleaches, no energy transfer occurs anymore from the Cy3.5 donor to the Cy5 acceptor. Because the donor is not yet bleached, normal emission of Cy3.5 is restored. Apparently some intensity remains in the acceptor channel indicating the cross talk from Cy3.5 emission into the red detection channel. The ratio between the fluorescence intensity in the donor and acceptor channel is a factor of three, indicating that the signal in the acceptor channel indeed comes from cross talk. After about 0.45 s also the Cy3.5 donor bleaches. The appearance of this particular time trace suggests that the observed energy transfer emerges from a statically arranged donor and acceptor pair. During the time of energy transfer the intensity level is rather constant. In case of dynamic changes within the molecule, different levels of energy transfer are supposed to show up.

The time trace represented in Figure 3.1.4.C is an example of the fluorescence behavior of a DNA molecule containing only an emitting Cy3.5 molecule. The intensity detected in the Cy3.5 channel is 2 to 3 times higher than in the Cy5 channel, indicating only signal from cross talk in the Cy5 channel. The alternating on and off periods are a representation of the blinking of this particular Cy3.5 molecule.



The fluorescence behavior of the Cy3.5 donor and Cy5 acceptor pair represented by the time trace of Figure 3.1.4.B was examined in more detail by binning the measured data with a smaller time bin. In Figure 3.1.5.A the same time trace as in Figure 3.1.4.A is shown after binning the data with a time bin of only 1 ms. It is obvious that strong fluctuations in fluorescence intensity become visible now, which were averaged out at a larger data bin.

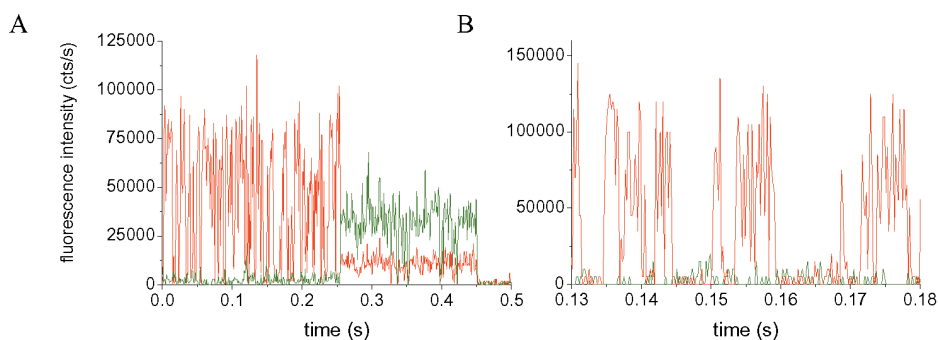


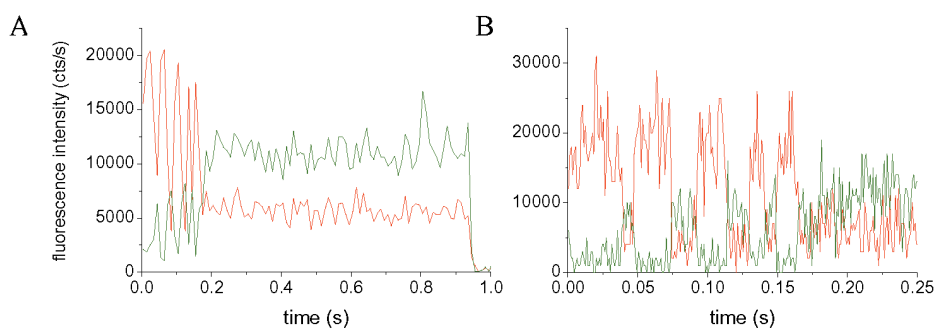
**Fig. 3.1.5.** Time trace of a single Cy3.5 and Cy5 double-labeled 4-way junction DNA molecule adhered to quartz, in the presence of 2 mM  $MgCl_2$ , displaying FRET, represented with different data bin times. A. Time traces represented with a data bin of 1 ms. B. Time interval from 0.13 to 0.18 s represented with a data bin of 0.2 ms. The signal detected in the Cy5 acceptor channel is in red, the signal in the Cy3.5 donor channel is in green. Excitation intensity was  $19 \text{ kW}\cdot\text{cm}^{-2}$  with a wavelength of 568 nm.

During the period that energy transfer occurs, the first 0.255 s of the time trace, several dark periods can be observed in the acceptor fluorescence. It is remarkable that these dark periods of the acceptor are not accompanied by an increased emission of the donor molecule. This phenomenon is even more clearly demonstrated by Figure 3.1.5.B which gives a more detailed view of the 0.13 to 0.18 s time interval after binning of the data with a 0.2 ms time bin. If conformational changes in the DNA molecule would be the reason for a decrease in acceptor fluorescence, then a simultaneous increase in donor emission would be expected. The absence of increased signal in the donor detection channel means that we have to do with another process here. It seems that the Cy5 molecules temporarily jump into a dark state in which they still can function as acceptor molecules. With respect to Cy5 two processes are known that may result in non-emitting molecules. These processes are singlet-triplet transition and trans-cis isomerization (see also paragraph 1.2). Singlet-triplet state transitions are unlikely, because they are supposed to occur at excitation intensities higher than applied in our measurements (10). Possibly at our excitation conditions Cy5 stays in a non-emissive state because of a trans-cis isomerization process. Only in the trans state Cy5 molecules are fluorescent, in the cis state fluorescence is hardly detected (11). It has been reported that Cy5 molecules in their cis state still work as acceptor dye molecules, owing to the close overlap of the absorption spectra of

the trans and cis isomers (11). Practically no fluorescence is however expected to be generated following energy transfer to the cis-state of Cy5. The assumption that Cy5 cis-states occur explains the absence of intensity from the donor during dark periods of the acceptor as represented in the fluorescence profiles of Figure 3.1.5. A and B.

Figure 3.1.5.A demonstrates that also during emission of Cy3.5 dark periods occur. It is evident that dark periods of Cy3.5 will not be accompanied by increased emission of Cy5, because Cy5 already bleached at an earlier moment.

In contrast to the above mentioned fluorescence behavior, where only one period of energy transfer is shown, we also observed molecules exhibiting several periods of FRET of different duration (Figure 3.1.6).



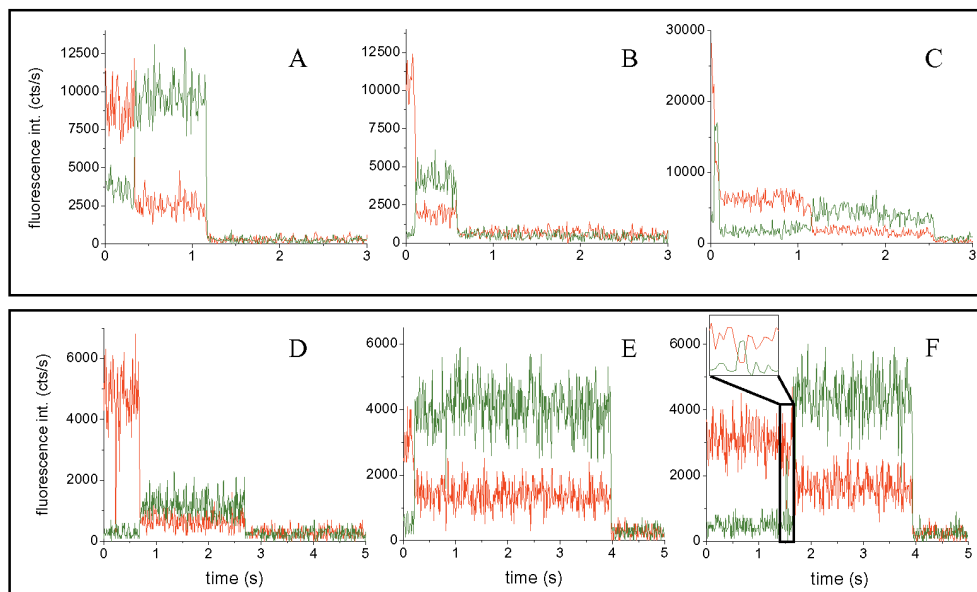
**Fig. 3.1.6.** Time traces of a single Cy3.5 and Cy5 double-labeled DNA molecule adhered to quartz, in the absence of  $\text{MgCl}_2$ , displaying FRET, represented with different data bin times. A. Time trace represented with a data bin of 10 ms. B. Time interval from 0 to 0.25 s represented with a data bin of 1 ms. The signal detected in the Cy5 acceptor channel is indicated in red, the signal in the Cy3.5 donor channel is in green. Excitation intensity was  $1.9 \text{ kW}\cdot\text{cm}^{-2}$  with a wavelength of 568 nm.

Figure 3.1.6.A shows a time trace with 5 periods of fluctuating FRET intensities measured on a DNA sample without  $\text{MgCl}_2$  present. Here a drop in acceptor emission is accompanied by an increase in donor emission. In Figure 3.1.6.B, where the same time trace is shown with a smaller data bin, this effect is even more clearly demonstrated. Provided that the surface adsorbed DNA molecules still have some motional freedom, conformational changes within the DNA molecule may be responsible for the changes in FRET efficiency.

It is not likely that differences in measurement conditions are responsible for the difference in appearance of the time traces of Figure 3.1.5 and Figure 3.1.6. The conditions were only different in  $\text{MgCl}_2$  concentration and the applied excitation intensity. In the absence of Mg the probability to observe energy transfer may be lower than with Mg present. However the observation of FRET in both situations

demonstrates that Mg is not absolutely required for energy transfer to occur. The 100 mM NaCl present in the DNA preparation may already provide sufficient cations to bring the DNA in such a conformation that FRET is possible. From a single molecule FRET study on conformational changes of immobilized RNA molecules it was shown that NaCl, if present at a 2,500 times higher concentration, can induce the same effect as MgCl<sub>2</sub> (12). Presumably also the difference in excitation power is not such that big differences in fluorophore characteristics should be expected. At intensities lower than 10 kW.cm<sup>-2</sup>, at 647 nm, mainly isomerization of Cy5 is supposed to occur and hardly any triplet formation (10). At excitation wavelengths other than 647 nm, where excitation is less efficient, similar isomerization properties were observed. Under FRET mediated excitation, the population of cis-isomers was found to be lower than under direct excitation of the Cy5 acceptor molecules. Nevertheless the loss of acceptor fluorescence due to non-fluorescent, but still FRET-active, cis-states was considerable. If we take into account the lower excitation efficiency of Cy5 at 568 nm, both the excitation powers used in the measurements of Figure 3.1.5 and Figure 3.1.6, correspond to 647 nm excitation powers lower than 10 kW.cm<sup>-2</sup>. The time traces shown in Figure 3.1.5 and Figure 3.1.6 should only be considered as examples of FRET, displaying different features. Probably the applied DNA deposition method results in a variety of DNA conformations at the surface. Differences in electrostatic interactions between the negatively charged Cy dyes, the DNA and the quartz surface within a particular buffer environment may result in different dipole orientations and distances between donor and acceptor. Because of the different conformations the donor and acceptor molecules may exhibit different FRET characteristics.

In Figure 3.1.7 several single molecule time traces have been collected that display different FRET characteristics at different measurement conditions. The purpose of this figure is to give an impression of the various observations that are obtained with the particular DNA preparation that we used. The time traces shown in the upper panel of Figure 3.1.7 are examples of possible observations within an environment of 2 mM MgCl<sub>2</sub>. The traces in Figure 3.1.7.A and B have been measured on the same sample at exactly the same conditions. Still the differences are remarkable. Where the initial intensity in the acceptor channel is higher in Figure 3.1.7.B, the accompanying intensity in the donor channel is lower than in Figure 3.1.7.A. Probably on the DNA molecule measured in Figure 3.1.7.B, the orientation of the Cy3.5 donor and Cy5 acceptor molecule as well as their distance are in favor of more efficient FRET.

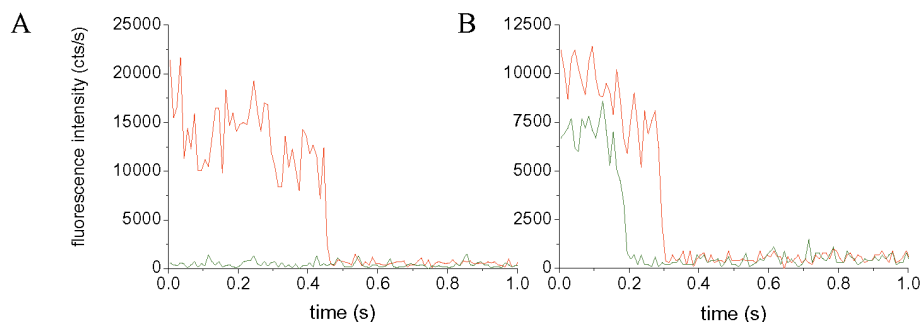


**Fig. 3.1.7.** Collection of FRET displaying time traces of individual Cy3.5 and Cy5 labeled DNA molecules immobilized on quartz obtained at different measurement conditions. Upper panel: with 2 mM MgCl<sub>2</sub>. A and B, 568 nm excitation intensity 1.9 kW.cm<sup>-2</sup>; C, 3.6 kW.cm<sup>-2</sup>. Lower panel: 0.9 kW.cm<sup>-2</sup>. D, 2 mM MgCl<sub>2</sub>; E, 5 mM MgCl<sub>2</sub>; F, 10 mM MgCl<sub>2</sub>. The inset in F is an enlarged view of the 1.45 to 1.62 s time interval. The signal detected in the Cy5 acceptor channel is indicated in red, the signal in the Cy3.5 donor channel is in green. Data bin in all time traces is 10 ms.

After acceptor bleaching the donor intensity in Figure 3.1.7.A is much higher than in Figure 3.1.7.B. Again the dipole orientation of Cy3.5 may determine the level of the emission intensity. The fluorescence behavior shown in Figure 3.1.7.C may be a reflection of a fast conformational change within the measured DNA molecule succeeded by a much slower change. It is less probable that dark states are responsible for the typical profile observed because of multiple steps with coupled donor and acceptor behavior.

In the lower panel of Figure 3.1.7 examples are shown of measurements on DNA molecules at one excitation power but at different Mg concentrations. Here once more a variety of fluorescence behaviors can be observed. Different intensity levels for donor as well as for acceptor fluorescence and different photobleaching times can be noticed. The inset in Figure 3.1.7.F accentuates a short-lived coupled intensity fluctuation in the donor and acceptor channel. Possibly this fluctuation is caused by a conformational change within the DNA molecule.

In Figure 3.1.8 examples are shown from other fluorescence characteristics possible to observe from single molecules within this particular DNA sample.



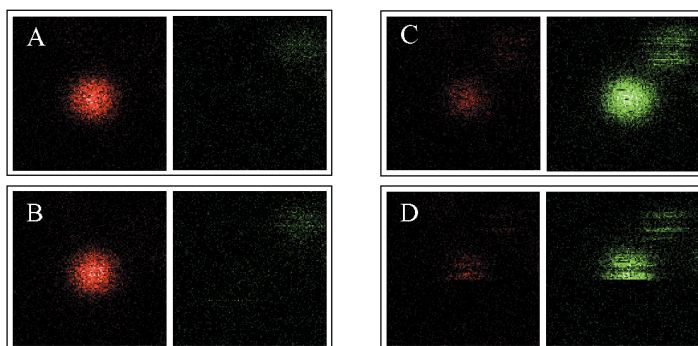
**Fig. 3.1.8.** Time traces of individual Cy labeled DNA molecules adhered to quartz in the presence of 2 mM  $MgCl_2$ . A. Time traces of a DNA molecule showing only fluorescence from Cy5. B. Time trace from a DNA molecule showing fluorescence from colocalized Cy3.5 and Cy5 without energy transfer. The signal detected in the Cy5 acceptor channel is indicated in red, the signal in the Cy3.5 donor channel is in green. Excitation was  $19 \text{ kW.cm}^{-2}$  with a wavelength of 568 nm. Data bin is 10 ms.

Figure 3.1.8.A shows the fluorescence emission pattern of only a Cy5 molecule upon excitation with a wavelength of 568 nm. There is no intensity present in the Cy3.5 detection channel. In relation with the gel electrophoresis result this probably indicates the fluorescence detected from a single Cy5 labeled oligomer. There also is a small chance that the DNA molecule contains an additional Cy3.5 labeled strand, from which the label was bleached already. The expected maximum fluorescence intensity of Cy5 at the applied  $19 \text{ kW.cm}^{-2}$  excitation at 568 nm, would be around  $6.4 \times 10^4$  counts/s. Here we only measure around  $1.5 \times 10^4$  counts/s. The lower intensity may be caused by the instability of the fluorescence of Cy5 molecules as already mentioned in paragraph 2.2.2. Figure 3.1.8.B shows intensity profiles for colocalized Cy3.5 and Cy5 molecules when no energy transfer takes place. During the 0.185 s period that both molecules are emitting, the average intensity in the Cy3.5 detection channel is about 0.75 times the intensity in the Cy5 channel. This is quite close to the expected ratio of 0.8, as mentioned before.

### FRET images

FRET was also observed in successively measured images. The images in Figure 3.1.9 illustrate clearly the FRET effect between a Cy3.5 donor molecule and a Cy5 acceptor molecule. Although excitation was performed only with 568 nm for excitation of Cy3.5, the first two sets of images only show emission from Cy5 (panel A and B). In the third panel (C), suddenly quite high intensity appears in the Cy3.5 detection channel while the intensity in the Cy5 detection channel almost disappeared. This indicates that during registration of the images in panel A and B fluorescence resonance energy transfer occurred from Cy3.5 to Cy5. Then apparently the fluorescence from the Cy5 molecule stopped because of

bleaching, resulting in emission from Cy3.5. Some low intensity remains in the Cy5 detection channel because of cross talk from Cy3.5 emission into this channel. During scanning of the next image pair (panel D) also the Cy3.5 molecule bleaches. Only part of the fluorescence spot is visible. In both images of panel D the intensity disappears at the same moment, which confirms that the intensity in the acceptor channel comes from cross talk.



**Fig. 3.1.9.** Scanning confocal images of Cy3.5 and Cy5 labeled DNA molecules adhered to quartz in the presence of 2 mM MgCl<sub>2</sub>. Four image pairs measured successively from the same area. Images are recorded simultaneously from emission detection of wavelengths longer than 665 nm (acceptor channel-red) and from detection in the 577-632 nm region (donor channel-green). Image size is 1.5×1.5 μm<sup>2</sup>, 128×128 pixels, dwell time 0.5 ms/pixel, excitation 1.9 kW.cm<sup>-2</sup> at 568 nm. All images are scaled on a maximum intensity of 17 counts.

### Estimation of energy transfer efficiency

From the time traces observed at different Mg concentrations and without Mg present it was not immediately clear if there is a relation between the observed degree of energy transfer and Mg concentration. Therefore we estimated the energy transfer efficiency (E) at different measurement conditions. The estimation method was according to Brasselet et al. (13):

$$E = \frac{1}{1 + \frac{Q_A}{Q_D} \cdot \frac{D}{\left[ \frac{I_A}{I_D} - L \right]}} \quad (3.1)$$

Where  $D$  is the ratio between the detection efficiencies of the acceptor and donor channels, which was estimated to be 1.67 accounting for the emission filters and dichroic beam splitter used in the confocal experiment.  $I_A$  and  $I_D$  are the time averages of the means of the acceptor and donor signals before a bleaching event,  $I_A$  being the intensity of the acceptor measured at wavelengths longer than 665 nm

and  $I_D$  the intensity of the donor measured in the 577 to 632 nm region.  $L$  is the proportion of the donor signal  $I_D$  (photons) leaking into the acceptor channel (0.20) as determined from donor only time traces.  $Q_A$  and  $Q_D$  are the quantum yields of the donor and acceptor, 0.15 and 0.27 respectively. We analyzed several time traces measured at Mg concentrations of 2, 5 and 10 mM and also without Mg present.

The number of measurements was not sufficiently high to draw definite conclusions about a possible dependence of the energy transfer efficiency on Mg concentration. The average estimated energy transfer efficiencies at each Mg concentration were between 0.7 and 0.8. The overall distribution of observed energy transfer efficiencies is given in Figure 3.1.10.

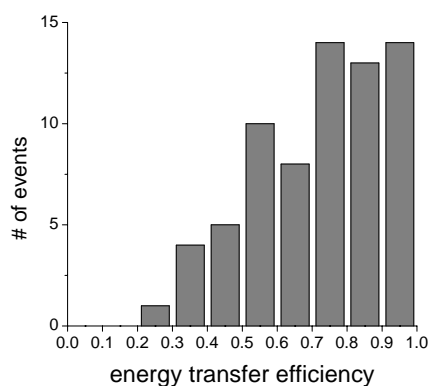


**Fig. 3.1.10.** Histogram of estimated energy transfer efficiencies between Cy3.5 donor and Cy5 acceptor present on surface immobilized DNA molecules. Results were combined from measurements in buffer containing 0, 2, 5 and 10 mM  $MgCl_2$ . In total 69 time traces were analyzed resulting in an average energy transfer efficiency of  $0.73 \pm 0.19$ .

The average energy transfer efficiency determined was  $0.73 \pm 0.19$  ( $N = 69$ ). The reason that we did not observe a significant difference in energy transfer at different Mg concentrations may lie in the presence of 100 mM NaCl in each sample. The NaCl concentration may be high enough to provide sufficient cations to bring the DNA in a FRET conformation. Even in the absence of Mg the observed energy transfer efficiencies were within the same range as with Mg present. This excludes an effect of the brief pretreatment of the quartz surface with 1 M  $MgCl_2$ , which was omitted in the measurements without Mg.

If we ignore dipole orientations, then the energy transfer efficiency ( $E$ ) is directly related to the distance between the donor and acceptor ( $R$ ). The relation, as mentioned in paragraph 1.2- equation 1.1 is (14):

$$E = \frac{1}{\left[1 + \left(\frac{R^6}{R_0^6}\right)\right]}$$

If we assume an  $R_0$  of 5.58 nm (is  $R_0$  for Cy3/Cy5 combination, for Cy3.5/Cy5  $R_0$  has not been determined yet), then the average transfer efficiency of 0.73 would correspond to a distance of 4.7 nm between Cy3.5 and Cy5. This would mean for 4-way junction DNA that the DNA is in a stacked conformation with an angle of about  $50^\circ$  between the Cy3.5 labeled arm and Cy5 labeled arm.

With an  $R_0$  of 5.58 nm, an energy transfer efficiency of 0.1 still can be expected from a planar DNA conformation, where the maximum distance between Cy3.5 and Cy5 is about 8 nm. If however  $R_0$  is larger, which is likely because of the larger overlap between the emission spectrum of Cy3.5 and the absorption spectrum of Cy5 than in case of a Cy3 and Cy5 combination, then in a planar conformation an energy transfer efficiency will be expected of 0.22. With a larger  $R_0$  also the distance corresponding to an energy transfer efficiency of 0.73 will be larger.

### 3.1.4 Discussion and Conclusions

In paragraph 3.1.3 we have shown different observations with confocal fluorescence microscopy from individual, surface immobilized, fluorescent DNA molecules. Fluorescence from single as well as double-labeled DNA molecules was detected with expected count rates. From molecules double labeled with Cy3.5 and Cy5 the fluorescence was detected simultaneously resulting in images containing colocalized fluorescence intensities. Besides colocalization we also observed fluorescence resonance energy transfer between the Cy3.5 donor molecule and Cy5 acceptor molecule. From the level of energy transfer observed it appears that the 4-way junction DNA is rather in a stacked than in a planar conformation at our measurement conditions. We can conclude that the Cy3.5/Cy5 donor-acceptor pair is very well suited for FRET studies. The results are promising in view of XPA protein binding to the 4-way junction DNA substrate. By using the Cy3.5/Cy5 pair indeed DNA conformational changes caused by XPA binding may be revealed from FRET analysis.



### 3.1.5 References

1. Busch, K., and Tampé, R. (2001) Single molecule research on surfaces: from analytics to construction and back. *Rev. Mol. Biotech.*, **82**, 3-24
2. Peterman, E.J.G., Brasselet, S., and Moerner, W.E. (1999) The fluorescence dynamics of single molecules of green fluorescent protein. *J. Phys. Chem. A*, **103**, 10553-1056
3. Brasselet, S., Peterman, E.J.G., Miyawaki, A., and Moerner, W.E. (2000) Single-molecule fluorescence resonant energy transfer in calcium concentration dependent cameleon. *J. Phys. Chem B*, **104**, 3676-3682
4. Kubitscheck, U., Kückmann, O., Kues, T., and Peters, R. (2000) Imaging and tracking of single GFP molecules in solution. *Biophys. J.*, **78**, 2170-2179
5. Moerner, W.E., Peterman, E.J.G., Brasselet, S., Kummer, S., and Dickson, R.M. (1999) Optical methods for exploring dynamics of single copies of green fluorescent protein. *Cytometry*, **36**, 232-238
6. Duckett, D.R., Murchie, A.I.H., Diekmann, S., von Kitzing E., Kemper, B., and Lilley, D.M.J. (1988) The structure of the Holliday junction and its resolution. *Cell*, **55**, 79-89
7. Clegg, R.M., Murchie, A.I.H., Zechel, A., Carlberg, C., Diekmann, S., and Lilley, D.M.J. (1992) Fluorescence resonance energy transfer analysis of the structure of the four-way DNA junction. *Biochemistry*, **31**, 4846-4856
8. Clegg, R.M., Murchie, A.I.H., and Lilley, D.M.J. (1994) The solution structure of the four-way DNA junction at low-salt conditions: a fluorescence resonance energy transfer analysis. *Biophys. J.*, **66**, 99-109
9. Missura, M., Buterin, T., Hindges, R., Hübscher, U., Kaspárková, J., Brabec, V., and Naegeli, H. (2001) Double-check probing of DNA bending and unwinding by XPA-RPA: an architectural function in DNA repair. *EMBO J.*, **20**, 2001
10. Widengren, J., Schweinberger, E., Berger, S., and Seidel, C.A.M. (2001) Two new concepts to measure fluorescence resonance energy transfer via fluorescence correlation spectroscopy: theory and experimental realization. *J. Phys. Chem.*, **105**, 6851-6866
11. Widengren, J., and Schwille, P. (2000) Characterization of photoinduced isomerization and back-isomerization of the cyanine dye Cy5 by fluorescence correlation spectroscopy. *J. Phys. Chem.*, **104**, 6416-6428
12. Kim, H.D., Nienhaus, G.U., Ha, T., Orr, J.W., Williamson, J.R., and Chu, S. (2002) Mg<sup>2+</sup>-dependent conformational change of RNA studied by fluorescence correlation and FRET on immobilized single molecules. *Proc. Natl. Acad. Sci. USA*, **99**, 4284-4289
13. Brasselet, S., Peterman, E.J.G., Miyawaki, A., and Moerner, W.E. (2000) Single-molecule fluorescence resonant energy transfer in calcium concentration dependent cameleon. *J. Phys. Chem B*, **104**, 3676-3682
14. Lakowicz, J.R. (1999) *Principles of fluorescence spectroscopy*. Kluwer Academic/Plenum, New York

## **3.2 Diffusion of DNA in an agarose matrix**

In this paragraph results are shown from confocal fluorescence microscopic examination of the diffusional behavior of different types of 5'-Cy3.5 labeled DNA within a 1% resp. 4% agarose gel. Because of their involvement in DNA-protein binding studies we included the following types of DNA in the diffusion experiments: single strand 90-nt DNA, 4-way junction DNA with arms of 17-bp (see paragraph 3.1.1), double strand 90-bp DNA and 90-bp bubble-DNA, containing a central 30-bp unpaired region. To get a more complete impression of DNA diffusion within agarose we also investigated the diffusion of two longer double strand types of DNA, a double strand 145-bp and a 1500-bp DNA.

### **3.2.1 Materials and Methods**

#### **DNA**

5'-Cy3.5 labeled 90-nt single strand DNA oligomers were purchased (DNA Technology A/S, Aarhus, Denmark). Cy3.5 is coupled to the 5'OH of the last nucleotide via a 3-carbon linker.

Bubble DNA was prepared as described in paragraph 4.2.

Double-strand 90-bp DNA was prepared in the same way as the bubble-DNA from a pair of complementary 90-nt oligomers. One of the oligomers had a 5'-Cy3.5 label (DNA Technology A/S, Aarhus, Denmark). The sequence of the unlabeled strand was the same as in the bubble-DNA. Formation of ds-DNA was checked by electrophoresis in 8% PAA gel. The ds-DNA was used without further purification.

5'-Cy3.5 labeled double-strand 145-bp and 1500-bp DNA were prepared by PCR from pUC19 template DNA (New England Biolabs, Beverly, MA, USA) by using a 5'-Cy3.5 labeled primer together with an unlabeled primer (Biozym, Landgraaf, the Netherlands). The PCR products were purified from primers with a Chromaspin-100 column (Clontech, Palo Alto, CA, USA).

4-Way junction DNA was prepared as described in paragraph 3.1.2.

#### **Visualization of PAA-gel electrophoresis result**

Before staining with ethidium bromide the gel was imaged with a fluorescence gel imager as described in paragraph 3.1.2. For detection of Cy3.5 an HQ560/55 excitation filter was used in combination with an HQ620/60 emission filter. Total DNA was detected after ethidium bromide staining.

### Sample preparation for confocal microscopy

For confocal measurements the DNA was diluted to concentrations of approximately  $2 \times 10^{-9}$  M in molten low melt agarose, 1% (w/v) or 4% (w/v), in 25 mM Hepes, 40 mM KCl, 60 mM NaCl, 10 mM MgCl<sub>2</sub>, pH 7.4 at 30° C. The DNA-agarose mixture was sandwiched between two 25 mm quartz cover slips.

### Scanning confocal fluorescence microscopy

For measurements on the Cy3.5-labeled DNA preparations the confocal microscope, described in paragraph 1.4, was used. For detection of Cy3.5 a 565EFLP emission filter (Omega Optical, Brattleboro, VT) was used.

### Diffusion analysis from time traces

For the purpose of quantitative analysis of diffusion, 60 s time traces were recorded with an integration time of 100 μs at 10 different positions within the sample. Normalized autocorrelation curves of measured time traces were determined with the MINITAB software package (MINITAB Ltd., Coventry, UK). In this procedure  $N$  observations are considered in a time series at uniform sampling time  $\Delta_t$ . Observation time  $t_k = k \cdot \Delta_t$  and the total duration of the time series is  $N \cdot \Delta_t$ . Time lag  $\tau$  is defined as  $m \cdot \Delta_t$ . The autocorrelation coefficient at lag  $m$  is now defined as:

$$G_m = \frac{\sum_{k=1}^{N-m} (F(k) - \langle F \rangle) \cdot (F(k+m) - \langle F \rangle)}{\sum_{k=1}^{N-m} (F(k) - \langle F \rangle)^2} \quad (3.2)$$

In equation 3.2  $F(k)$  is the fluorescence intensity at  $t_k$ ,  $\langle F \rangle$  is the average fluorescence intensity over  $N \cdot \Delta_t$  time intervals,  $F(k+m)$  is the fluorescence intensity at lag  $m$  with respect to  $t_k$ .

Diffusion coefficients were determined by non-linear least squares fitting (Origin software, Microcal Inc., Northampton, MA, USA) of the theoretical autocorrelation function to the experimental data for one freely diffusing fluorescent species in three dimensions, according to (1, 2):

$$G(\tau) = \left[ \frac{1}{V_{eff} \cdot \langle C \rangle} \cdot \frac{1}{\left(1 + \frac{\tau}{\tau_D}\right)} \cdot \frac{1}{\sqrt{1 + \frac{\tau}{\tau_D} \cdot \left(\frac{r_0}{z_0}\right)}} \right] + c \quad (3.3)$$

In equation 3.3  $V_{eff}$  is the probe volume described by a Gaussian distribution in three dimensions, with a waist radius of  $r_0$  in the lateral direction and  $z_0$  the half length in the axial direction at an intensity of  $1/e^2$ . In this case  $V_{eff}$  is equal to  $\pi^{3/2} \cdot r_0^2 \cdot z_0^2$ . For our confocal setup we determined  $r_0$  to be  $0.2 \mu\text{m}$  and  $z_0$   $1.34 \mu\text{m}$ . If only translational diffusion is assumed, the autocorrelation curve as calculated from equation 3.2 can be fitted to equation 3.3 using  $r_0$  and  $z_0$  as fixed parameters and the average particle number in the focal volume  $\langle N \rangle$  and  $\tau_D$  as free parameters. Sometimes the inclusion of a certain background value  $c$ , as a free parameter, improves the fitting results.

From the obtained value of  $\tau_D$  the corresponding diffusion coefficient  $D$  is calculated according to:

$$D = \frac{r_0^2}{4 \cdot \tau_D} \quad (3.4)$$

### Expected observations

To illustrate the image acquisition procedure and the predicted scanning confocal result from a diffusing fluorescent molecule a schematic drawing is shown in Figure 3.2.1. This figure demonstrates that diffusing fluorescently labeled molecules give rise to a stripy pattern in confocal images obtained by scanning. During scanning, by moving the sample through the focus, photons emitted by molecules present in the confocal volume, are detected. As long as a diffusing fluorescent molecule stays within the focus it will give rise to a row of bright pixels. If a molecule, present in the focus, keeps on moving in the scan direction with the same velocity as the speed of scanning, this will result in a long bright stripe in the image. A molecule that crosses the focus in a direction perpendicular to the scan direction will result in a smaller number of bright pixels. The intensity of the stripe reflects the position of the molecule within the focus. In Figure 3.2.1.C expected images are represented for two different diffusion rates. It shows that shorter stripes appear when the diffusion is faster. Although only diffusion in one plane is considered it gives a valid representation also for three-dimensional diffusion. If diffusion in the third dimension is taken into account only the intensity distribution along the lines as well as the length of the lines will be different. Still the stripy pattern will remain.

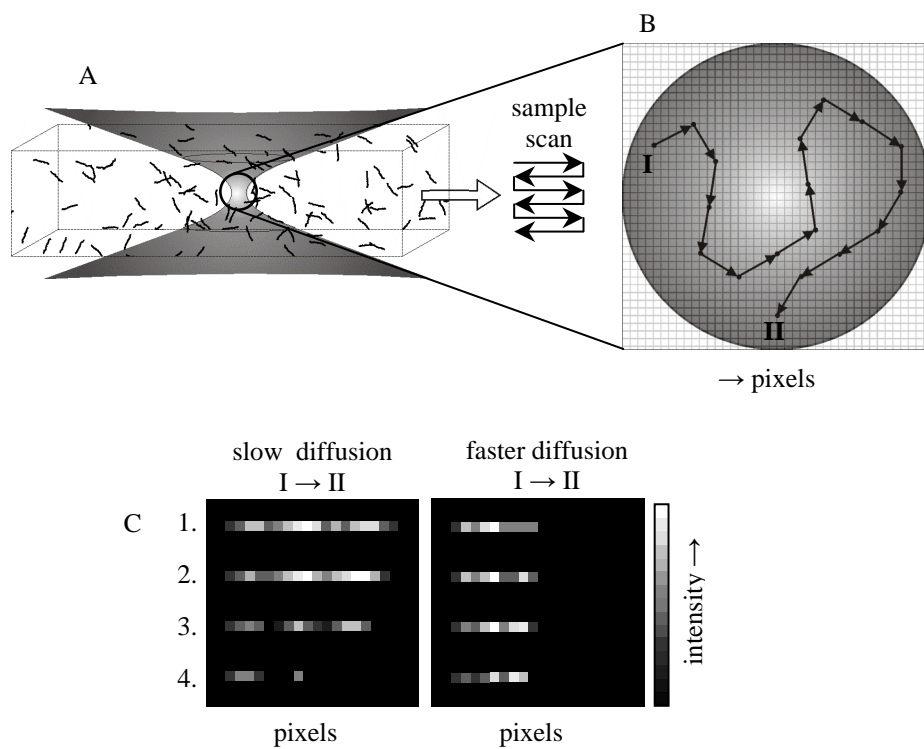


**Fig.3.2.1.** Schematic representation of predicted scanning confocal imaging result of diffusing molecules. In A the position of the focus is shown within the sample. During scanning of the sample diffusing fluorescent molecules pass through the focus. In B an enlarged view is shown of the focus with one diffusing molecule. Arrow segments indicate the path of the hypothetical diffusion track running from I to II. For convenience only diffusion in one plane is shown. The appearance of scanning confocal images depends on the diffusion rate in combination with a certain scan speed. In C examples of possible results are shown with 4 different scan speeds and two different diffusion rates. Left panel: diffusion rate equal to one arrow distance per time unit ( $\Delta_t$ ). Right panel: diffusion rate equal to two arrow distances per  $\Delta_t$ . Lane 1, scan speed  $0.5 \text{ pixel}/\Delta_t$ ; lane 2, scan speed  $1 \text{ pixel}/\Delta_t$ ; lane 3, scan speed  $2 \text{ pixels}/\Delta_t$ ; lane 4, scan speed  $3 \text{ pixels}/\Delta_t$ .

## 3.2.2 Results

### Preparation of DNA samples

In Figure 3.2.2.A and B the result is shown of electrophoresis of the annealing products for preparation of the 90-bp double strand DNA and bubble-DNA on an 8% polyacrylamide gel.

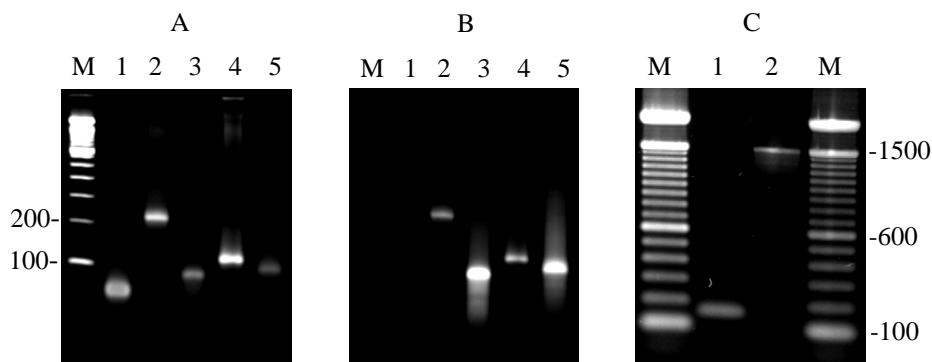


**Fig.3.2.2.** Result of electrophoresis of DNA preparations. Panel A and B: 90-bp double strand and bubble DNA preparations. Samples are run on an 8% non-denaturing polyacrylamide gel in 1X TBE buffer (0.09 M Tris-borate, 2 mM EDTA, pH 8.0). A: ethidium bromide stained gel visualizing total DNA; B: unstained gel illuminated with yellow light (533-588 nm) in combination with emission detection at 590-650 nm visualizing the Cy3.5 label. Lane M: 100-bp ds-DNA marker; lane 1: unlabeled 90-mer; lane 2: Cy3.5-bubble-DNA; lane 3: Cy3.5 labeled 90-mer used to prepare ds-90-bp DNA; lane 4: Cy3.5-ds-90-bp DNA; lane 5: Cy3.5 labeled 90-mer used to prepare bubble-DNA. Panel C: 145-bp and 1500-bp PCR products. Samples were run on a 1% agarose gel in 1X TAE buffer (0.04 M Tris-acetate, 1 mM EDTA, pH 8.0). Lane M: 100-bp ds-DNA marker; lane 1: Cy3.5-145-bp-DNA; lane 2: Cy3.5-1500-bp DNA.

From this gel we can conclude that the preparations mainly consist of the desired products. In these figures we can clearly observe a difference in mobility in the gel during electrophoresis between the bubble-DNA (lane 2) and the ds-90-bp analogue (lane 4). We may expect that the bubble-DNA stays behind the ds-DNA because of conformational differences. It is conceivable that the bubble-DNA has a more kinked structure than the double strand DNA, resulting in a slower migration rate in the gel. In Figure 3.2.2.C the electrophoresis result is shown of the 145-bp and 1500-bp PCR products. Both products appear in the gel as one band at their expected positions. From the electrophoresis results the DNA preparations are considered to be sufficiently pure for the purpose of studying their diffusion within agarose gels.

### Confocal imaging of diffusing DNA molecules within agarose gels

Figure 3.2.3 gives an impression of the appearance of confocal images scanned from Cy3.5 labeled double-strand 90-bp DNA within a 1% agarose (A) and a 4% agarose (B) environment. For comparison in Figure 3.2.3.C an image is shown obtained from Cy3.5 labeled DNA molecules immobilized on quartz. The single molecule spots with a two-dimensional Gaussian intensity distribution represent the intensity profile of the diffraction-limited focus.

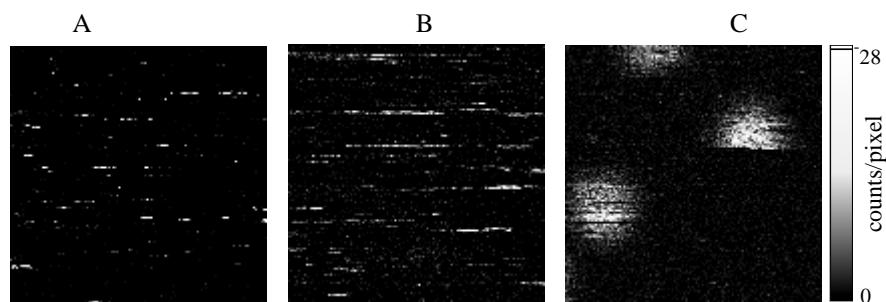


**Fig. 3.2.3.** Scanning confocal images of Cy3.5 labeled DNA. A. Double-strand Cy3.5-90-bp DNA in 1% agarose. B. Double-strand Cy3.5-90-bp DNA in 4% agarose. Image size is  $1.5 \times 1.5 \mu\text{m}^2$ ,  $128 \times 128$  pixels, dwell time 0.25 ms/pixel, excitation  $19 \text{ kW}\cdot\text{cm}^{-2}$  at 568 nm. Emission was detected at wavelengths longer than 565 nm by using a 565 nm long pass filter. C. Single-strand Cy3.5-90-nt DNA adsorbed to quartz. Image size is  $1.5 \times 1.5 \mu\text{m}^2$ ,  $128 \times 128$  pixels, dwell time 0.5 ms/pixel, excitation  $5 \text{ kW}\cdot\text{cm}^{-2}$  at 568 nm. Emission was detected at wavelengths from 577-632 nm by using a 605/55 nm band pass filter. All three images are scaled on a maximum of 28 counts/pixel.

In Figure 3.2.3.A and B we indeed can observe that Cy3.5 labeled double-strand DNA molecules, diffusing in agarose gels, give rise to a stripy pattern in confocal images during scanning. The shorter average length of the bright lines in the image obtained from DNA in 1% agarose (A) than in 4% agarose (B) is in correspondence with expected faster diffusion in a lower density medium. This result is in agreement with Figure 3.2.2.C where the right panel represents diffusion twice as fast as in the left panel. Here also faster diffusion results in shorter stripes. Also in a 4% agarose gel the DNA molecules have not been trapped within the pores of the gel.

### Diffusion analysis from time traces

For the purpose of quantitative determination of diffusion rates of different DNA molecules within agarose gels time traces were measured at several positions within a sample. In Figure 3.2.4.A as a representative example part of a time trace is shown measured from diffusing bubble-DNA molecules within 1% agarose with an integration time of 100  $\mu\text{s}$ . Clearly the bursts of photons can be observed upon passage of a Cy3.5 labeled DNA molecule through the focus. In Figure 3.2.4.B 10 autocorrelation curves of bubble-DNA molecules diffusing within 1% agarose are shown from time traces measured for 60 s at 10 different positions within the sample. The number of 100  $\mu\text{s}$  time lags included in the calculation of the autocorrelation curves was 1000. From this figure it is demonstrated that the reproducibility within one sample is good. Fitting of this set of 10 autocorrelation curves results in a diffusion time of  $0.637 \pm 0.001$  ms and a corresponding diffusion coefficient of  $1.57 \times 10^{-7} \text{ cm}^2/\text{s}$ .

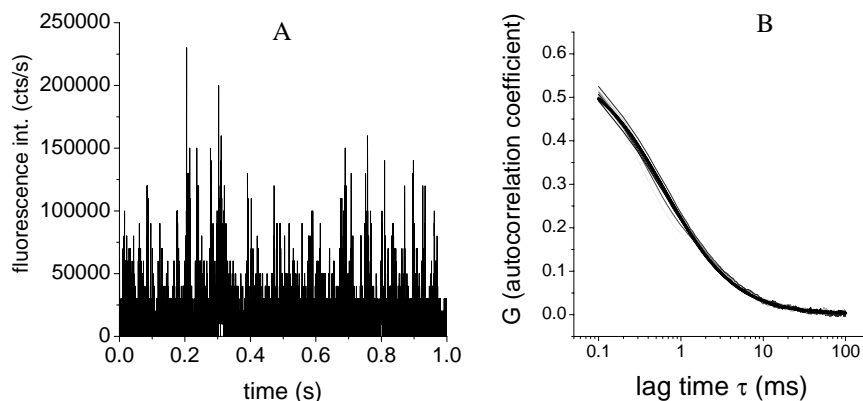


**Fig. 3.2.4.** Analysis of diffusion of Cy3.5-labeled bubble-DNA molecules within a 1% agarose matrix. A. First 1 s part of a 60 s time trace measured and represented with an integration time of 100  $\mu$ s. B. Autocorrelation curves determined from 10 time traces measured at different positions within the sample. Upon fitting the autocorrelation curves (fit result is thick black line) according to equation 3.3, a diffusion time  $\tau_D$  was obtained of  $0.637 \pm 0.001$  ms.

Time traces were measured in 1% and in 4% agarose to determine the dependence of the diffusion rate on the density and pore size of the matrix. This was performed for different types of DNA to investigate the diffusional properties in relation with later single molecule protein-DNA binding studies (chapter 4, 5).

In the histogram of Figure 3.2.5 the results of the diffusion analysis have been summarized for the different types of DNA included in this investigation. A general conclusion from this figure is that diffusion is faster in 1% agarose than in 4% agarose for all types of DNA. This is in correspondence with the density of the gels. The pore size is larger in a 1% gel (3,4) than in a 4% gel resulting in less hindered diffusion within a more open network. Apparently single strand 90-nt DNA has a higher mobility than double strand DNA of the same size (ds-90-bp) (5). The difference in diffusion coefficients reflects the difference in flexibility between single strand and double strand DNA. The persistence length is about 50 nm for double strand DNA and only a few nm for single strand DNA (6,7) at salt conditions similar to the conditions in our experiments. Because of a more globular conformation the 90-nt single strand DNA may experience less resistance during movement through an agarose matrix than the rod-like double strand 90-bp DNA.



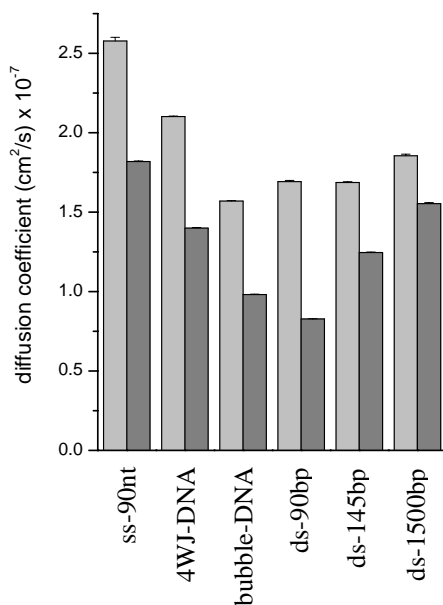


**Fig. 3.2.5.** Analysis of diffusion of different types of Cy3.5 labeled DNA within 1% (light gray bars) and 4% (dark gray bars) agarose. Time traces were measured for 60 s with an integration time of 100  $\mu$ s. Autocorrelation curves were determined from 10 time traces measured at different positions within the samples. The autocorrelation curves were fitted according to equation 3.3. to obtain the diffusion times ( $\tau_D$ ). The corresponding diffusion coefficients, calculated with equation 3.4, are plotted in this histogram.

4-Way junction DNA diffuses more slowly than single strand DNA, but has a higher diffusion coefficient than the double strand versions of DNA. The distance between the ends of two opposite arms is about 11 nm, which is small compared to the other double stranded DNA molecules involved. Possibly 4-way junction DNA experiences a little more friction in the gel than single strand DNA, but less than double-strand DNA, because of a rather compact three-dimensional conformation.

In 1% agarose the diffusion rates of the bubble-DNA and the double-strand DNA's of 90-bp, 145-bp and 1500-bp length are similar, while in 4% agarose some difference in diffusion rates can be observed. Probably the characteristics of the denser medium are just suitable to distinguish differences in diffusional behavior of the types of DNA included in this study. The constitution of a 1% agarose gel may be such that only differences in diffusion can be observed from molecules that have a highly dissimilar conformation. This is illustrated by the faster diffusion of single strand and 4-way junction DNA compared to the DNA molecules with a more double strand content.

In 4% agarose larger DNA molecules show faster diffusion than smaller molecules. This is surprising because during gel electrophoresis, even in 1% agarose, 1500-bp DNA molecules show a lower mobility than 90- and 145-bp DNA molecules (Figure 3.2.1.C). During electrophoresis larger molecules migrate more slowly because of higher friction and because they find their way through the pores of the gel less efficiently than smaller molecules (8-10). In electrophoresis molecules are forced to move in one direction because of the applied electrical field. In our experiments however the DNA molecules are freely diffusing without any external force. Our results indicate that the movement of DNA molecules within an agarose medium is different in the absence and presence of a driving force.

In a recent paper (5) it was shown that the free solution mobility of DNA becomes independent of molecular weight at lengths longer than 170-bp. Here it was suggested that the approach of DNA mobilities to a constant value with increasing molecular weights is associated with the transition from a rod-like to a coil-like conformation in solution. Probably the faster diffusion of the 1500-bp DNA molecules can be attributed to their higher flexibility. Perhaps longer double strand DNA molecules are able to snake through the matrix more efficiently than shorter more rigid molecules.

The rather low number of reports that have been published for diffusion of various types of DNA within different environments show a quite large variation. For 280-nt single-strand DNA in solution a diffusion coefficient of  $1.9 \times 10^{-7}$  cm<sup>2</sup>/s was determined with FRAP (6). For 100-bp DNA within 2% agarose a diffusion coefficient was measured of about  $10^{-7}$  cm<sup>2</sup>/s by FRAP (fluorescence recovery after photobleaching) (11). A diffusion coefficient of  $1.7 \times 10^{-8}$  cm<sup>2</sup>/s was obtained for 1 kilobase DNA in 1% agarose from measurement of band spreading (12) as well as in 2% agarose measured with FRAP (11). The equal diffusion coefficients measured for 1 kb DNA in media of different density show that the results are not very consistent. Probably this is caused by differences in measurement conditions, like temperature and salt concentration.

### **3.2.3 Discussion and Conclusions**

In this paragraph we have shown that confocal fluorescence microscopy is a suitable technique to study not only immobilized but also diffusing fluorescent molecules. In scanning mode the appearing stripy pattern is a representation of the diffusion of fluorescent molecules within the focal volume. The length of the stripes reflects the residence time in the focus. Within a denser matrix of 4% agarose we observe longer stripes than in a more open matrix of 1% agarose. In general faster diffusion gives rise to shorter stripes. The analysis of

autocorrelation curves, calculated from measured time traces, results in diffusion coefficients that fit well within the range of diffusion coefficients obtained from similar DNA molecules with other techniques. In general the more flexible the DNA molecules, the faster their observed diffusion is.

In later confocal measurements the immobilization of 90-bp bubble-DNA and 90-bp double strand DNA by protein binding within a 1% agarose matrix is utilized to study NER protein-DNA complex formation (see paragraph 3.3 and chapter 4 and 5). From the diffusion results we can conclude that the mobility of 90-bp bubble-DNA and double strand 90-bp DNA in 1% agarose is comparable. This information is relevant for the interpretation of the protein-DNA binding results to be discussed in chapter 5.

### 3.2.4 References

1. Aragon, S.R., and Pecora, R. (1976) Fluorescence correlation spectroscopy as a probe of molecular dynamics. *J. Chem. Phys.*, **64**, 1791-1803
2. Schwille, P., Bieschke, J., and Oehlenschläger, F. (1997) Kinetic investigations by fluorescence correlation spectroscopy: the analytical and diagnostic potential of diffusion studies. *Biophys. Chem.*, **66**, 211-228
3. Brasselet, S., Peterman, E.J.G., Miyawaki, A., and Moerner, W.E. (2000) Single-molecule fluorescence resonant energy transfer in calcium concentration dependent cameleon. *J. Phys. Chem B*, **104**, 3676-3682
4. Rees, D. (1972) Shapely polysaccharides. *Biochem. J.*, **126**, 257-273
5. Stellwagen, E., and Stellwagen, N. (2002) Determining the electrophoretic mobility and translational diffusion coefficients of DNA molecules in free solution. *Electrophoresis*, **23**, 2794-2803
6. Tinland, B., Pluen, A., Sturm, J., and Weill, G. (1997) Persistence length of single-stranded DNA. *Macromolecules*, **30**, 5763-5765
7. Rivetti, C., Walker, Bustamante, C. (1998) Polymer chain statistics and conformational analysis of DNA molecules with bends or sections of different flexibility. *J. Mol. Biol.*, **280**, 41-59
8. Fisher, M.P., and Dingman, C.W. (1971) Role of molecular conformation in determining the electrophoretic properties of polynucleotides in agarose-acrylamide composite gels. *Biochemistry*, **10**, 1895-1899
9. Aaij, C., and Borst, P. (1972) The gel electrophoresis of DNA. *Biochim. Biophys. Acta*, **269**, 192-200
10. Helling, R.B., Goodman, H.M., and Boyer, H.W. (1974) Analysis of endonuclease R-EcoRI fragments of DNA from lambdaoid bacteriophages and other viruses by agarose-gel electrophoresis. *J. Virol.*, **14**, 1235-1244
11. Pluen, A., Netti, P.A., Jain, R.K., and Berk, D.A. (1999) Diffusion of macromolecules in agarose gels: comparison of linear and globular configurations. *Biophys. J.*, **77**, 542-552
12. Yarmola, E., Sokoloff, H., and Chrambach, A. (1996) The relative contributions of dispersion and diffusion to band spreading (resolution) in gel electrophoresis. *Electrophoresis*, **17**, 1416-1419

### **3.3 Immobilization of DNA in an agarose matrix by protein binding**

In this paragraph results are shown of immobilization in agarose of fluorescently labeled DNA molecules as a result of binding by different NER-proteins. The RPA protein, a single-strand DNA binding protein involved in the NER process and also in DNA replication (1-4), is used in unlabeled form. The ERCC1-XPF protein complex, responsible for DNA incision at the 5'-side of a damage (5,6) was fluorescently labeled by fusion to EYFP. The proteins mentioned were combined with different DNA substrates, like single strand DNA and bubble-DNA. We show that our DNA immobilization method can be used for the quantitative determination of protein-DNA binding even when the protein is non-fluorescent.

#### **3.3.1 Materials and Methods**

##### **DNA substrates**

5'-Cy3.5 labeled 90-nt single strand DNA oligomers were purchased (DNA Technology A/S, Aarhus, Denmark). Cy3.5 is coupled to the 5'OH of the last nucleotide via a 3-carbon linker.

Bubble DNA was prepared as described in paragraph 4.2.

##### **Proteins**

###### **RPA**

The recombinant human RPA complex, utilized in our studies, purified from *E.coli* cells was kindly provided by M. Modesti and A. Janicijevic (Genetics, Rotterdam)(7,8).

###### **ERCC1-EYFP/XPF**

ERCC1-EYFP/XPF was prepared at the Department of Cell Biology & Genetics, Erasmus MC, Rotterdam, the Netherlands as described in paragraph 2.1.1.

The DNA-cutting activity of the purified ERCC1-EYFP/XPF protein was tested by means of a nuclease assay. Radioactively labeled substrate DNA was combined with the ERCC1-EYFP/XPF protein and the reaction products were quantified after separation by electrophoresis. A comparison was made with the nuclease activity of wild-type ERCC1/XPF. Moreover the activity of the purified ERCC1-EYFP/XPF protein was determined by microinjecting fractions into XPF

deficient cells and subsequently testing the DNA repair capacity, as described previously (9) and analogous to the procedure described for EGFP-XPA (paragraph 4.2).

## **DNA binding reactions**

### **RPA binding to single-strand DNA**

RPA was combined with single-strand DNA at a molar ratio of 1:20. During incubation the RPA concentration was approximately  $3 \times 10^{-9}$  M and the DNA concentration was  $6 \times 10^{-8}$  M in a 5.3  $\mu$ l volume of 25 mM Hepes, 40 mM KCl, 60 mM NaCl, 7 mM MgCl<sub>2</sub>, 0.4 mM DTT, 0.02% NP-40, 2.6% glycerol, pH 7.5. Incubation was performed for 30 min. at room temperature.

### **ERCC1-EYFP/XPF binding to bubble-DNA**

ERCC1-EYFP/XPF was combined with Cy3.5-labeled bubble-DNA in a molar ratio of 1:20. During incubation the ERCC1-EYFP/XPF concentration was  $4 \times 10^{-9}$  M and the DNA concentration was  $8 \times 10^{-8}$  M in a 5.3  $\mu$ l volume of 25 mM Hepes, 40 mM KCl, 60 mM NaCl, 5 mM CaCl<sub>2</sub>, 0.4 mM DTT, 0.02% NP-40, 2.6% glycerol, pH 7.5. Incubation was performed for 30 min. at room temperature.

Binding of ERCC1-EYFP/XPF to bubble-DNA was also performed in the presence of unlabeled RPA protein. For this purpose Cy3.5-labeled bubble-DNA and RPA were combined in a molar ratio of 20:1 and incubated in a 4  $\mu$ l volume of 25 mM Hepes, 40 mM KCl, 60 mM NaCl, 5 mM CaCl<sub>2</sub>, 0.4 mM DTT, 0.02% NP-40, 2.6% glycerol, pH 7.5. During incubation the RPA concentration was approximately  $4 \times 10^{-9}$  M and DNA concentration was  $8 \times 10^{-8}$  M. After 10 min. at 30° C a 1  $\mu$ l volume of ERCC1-EYFP/XPF protein in 25 mM Hepes, 40 mM KCl, 60 mM NaCl, 5 mM CaCl<sub>2</sub>, 0.4 mM DTT, 0.02% NP-40, 2.6% glycerol pH 7.5 was added to a final concentration of  $4 \times 10^{-9}$  M. The resulting reaction mixture contained a 1:1:20 molar ratio of RPA:ERCC1-EYFP/XPF:DNA and was incubated for an extra 10 min. at 30° C.

### **Sample preparation for confocal fluorescence microscopy**

For single molecule confocal measurements, reaction mixtures containing RPA/ss-DNA complexes were diluted to concentrations of approximately  $5 \times 10^{-10}$  M with respect to RPA at 30° C in molten low melt agarose, 1% (w/v) in 25 mM Hepes, 40 mM KCl, 60 mM NaCl, 7 mM MgCl<sub>2</sub>, pH 7.5.

Reaction mixtures containing ERCC1-EYFP/XPF and bubble-DNA, in the presence or absence of RPA, were diluted to approximately  $5 \times 10^{-10}$  M with respect to ERCC1-EYFP/XPF and RPA at 30° C in molten low melt agarose, 1% (w/v) in 25 mM Hepes, 40 mM KCl, 60 mM NaCl, 5 mM CaCl<sub>2</sub>, pH 7.5. The agarose mixtures were sandwiched between two quartz cover slips, diameter 25 mm.

### **Scanning confocal fluorescence microscopy**

The confocal microscope, described in paragraph 1.4, was used for measurements on reaction mixtures containing complexes of NER proteins with Cy3.5 labeled DNA substrates. For measurements on RPA/single-strand DNA complexes, the 568 nm line was selected from the Ar-Kr laser. Cy3.5 emission was detected with a D605/55 emission filter.

For measurements on ERCC1-EYFP/XPF complexes with Cy3.5 labeled bubble-DNA the 488 nm and 568 nm excitation wavelengths were selected. Reflected excitation light was suppressed by a 488 nm and a 568 nm notch filter. For spectral separation of Cy3.5 and EGFP or EYFP fluorescence a 565DCXR dichroic beam splitter was used. The emission filter for EGFP and EYFP was an HQ525/50m filter and for Cy3.5 it was a D605/55m filter. All filters and dichroics were purchased from Chroma Technology Corporation, Brattleboro, VT.

### **3.3.2 Results**

#### **Protein production and purification**

Because the DNA binding properties of the proteins will be utilized, it is important to check that the produced proteins are functional. The RPA preparation used had been shown to be active from other applications (7,8). The ERCC1-EYFP/XPF complex turned out to be almost as active as wild-type ERCC1/XPF in the nuclease assay. After microinjection of XPF deficient cells with ERCC1-EYFP/XPF protein and UV irradiation the repair deficiency was corrected up to the wild-type level. The number of autoradiographic grains above injected cells was comparable for XPF deficient cells injected with the EYFP labeled ERCC1/XPF and injected with wild-type ERCC1/XPF. From these observations, a positive nuclease assay and restoration of repair deficiency, the ERCC1-EYFP/XPF was considered to be a proper preparation for the use in DNA binding reactions.

#### ***Single molecule imaging of NER-protein/DNA complexes***

##### **RPA binding to single-strand DNA**

In paragraph 3.2 we have shown that confocal scanning of Cy3.5 labeled DNA present in a 1% agarose matrix results in images with a stripy intensity pattern. If the unlabeled RPA protein and Cy3.5 labeled single-strand DNA are present in the sample as independent components we expect to observe similar images. In Figure 3.3.1.A an example is shown of a confocal fluorescence image measured from a sample of RPA combined with ss-90-nt-DNA.

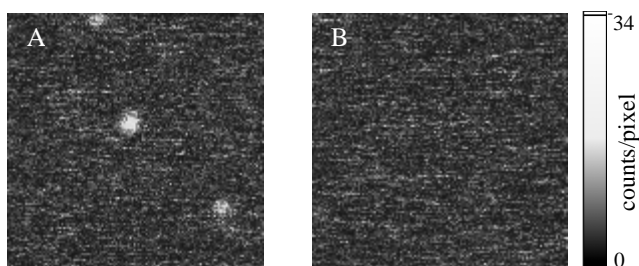


**Fig.3.3.1.** Scanning confocal images from unlabeled RPA protein together with Cy3.5-labeled single-strand DNA (A) and from only Cy3.5-labeled single-strand DNA (B) in 1% agarose. Image size is  $6.2 \times 6.2 \mu\text{m}^2$ ,  $128 \times 128$  pixels, dwell time 0.5 ms/pixel, excitation  $6 \text{ kW.cm}^{-2}$ .

In Figure 3.3.1.A three discrete spots can be observed on top of some background intensity from diffusing DNA. The concentration of DNA within the agarose is about 10 times higher than used in the diffusion experiments (see Figure 3.2.3). This results in a more homogeneous distribution of intensities than at lower DNA concentrations. For comparison in Figure 3.3.1.B a confocal image is shown from only Cy3.5-labeled DNA in 1% agarose with the same DNA concentration as in Figure 3.3.1.A. The fluorescence intensity present in the spots in Figure 3.3.1.A only can come from Cy3.5-labeled DNA bound by unlabeled RPA protein. The DNA is immobilized in the pores of the gel together with the RPA protein. In 188 images of  $6.2 \times 6.2 \mu\text{m}$  we counted on average 5.0 single molecule spots. Because the RPA protein is unlabeled it is not possible to accurately determine the DNA-bound RPA fraction. For quantitative purposes the RPA protein needs to be fluorescently labeled too. These results demonstrate that immobilization of DNA in an agarose matrix by protein binding is a useful method in the study of single molecule protein-DNA interactions, even if the protein of interest is non-fluorescent.

### ERCC1-EYFP/XPF binding to bubble-DNA

The incision activity of the ERCC1/XPF complex has been shown to be absolutely dependent on the presence of divalent cations like Mg and Mn (6,10). To achieve only binding of protein without cutting of the DNA, the ERCC1-EYFP/XPF complex was combined with Cy3.5 labeled 90-bp bubble-DNA in the presence of calcium. In the confocal images obtained from this binding reaction we did not observe any immobilization of DNA. It means that no complex formation occurs between ERCC1-EYFP/XPF and Cy3.5 labeled 90-bp bubble-DNA at the applied conditions. This result is consistent with the result of a pull-down assay in which only weak binding of ERCC1/XPF complex to an identical 90-bp-bubble-DNA substrate was observed (11). When however ERCC1/XPF was incubated with the DNA substrate in the presence of the RPA protein, significantly more ERCC1/XPF bound to the bubble-substrate.

To investigate the effect of RPA also on the single molecule level we also combined the ERCC1-EYFP/XPF with the Cy3.5-labeled bubble-DNA in the presence of unlabeled RPA and calcium. As a control, we first imaged the immobilized DNA by illuminating with only 568 nm. Then we only observed fluorescence intensity in the Cy3.5 detection channel (Figure 3.3.2-upper panel), which means that EYFP is not excited by 568 nm light.

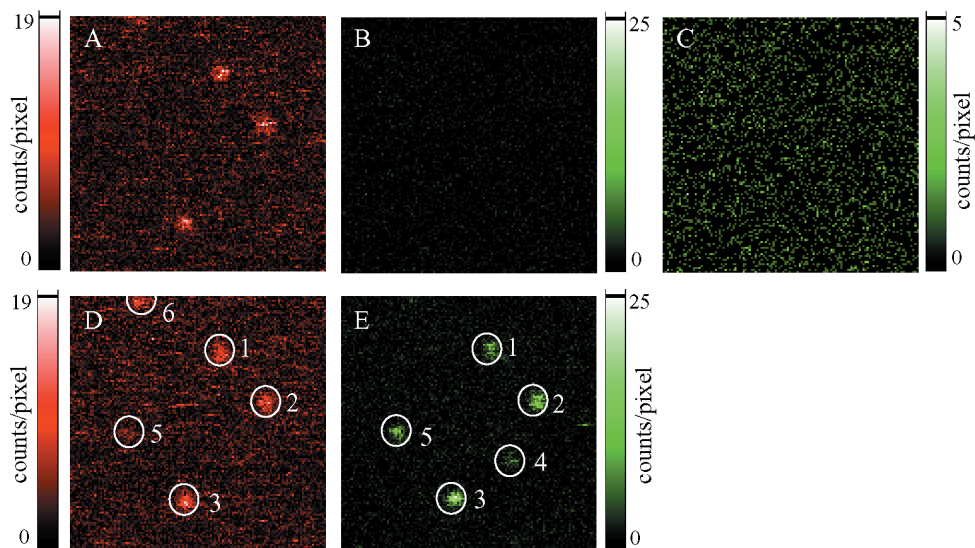


**Fig. 3.3.2.** Scanning confocal images from complexes of ERCC1-EYFP/XPF, RPA and Cy3.5-bubble-DNA (ratio 1:1:20) in a 1% agarose matrix. Upper panel: excitation with 568 nm only. Lower panel: simultaneous excitation with 488 and 568 nm. Emission was detected simultaneously in the Cy3.5 channel from 577-632 nm (images A and D) and in the EYFP channel from 500-550 nm (images B, C and E). Image C is the same as image B, but only scaled on its own intensity maximum. Image size is  $6.2 \times 6.2 \mu\text{m}^2$ ,  $128 \times 128$  pixels, dwell time 0.5 ms/pixel, excitation  $5 \text{ kW}\cdot\text{cm}^{-2}$  at 488 and  $3 \text{ kW}\cdot\text{cm}^{-2}$  568 nm. Circled positions 1, 2 and 3 indicate colocalization of ERCC1-EYFP/XPF and Cy3.5-bubble-DNA. Positions 4 and 5 indicate ERCC1-EYFP/XPF with cross talk. At position 6 Cy3.5-bubble-DNA is immobilized by only RPA.

The appearance of fluorescence spots indicates the presence of complexes of ERCC1-EYFP/XPF and bubble-DNA. To verify if indeed at the positions of immobilized DNA also protein is present, we next illuminated the same area simultaneously with 488 nm and 568 nm excitation light. In the EYFP detection channel now also single molecule spots appeared (Figure 3.3.2-lower panel). Some of these spots colocalize with spots observed in the Cy3.5 detection channel of the upper panel (molecules 1, 2 and 3) as well as with spots in the simultaneously measured Cy3.5 image. Obviously it means that there are complexes of ERCC1-EYFP and Cy3.5-labeled bubble-DNA at the positions where colocalized Cy3.5 and EYFP fluorescence intensities are detected



(molecules 1, 2 and 3). It is likely that the complexes also contain RPA protein, because we did not observe any immobilization of DNA in the absence of RPA. At position 4 and 5 probably there is only ERCC1-EYFP/XPF present, because these spots were not present in the upper panel with only 568 nm excitation. The accompanying spot at position 5 in the left image of the lower panel is the result of cross talk from EYFP emission into the Cy3.5 detection channel. At position 6 there probably is a Cy3.5 labeled bubble-DNA molecule immobilized by binding to RPA only that was not yet present during scanning of the upper panel images.

In total we analyzed 144 molecules for complex formation by the detection of colocalized Cy3.5 and EYFP intensities. From these molecules 72 molecules showed the presence of Cy3.5-labeled bubble-DNA together with EYFP-labeled ERCC1/XPF protein at the same position in the images. This means that 50% of the ERCC1/XPF molecules formed complexes with the Cy3.5-labeled bubble-DNA, probably together with RPA. From the total number of 83 spots in the Cy3.5 detection channel 87% showed colocalized EYFP intensities. The remaining 13% of immobilized Cy3.5-labeled bubble-DNA molecules will be associated with RPA only.

These results demonstrate that also at the single molecule level a positive effect of the presence of RPA on the DNA binding affinity of ERCC1-EYFP/XPF is observed.

### **3.3.3 Discussion and Conclusions**

The immobilization in agarose of Cy3.5-labeled single-strand DNA because of binding by RPA demonstrates that this is a suitable method to study protein-DNA complex formation on the single molecule level.

The ERCC1-EYFP/XPF binding to Cy3.5-labeled bubble-DNA is an example of a single molecule protein-DNA binding study where colocalization of fluorescent labels is indicative of complex formation. Although the total number of molecules investigated is too low to assess binding affinities quantitatively, these results give a clear demonstration of the possibilities offered by single molecule fluorescence methods. Only together with RPA the ERCC1-EYFP/XPF complex was able to immobilize the bubble-DNA. This effect also has been observed in bulk biochemical methods where the RPA and ERCC1/XPF proteins were incubated with bead-immobilized bubble-DNA (11). In the absence of RPA hardly any binding of ERCC1/XPF to the bubble-DNA was detected, while in the presence of RPA ERCC1/XPF binding was enhanced. It was suggested that RPA directs the ERCC1/XPF complex onto the DNA through protein-protein interaction or by creating an adequate DNA structure for protein binding. In a later report it was shown that the RPA protein binds with defined polarity to the

undamaged DNA strand and positions the ERCC1/XPF complex at the 5'-side of a damage to make an incision (8). The potential of single molecule fluorescence imaging is indicated by the good correspondence of our results with results from biochemical methods.

### 3.3.4 References

1. Kim, C., Paulus, B.F., and Wold, M.S. (1994) Interactions of human replication protein A with oligonucleotides. *Biochemistry*, **33**, 14197-14206
2. Stigger, E., Drissi, R., and Lee, S.-H. (1998) Functional analysis of human replication protein A in nucleotide excision repair. *J. Biol. Chem.*, **273**, 9337-9343
3. Burns, J.L., Guzder, S.N., Sung, P., Prakash, S., and Prakash, L. (1996) An affinity of human replication protein A for ultraviolet-damaged DNA. *J. Biol. Chem.*, **271**, 11607-11610
4. He, Z., Henriksen, L.A., Wold, M.S., and Ingles C.J. (1995) RPA involvement in the damage-recognition and incision steps of nucleotide excision repair. *Nature*, **374**, 566-569
5. van Vuuren, A.J., Appeldoorn, E., Odijk, H., Humbert, S., Moncollin, V., Eker, A.P.M., Jaspers, N.G.J., Egly, J.-M., and Hoeijmakers, J.H.J. (1995) Partial characterization of the DNA repair protein complex containing the ERCC1, ERCC4, ERCC11 and XPF correcting activities. *Mut. Res.*, **337**, 25-39
6. Sijbers, A.M., de Laat, W.L., Ariza, R.R., Biggerstaff M., Wei, Y.F., Moggs, J.G., Carter, K.C., Shell, B.K., Evans, E., de Jong, M.C., Rademakers, S., de Rooij, J., Jaspers, N.G., Hoeijmakers, J.H.J., and Wood, R.D. (1996) Xeroderma pigmentosum group F caused by a defect in a structure-specific DNA repair endonuclease. *Cell*, **86**, 811-822
7. Henriksen, L.A., Umbricht, C.B., and Wold, M.S. (1994) Recombinant replication protein A: expression, complex formation and functional characterization. *J. Biol. Chem.*, **269**, 11121-11132
8. de Laat W.L., Appeldoorn, E., Sugasawa, K., Weterings, E., Jaspers, N.G., and Hoeijmakers, J.H. (1998) DNA-binding polarity of human replication protein A positions nucleases in nucleotide excision repair. *Genes Dev.*, **12**, 2598-2609).
9. Vermeulen, W., van Vuuren, A.J., Chipoulet, M., Schaeffer, L., Appeldoorn, E., Weeda, G., Jaspers, N.G., Priestley, A., Arlett, C.F., and Lehmann, A.R. et al. (1994) Three unusual repair deficiencies associated with transcription factor BTF2(TFIID): evidence for the existence of a transcription syndrome. *Cold Spring Harb Symp Quant Biol.*, **59**, 317-329
10. de Laat, W.L., Appeldoorn, E., Sugasawa, K., Weterings, E., Jaspers, N.G., and Hoeijmakers, J.H.J. (1998) DNA structural elements required for ERCC1-XPF endonuclease activity. *J. Biol. Chem.*, **273**, 7835-7842
11. Matsunaga, T., Park, C.H., Bessho, T., Mu, D., and Sancar, A. (1996) Replication protein A confers structure-specific endonuclease activities to the XPF-ERCC1 and XPG subunits of human DNA repair excision nuclease. *J. Biol. Chem.*, **271**, 11047-11050

### **3.4 Colocalization of NER proteins and DNA**

Within each project on the mechanism of Nucleotide Excision Repair a highly interesting issue is to determine the exact location of different molecular components within intermediate NER complexes. From the present knowledge about NER it can be foreseen that the required localization accuracy must be at least 10 to 15 nm or better. In confocal fluorescence microscopy different fluorescently labeled components within a NER complex will always colocalize within one spot on the detector, because of diffraction limited resolution. Mutual distances between proteins, within a NER complex may then be determined by FRET measurements. The required conjugates for FRET studies are under development, and it is therefore presently not possible to use FRET for this purpose. Therefore we started to apply an alternative method for high-resolution localization of individual fluorescent molecules in images obtained with a scanning confocal fluorescence microscope.

We determined the center of the emission intensity distribution of single molecules in confocal images by fitting the observed distribution with a Gaussian function. Using a chi-square minimization procedure the probability and a confidence level is obtained of finding a molecule at some position.

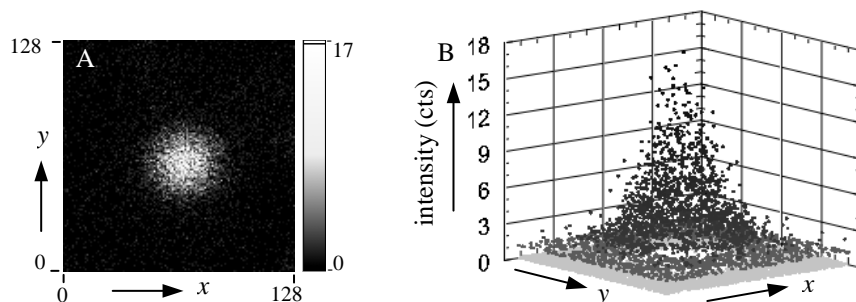
With our confocal configuration, distance determination between individual molecules, imaged simultaneously at different excitation wavelengths, requires a perfect overlap of the excitation beams. Currently we are solving the issue of the relatively large systematic error that may be introduced in the excitation path using two wavelengths. Consequently we did not yet have the opportunity to apply the localization method for real distance measurements between colocalized GFP-NER proteins and Cy3.5-labeled DNA (as shown in chapter 4). So far we determined the localization accuracy for single EGFP-XPA molecules embedded in agarose and for Cy3.5 or Cy5 labeled DNA molecules adsorbed on quartz. The results are promising in view of accurate distance measurements within NER complexes and indicate that the agarose gels can be used for these purposes.

#### **3.4.1 Localization of single molecules in confocal fluorescence microscopy images**

In the applied fitting procedure, based on chi-square minimization, 7 parameters were included, being the average background level, the maximum amplitude, the width of the intensity distribution in the x- and in the y-direction, the x- and y-position of the intensity maximum, and the orientation of the spot. The accuracy of the fit was expressed for all parameters in their variances. From the variances localization accuracies were calculated for the position of the intensity maximum.

### Localization results

In Figure 3.4.1 a scanning confocal image is shown measured from a Cy5 labeled 90-nt DNA molecule adsorbed on quartz.



Spot specifications	
Max. intensity of image	17 cts
Max. intensity of fit	8.37 cts
Peak width ( $\sigma$ )	$(9.8 \pm 0.3)$ pixels
Average background	1.13 cts
Total intensity in spot	6245 cts
Position of max. intensity (x;y)	$(65,69; 62,71)$ pixels
Pixel size	12.1 nm
RMS error in x-position	0.095 pixels
RMS error in y-position	0.101 pixels

**Fig. 3.4.1.** A. Scanning confocal image of a Cy5 labeled 90-nt DNA molecule adsorbed on quartz. Image size is  $1.55 \times 1.55 \mu\text{m}^2$ ,  $128 \times 128$  pixels. B. 3-D plot of the intensity distribution of the spot shown in A.

The resulting localization accuracy for this individual Cy5 molecule was, for a  $1\sigma$  confidence level, 0.095 pixels in the x-direction and 0.101 pixels in the y-direction. For a  $2\sigma$  confidence level and a pixel size of 12.1 nm, we find that the molecule is located with 95% probability within an almost spherical spot (ellipsoidal with aspect ratio 0.96) with a radius of 2.4 nm.

In the same way as shown in the example, we analyzed several single molecule spots in confocal images of both surface adsorbed molecules and molecules embedded in agarose gel. Only fluorescence spots from non-blinking molecules were included. At this point we did not take into account bleaching effects. The result is shown in Figure 3.4.2.

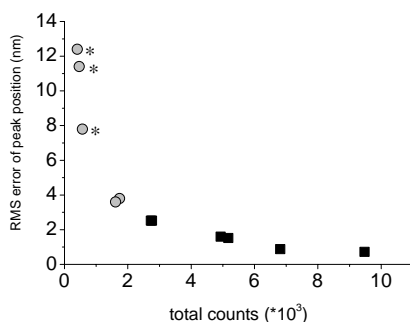


**Fig. 3.4.2.** Result of localization analysis with a  $2\sigma$  confidence level for different types of single molecules. The black square data points are from Cy3.5 labeled 90-nt DNA molecules adsorbed to quartz, the round gray data points from EGFP-XPA molecules embedded in agarose. Molecules indicated with \* were measured with 2.5 pixels within a length corresponding to the size of  $d$ , where  $d$  is the standard deviation of the Gaussian beam profile, all other molecules were measured with 5 pixels within  $d$ .

From Figure 3.4.2 we can conclude that the localization accuracy is mainly determined by photon statistics. The higher the total number of counts collected, the more accurate the position of a molecule can be determined. This holds not only for surface immobilized molecules, but even for gel embedded molecules. So far we could not determine the contribution from other errors. Repeated measurements on one molecule are not well possible because of bleaching effects. For this purpose we will have to analyze and compare molecules that are measured under the same scanning conditions and that show similar intensities. Also systematic errors were not considered yet. The localization accuracy of the surface adhered Cy3.5 labeled DNA molecules shown in Figure 3.4.2 varies from 0.7 to 2.5 nm for a  $2\sigma$  confidence level and for the EGFP-XPA molecules from 3.8 to 12.4 nm. Although the signal to background ratio for the measured molecules was different and varied between 38 and 5, we can conclude from Figure 3.4.2 that these ratios are so high that they were not the determining factors for the accuracy of localization.

**Optimal scanning conditions** The results shown in Figure 3.4.2 indicate that we can localize individual molecules with accuracies of less than 20 nm. From this figure it is not clear if during measurement the applied number of pixels ( $N$ ) that fit within a length corresponding to the size of  $d$  (the standard deviation of the Gaussian beam profile), was optimal for localization purposes. To determine if we still can improve the accuracy with which we can localize a molecule in an image we determined the relation between the localization accuracy and the number of pixels within  $d$ . Now we kept the volume under the Gaussian curve (= total number of counts) constant for each value of  $N$ . In Figure 3.4.3 the resulting graphs are shown for two different numbers of total counts and different signal to

background ratios. Figure 3.4.3 demonstrates that there is an optimum number of pixels in  $d$  in both curves. We can conclude that, at the applied number of counts and signal to background ratios, the pixel size should be about equal to the size of  $d$  for most accurate localization. It means that the localization accuracy of the molecules indicated in Figure 3.4.2 still can be improved by measuring with only 1 pixel in  $d$ .

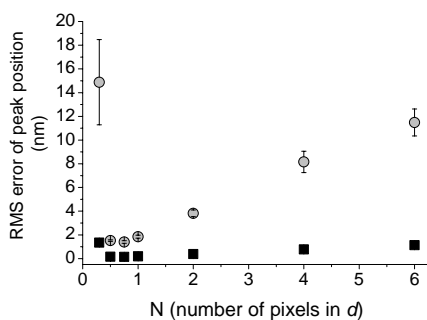


**Fig.3.4.3.** Localization accuracy as a function of the number of pixels in  $d$  at a constant total number of counts for a  $2\sigma$  confidence level. A constant ratio between the amplitude and the background was applied over the whole curve. The black square data points are from a total number of counts of 6245 and a signal to background ratio of 7.4, the gray data points are from a total number of counts of 566 and a signal to background ratio of 8.6.

### 3.4.2 Discussion and Conclusions

The results from our localization analysis show that we can localize individual EGFP-XPA and Cy3.5 labeled DNA molecules with an accuracy much smaller than the actual signal width ( $d$ ) and even smaller than the size of one pixel. This holds even though the measurements were done at room temperature and for molecules embedded in agarose (EGFP-XPA). This is promising with respect to distance determination between individual components within a NER complex.

Figure 3.4.3 shows that the localization accuracy of the molecules included in Figure 3.4.2 will be improved by decreasing the number of pixels ( $N$ ) in  $d$ . It is most important to collect as many photons as possible during scanning with a low number of pixels within  $d$ . The purpose of a measurement will determine the allowed dwell time per pixel. If a molecule needs to be imaged only once, longer dwell times will be allowed than for tracking of a single fluorescent molecule in several sequential images.

By successively scanning a single molecule or a small scattering bead systematic errors will be determined. The standard deviation of the resulting set of maximum positions will indicate whether the applied methods give a good representation of the practical situation. So far, in all analysis possible blinking and bleaching of fluorescent molecules have not been taken into consideration. Determination of the localization accuracy of strongly blinking or rapidly bleaching molecules will require alternative methods.

### **3.4.3 References**

1. Bobroff, N., (1986) Position measurement with a resolution and noise-limited system. *Rev. Scient. Instr.*, **57**
2. Kubitscheck, U., Kückmann, O., Kues, T., and Peters, R. (2000) Imaging and tracking of single GFP molecules in solution. *Biophys. J.*, **78**, 2170-2179
3. Thompson, R.E., Larson, D.R., and Webb, W.W. (2002) Precise nanometer localization analysis for individual fluorescent probes. *Biophys. J.*, **82**, 2775-2783
4. Lacoste T.D., Michalet X., Pinaud, F., Chemla, D.S., Allvisatos, P., and Weiss, S. (2000) Ultrahigh-resolution multicolor colocalization of single fluorescent probes. *Proc. Natl. Acad. Sci. USA*, **97**, 9461-9466





# 4

## SINGLE MOLECULE STUDY on NUCLEOTIDE EXCISION REPAIR:

### COMPLEX FORMATION of XPA/RPA with BUBBLE-DNA

*In this chapter results are shown from single molecule fluorescence investigations on the Nucleotide Excision Repair system. We studied complex formation between a model DNA bubble- substrate and the XPA and RPA proteins. Binding of EGFP-labeled XPA protein to a Cy3.5-labeled DNA substrate, in the presence and absence of RPA, was assessed quantitatively by simultaneous excitation and emission detection of both fluorophores. On the single molecule level we observed a low binding affinity of XPA for bubble-DNA. In the presence of RPA, XPA-DNA binding was significantly enhanced. These results are in good correspondence with those obtained in bulk experiments.*

---

The content of this chapter is based on:

Segers-Nolten, G.M.J., Wyman, C., Wijgers, N., Vermeulen, W., Lenferink, A.T.M., Hoeijmakers, J.H.J., Greve, J. and Otto C. (2002) Scanning confocal fluorescence microscopy for single molecule analysis of Nucleotide Excision Repair complexes, *Nucl. Acids Res.*, **30**, 4720-4727

## 4.1 Introduction

We studied complex formation between a model DNA substrate and proteins involved in nucleotide excision repair (NER). NER is one of the most important mammalian DNA repair processes responsible for removing a wide variety of helix distorting lesions from genomic DNA (see paragraph 1.5 for details about NER and 1-4). To see whether scanning confocal fluorescence microscopy of single molecules embedded in gel matrices provides valid information on the dynamics of protein/DNA complex assembly we used a relatively simple DNA/(NER) protein complex that has already been characterized in bulk biochemical experiments. We first analyzed the interaction of human XPA protein with a 90-bp double stranded DNA molecule that has a central 30-nt unpaired region, subsequently referred to as 'bubble DNA'. XPA plays a crucial role in NER and binds to bubble-DNA (5,6). In addition, RPA is known to enhance the binding of XPA to DNA (5-12). This protein/DNA complex is suggested to be important for damage verification and proper orientation of excision activities (13). To visualize individual components with scanning confocal fluorescence microscopy, both DNA and XPA were fluorescently labeled. One DNA strand was 5'-labeled with a single Cy3.5 molecule. EGFP was fused in frame to XPA, which was then overproduced in *E.coli* and purified to near homogeneity. For illustration in Figure 4.1.1 the possible position of the XPA and RPA proteins is accentuated within a proposed intermediate NER complex including Cy3.5-labeled damaged DNA and the EGFP label on XPA.

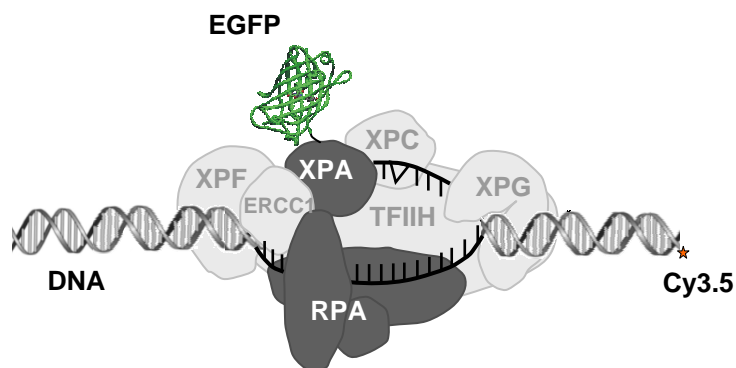


**Fig. 4.1.1** Schematic representation of the position of the XPA/RPA protein in a possible NER complex. A 90-'bp' damaged DNA molecule is drawn (damage indicated as a triangle), which length is equal to about 30 nm. EGFP is a cylinder with a diameter of 2 nm and a length of 4 nm. As far as possible the drawing is to scale, the dimensions of the NER proteins are estimated on the basis of their molecular mass.

The measured affinity of XPA for the bubble-DNA substrate and the influence of RPA on this affinity, as determined here using single molecule scanning confocal fluorescence microscopy, are in good agreement with results obtained from bulk biochemical methods. Moreover, we show that the applied procedure of DNA immobilization by protein binding in a gel is very well suited for single molecule protein-DNA binding studies in general. Our results demonstrate that single molecule spectroscopic imaging is a promising new technique that will allow us to identify and study the dynamic interactions of even more complex intermediates in NER. This method also has the potential to provide new insights into the mechanism of other complex DNA transactions.

## **4.2 Materials and methods**

### **Production and Purification of His<sub>9</sub>HA-EGFP tagged XPA**

The procedure for production and purification of His<sub>9</sub>HA-EGFP-XPA has been published (14). Here we will give only a brief description. EGFP-tagged XPA was generated by fusing the cDNA coding for the enhanced green fluorescent protein (EGFP) to XPA cDNA. An extra sequence encoding for both a nine histidine (His<sub>9</sub>) stretch and a HA-epitope were added to the N-terminal coding part of EGFP. Protein overexpression was induced in *E.coli* BL21(DE3)LysS with 2 mM IPTG. To isolate the recombinant protein cells were lysed by sonication. The whole cell extract was cleared from insoluble particles by centrifugation. The supernatant was subsequently purified on a Heparin-sepharose column, a Phosphocellulose column and a Ni-NTA column. Protein fractions at each stage during production and purification were analyzed by standard SDS-PAGE and immunoblotting. The recombinant human RPA complex, utilized in our studies, purified from *E.coli* cells was kindly provided by M. Modesti and A. Janicijevic (Genetics, Rotterdam)(15,16).

### **Microinjection and DNA repair synthesis**

The activity of the purified EGFP-XPA protein was assayed by microinjecting fractions into XPA deficient human fibroblasts and subsequently testing the DNA repair capacity, as described previously (17). After fluorescent image recording, DNA repair capacity was determined by measuring unscheduled DNA synthesis (UDS) (17). Human fibroblasts were UV-irradiated, labeled with [<sup>3</sup>H]thymidine and fixed for autoradiography. Autoradiographic grains above the nuclei of injected polykaryons were counted and compared with the number of grains above nuclei of wild-type fibroblasts assayed in parallel.

### **DNA substrate**

DNA substrates that model NER intermediates were prepared from a pair of 90 nucleotide oligomers, one of which had a 5'-Cy3.5 label (Biozym, Landgraaf, the Netherlands). The sequence of the oligomers was the same as described in Matsunaga et al (18). Upon annealing equimolar amounts of 90-mers in 25 mM Hepes, pH 7.5, 100 mM NaCl, 10 mM MgCl<sub>2</sub> in a final concentration of 10<sup>-6</sup> M, double stranded DNA with a central 30-bp unpaired region, bubble-DNA substrates, was produced. Formation of bubble-DNA was checked by electrophoresis in 8% non-denaturing PAA gel and determined to be in the bubble configuration for about 91% (shown in paragraph 3.2-Figure 3.2.2). From the gel we can conclude that the preparation does not contain free Cy3.5-oligomers. The 9% impurities are only on the higher molecular mass side of the gel. Probably a small amount of higher order structures is present, containing 4, 6, etc. oligomers, which are supposed not to be of significant importance in the interpretation of our results. The bubble-DNA was used without further purification.

### **Binding reactions**

EGFP-XPA/DNA complexes were prepared by combining DNA bubble-substrate and EGFP-XPA at a molar ratio of 20:1. During incubation EGFP-XPA concentration was approximately 3×10<sup>-9</sup> M and DNA concentration was 6×10<sup>-8</sup> M in a 5.3 μl volume of 25 mM Hepes, 40 mM KCl, 60 mM NaCl, 7 mM MgCl<sub>2</sub>, 0.4 mM DTT, 0.02% NP-40, 2.6% glycerol, pH 7.5. For preparation of XPA/RPA/DNA complexes DNA, EGFP-XPA and RPA were combined as above in a molar ratio of 20:1:1. Binding reactions were incubated for 30 minutes at room temperature.

### **Sample preparation for confocal microscopy**

For single molecule confocal measurements, proteins and reactions containing complexes of protein and DNA were diluted to concentrations of approximately 5×10<sup>-10</sup> M with respect to EGFP-XPA at 30° C in molten low melt agarose, 1% (w/v) in 25 mM Hepes, 40 mM KCl, 60 mM NaCl, 7 mM MgCl<sub>2</sub>, pH 7.5. The agarose mixture was sandwiched between two quartz cover slips, diameter 25 mm. Adsorption of bubble-DNA only, was achieved by applying 10 μl of a 10<sup>-9</sup> M solution of Cy3.5-labeled DNA in buffer between two 25 mm diameter quartz cover slips.

### **Scanning confocal fluorescence microscopy**

The measurements on DNA/NER-protein complexes were performed with our home-built confocal microscope, described in paragraph 1.4. For spectral separation of EGFP and Cy3.5 fluorescence a 565DCXR dichroic beam splitter was used (Chroma Technology Corporation, Brattleboro, VT).

### 4.3. Results

#### Preparation of EGFP-XPA

As shown in Figure 4.3.1, a protein migrating at the expected position for the tagged-XPA in SDS-PAGE was visible (arrow, lanes D and E). Because of the known aberrant mobility of XPA in SDS-PAGE the His<sub>9</sub>HA-EGFP-XPA fusion protein appears as a protein with higher MW than the calculated 62.5 kDa. Immunoblot analysis, using XPA specific antibodies, confirmed that indeed the desired fusion product was induced (data not shown). For each of the subsequent steps of purification, respectively, Heparin-sepharose, Phosphocellulose and Ni-NTA agarose, purity and yield of the fusion protein were monitored by gel-staining (Figure 4.3.1) and immuno-blotting. The elution fractions of the last purification step contained predominantly intact EGFP-XPA polypeptide with some proteolytic degradation products.

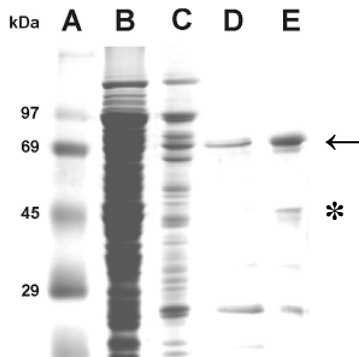


**Fig.4.3.1.** Protein profile of EGFP-XPA purification. Purification of EGFP-XPA was followed by loading samples of fractions from the purification steps on SDS-PAGE and staining with Coomassie brilliant blue. A. Standard prestained molecular weight markers, molecular size is indicated in kDa. B. Crude extract. C. Fractions eluted from the Heparin column and loaded onto the Phosphocellulose column. D. Fractions eluted from the Phosphocellulose column and loaded onto the Ni-NTA column. E. Fraction eluted from the Ni-NTA column with 200 mM imidazole. The arrow indicates the fusion protein of His<sub>9</sub>HA-EGFP-XPA, running at ~70 kDa. A minority of the fusion protein is degraded as shown by the asterisk, likely free XPA (without EGFP-tag), since it cross reacts with anti-XPA in Western blotting (not shown).

The isolated recombinant polypeptide (> 95% purity) was tested for its biological activity. To that aim the protein was introduced, via microneedle injection into XPA-deficient cells. NER activity of the injected cells was measured by determining DNA repair synthesis after UV-irradiation (UDS). Within 15 min.

after microinjection, a bright fluorescent signal was observed in the nuclei of the majority of injected cells. After fluorescence image recording, cells were assayed for their repair activity. The cells with green fluorescent nuclei were also corrected (up to wild type levels) for the severe UDS-defect, present in XP-A cells. The number of autoradiographic grains above the injected cell nuclei was significantly higher than above the non-injected neighboring cells (data not shown) and comparable to results from microinjection with non-tagged XPA (19). Both nuclear targeting and the complete restoration of UDS, indicate that the His<sub>9</sub>HA-EGFP tag does not interfere with the proper function of XPA, and that the purified protein is biologically active. In conclusion, both the purity and the biological activity indicate that this protein is a bonafide NER reagent to be applied in single molecule studies.

### **Imaging single EGFP-XPA proteins**

To image single fluorescent molecules by scanning confocal fluorescence microscopy it is necessary to immobilize these molecules during the scanning interval. For this purpose we used an agarose gel matrix, which offers the advantage of working in buffer and the ability to control the concentration of molecules in the sample.

Figure 4.3.2.C is a scanning confocal image of EGFP-XPA molecules immobilized in a 1% agarose gel, emission was detected between 500-550 nm. The bright spots in this image represent the emission profiles from immobilized EGFP-XPA molecules that can easily be distinguished from background signal. The observed one-step bleaching and blinking (characteristic for GFP) behavior (20-22), as detected by acquiring time traces (figure 4.3.2.D), strongly suggest that fluorescent spots are derived from single molecule emission. This behavior, together with the expected fluorescence intensity level, confirms that we observe individual EGFP-XPA molecules.

Simultaneously with the image in figure 4.3.2.C, an image was recorded from the EGFP sample with the detection wavelength in the 577-632 nm region, the detection window for Cy3.5 emission (figure 4.3.2.A and B). The low intensity of this image and the absence of localized spots show that there is virtually no cross talk from EGFP emission into the Cy3.5 detection channel.

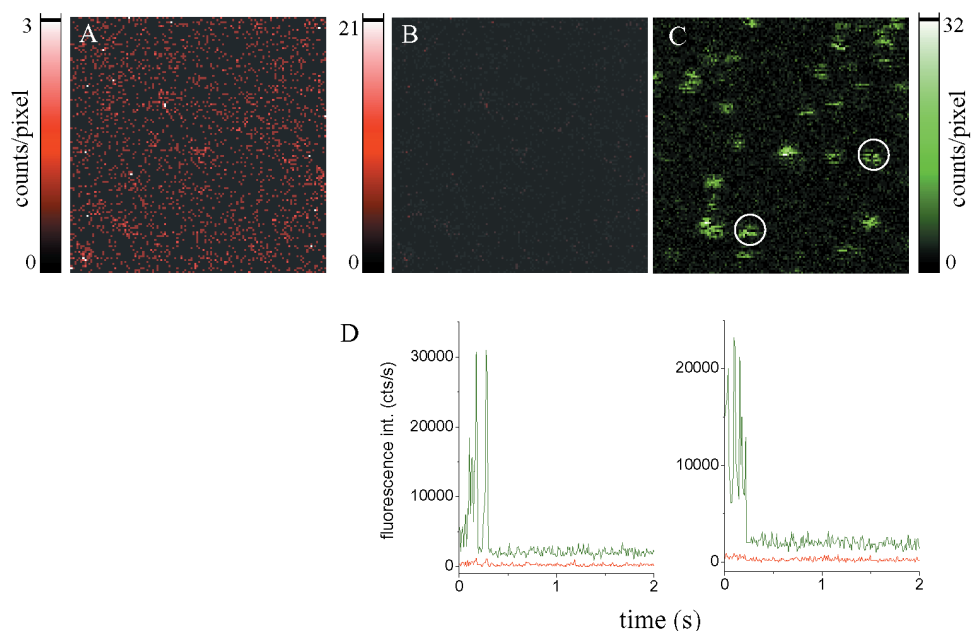


**Fig.4.3.2.** Confocal results of individual EGFP-XPA molecules immobilized in 1% agarose gel. A. Confocal image recorded from EGFP emission detected in the Cy3.5 detection channel, 577-632 nm region; scaling is on the maximum intensity of the image. Image A is also shown in B, but now the scaling is the same as in the other images recorded from signal in the Cy3.5 channel shown in this chapter. C. Confocal image recorded from EGFP emission detected in the EGFP detection channel, 500-550 nm region. Image size is  $6.2 \times 6.2 \mu\text{m}^2$ ,  $128 \times 128$  pixels, dwell time is 0.5 ms/pixel. D. Representative time traces of individual EGFP-XPA molecules measured simultaneously in both detection channels, data bin time 10 ms. The left time traces have been measured at the lower-left circled position, the right time traces at the upper-right circled position in image C. The fluorescence behavior in the Cy3.5 detection channel is indicated in red, the fluorescence behavior in the EGFP detection channel is in green. Excitation was  $4 \text{ kW.cm}^{-2}$  at 488 nm.

### Imaging bubble DNA

In contrast to EGFP-XPA molecules, 90-bp bubble DNA molecules are not immobilized in a 1% agarose matrix. The images obtained after scanning of Cy3.5-labeled bubble-DNA molecules alone in a 1% agarose matrix (figure 4.3.3.A), showed only diffusing DNA molecules. For comparison figure 4.3.3.B is a confocal image of Cy3.5 labeled bubble-DNA molecules immobilized on quartz.

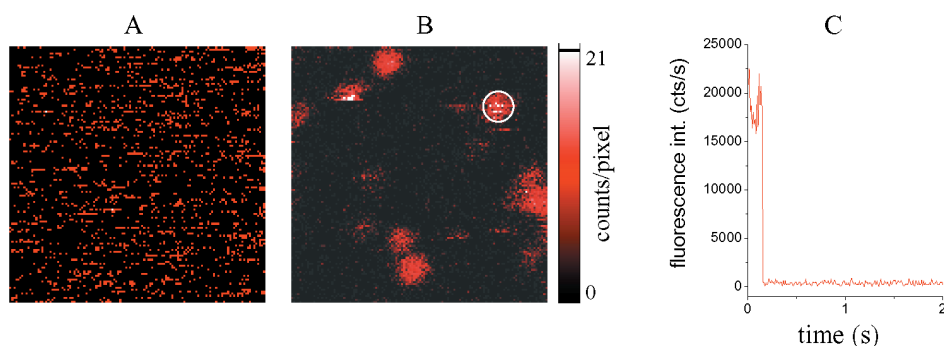


**Fig. 4.3.3.** Confocal results of Cy3.5-bubble-DNA molecules. Images are recorded from Cy3.5 emission detected in the Cy3.5 detection channel, 577-632 nm region. A. In 1% agarose, B. Adsorbed to quartz. Image size is  $6.2 \times 6.2 \mu\text{m}^2$ ,  $128 \times 128$  pixels, dwell time 0.5 ms/pixel. Images A and B are both scaled on a maximum of 21 counts/pixel. C. Typical time trace of an individual Cy3.5-bubble-DNA molecule measured at the circled position in image B with data bin time of 10 ms and emission detection from 577-632 nm. Excitation was  $4 \text{ kW.cm}^{-2}$  at 568 nm.

Again, the time trace of a representative fluorescent spot (figure 4.3.3.C) shows signal intensity and sudden bleaching characteristic of a single Cy3.5 molecule. Because we know from the image in figure 4.3.2.C that EGFP-XPA is immobilized in 1% agarose, we presume that after binding of EGFP-XPA protein to the DNA, the DNA will also be immobilized.

### Single molecule imaging of EGFP-XPA/bubble DNA complexes

EGFP-XPA was incubated with Cy3.5-bubble-DNA as described, after which the mixture was diluted to a concentration of approximately  $5 \times 10^{-10}$  M EGFP-XPA in 1% agarose and prepared for scanning confocal fluorescence microscopy.

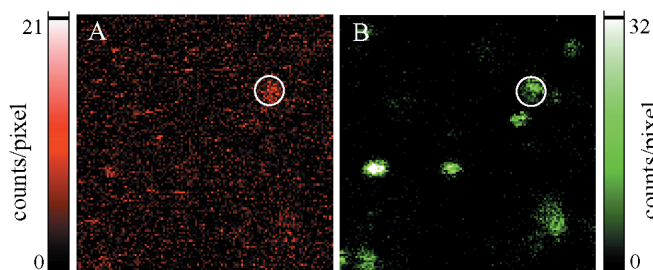


**Fig. 4.3.4.** Confocal images from complexes of EGFP-XPA and Cy3.5-bubble-DNA (ratio 1:20) in a 1% agarose matrix with simultaneous excitation and emission detection of EGFP and Cy3.5 labels. A, Cy3.5 emission 577-632 nm; B, EGFP emission 500-550 nm. Image size is  $6.2 \times 6.2 \mu\text{m}^2$ ,  $128 \times 128$  pixels, dwell time 0.5 ms/pixel; excitation  $4 \text{ kW.cm}^{-2}$  at both 488 nm and 568 nm. The circled position indicates the presence of a complex between EGFP-XPA and Cy3.5-bubble-DNA.



Images were recorded simultaneously for the Cy3.5 and the EGFP fluorescent labels (Figure 4.3.4.A and B respectively). The apparent colocalization of Cy3.5 and EGFP signals within the same diffraction limited spot, indicates that a DNA molecule is trapped by EGFP-XPA, suggesting the presence of a complex between XPA and the bubble DNA. DNA unbound by protein is still freely diffusing in the agarose matrix. A control experiment in which we combined pure EGFP with bubble DNA did not result in any immobilization of DNA (data not shown).

Complex formation was assessed quantitatively by determining the percentage of EGFP-XPA spots that colocalized with Cy3.5. In all analysis only molecules with single molecule fluorescence intensity were included. From analysis of 361 pairs of images containing in total 4340 EGFP-XPA molecules, we observed that a  $(10.1 \pm 0.5)\%$  fraction of EGFP-XPA molecules colocalizes with Cy3.5-bubble-DNA, indicating XPA-DNA complexes. This fraction of EGFP-XPA/bubble-DNA complexes corresponds to an equilibrium dissociation constant  $K_D$  of  $89 \pm 14$  nM, taking into account the actual concentrations in the sample during measurement,  $5 \times 10^{-10}$  M for EGFP-XPA and  $10^{-8}$  M for DNA. Recently, fluorescence anisotropy (5) has been used to determine the equilibrium dissociation constant for XPA binding to DNA. With that method, an equilibrium dissociation constant of  $380 \pm 45$  nM was determined. However, the applied experimental conditions were significantly different from ours. They used 36-bp DNA with a 6-nt bubble in reaction buffer without KCl containing 2 mM  $MgCl_2$ , where we used 40 mM KCl together with 7 mM  $MgCl_2$ . Nevertheless the binding constant for XPA-DNA interaction, that we determined here, is well within the large range of  $K_D$  values obtained by more established bulk methods, varying from several nanomolar to even micromolar concentrations (5,10-12).

### **RPA stabilizes the EGFP-XPA/bubble DNA complexes**

Although we were able to detect binding of XPA to a bubble DNA substrate, it does so with a relatively weak association constant. Several studies employing standard biochemical measurements have demonstrated that RPA enhances the binding of XPA to various DNA substrates (5-9,11,12,23). We tested the ability of our single molecule scanning confocal fluorescence microscope to detect this RPA-induced stabilization of XPA-DNA complexes. EGFP-XPA, RPA and DNA were combined in binding reactions as described in Materials and Methods before immobilization in agarose and confocal imaging. Images registering fluorescence simultaneously from EGFP-XPA and Cy3.5-DNA were collected and the percentage of XPA-DNA complexes determined from the colocalizing spots. As shown in two representative image pairs in Figure 4.3.5, the number of complexes, indicated by the number of colocalized spots, is higher with RPA than in the presence of XPA alone (compare with Figure 4.3.4).

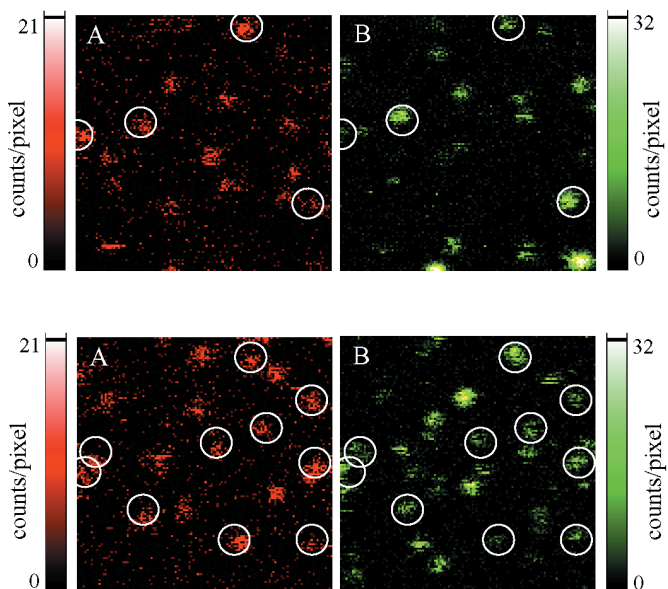


**Fig. 4.3.5.** Scanning confocal images from complexes of EGFP-XPA, RPA and Cy3.5-bubble-DNA (ratio 1:1:20) in a 1% agarose matrix with simultaneous excitation and emission detection of EGFP and Cy3.5 label. A, Cy3.5 emission 577-632 nm; B, EGFP emission 500-550 nm. Image size is  $6.2 \times 6.2 \mu\text{m}^2$ ,  $128 \times 128$  pixels, dwell time 0.5 ms/pixel, excitation  $4 \text{ kW}\cdot\text{cm}^{-2}$  at both 488 and 568 nm. Circled positions indicate colocalization of EGFP-XPA and Cy3.5-bubble-DNA.

In Figure 4.3.6 representative time traces of the fluorescence emission in two channels are shown in which colocalization of EGFP and Cy3.5 signal can be observed.

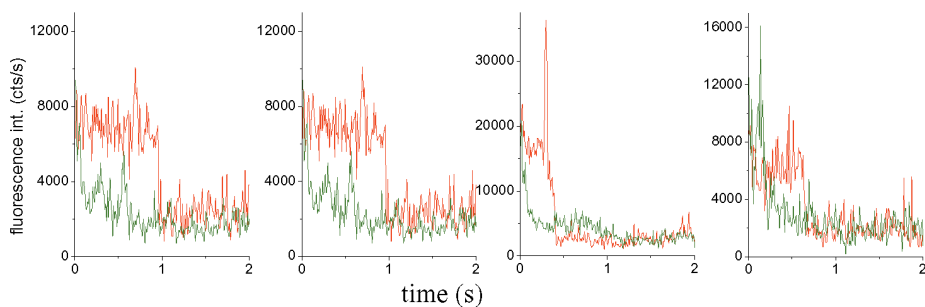


**Fig.4.3.6.** Representative time traces measured simultaneously in both detection channels at positions of colocalized EGFP and Cy3.5 signal with a data bin time of 10 ms. The fluorescence behavior in the Cy3.5 detection channel is indicated in red, the fluorescence behavior in the EGFP detection channel is in green. Excitation was  $4 \text{ kW}\cdot\text{cm}^{-2}$  at both 488 and 568 nm.

From analysis of 351 pairs of images, including 4352 EGFP-XPA molecules, we observed  $(31.8 \pm 0.8)\%$  of the XPA to be bound to DNA in the presence of RPA. This confirms the previously reported enhancement of RPA on the binding of XPA to different DNA substrates (5-9,11,12,23). The corresponding  $K_D$  for binding of XPA in the presence of RPA to bubble-DNA is calculated to be  $21 \pm 3.4$  nM. There is however no published data available from equilibrium binding experiments to compare this number. In other studies different DNA substrates and salt conditions are used, as well as affinity tagged and untagged versions of proteins (24,25).

We also observe immobilized bubble-DNA molecules in figure 4.3.5.A that do not colocalize with EGFP-XPA fluorescence. From the fact that these DNA-molecules are not freely diffusing we conclude that they are likely in complex with RPA only. Analysis of the images reveals that on average 71.9% of the immobilized protein-bound DNA molecules are immobilized by EGFP-XPA or by the combination of EGFP-XPA and RPA. Consequently 28.1% of the protein-bound DNA fraction includes no fluorescent protein and are likely RPA-DNA complexes. In the determination of this fraction we should however consider that our EGFP-XPA contains a small fraction of degradation products, free XPA and EGFP (figure 4.3.1). The unlabeled XPA present might still be able to bind to DNA and in this way contribute to the immobilized DNA fraction without showing an accompanying EGFP signal. Also the fluorescence capacity of part of the EGFP-labeled XPA molecules may have been lost. In the absence however of RPA, the EGFP-XPA binding experiments to bubble-DNA resulted in only a low number of immobilized DNA molecules, non-colocalizing with EGFP (Figure 4.3.4). This means that the fraction of XPA, present either as unlabeled or non-fluorescent, does not have a significant contribution in the binding experiments. Also the chance that EGFP-XPA accidentally colocalizes with RPA-bound DNA is very small. The EGFP-XPA concentration is  $5 \times 10^{-10}$  M and equal to the RPA concentration. At this concentration there are in average only 0.06 EGFP-XPA molecules per measurement volume. Indeed specific binding of RPA to DNA-bubble substrates has been reported (18), with a 30nt-bubble being the minimum size for high affinity RPA binding (26). Our results show that DNA immobilization can be used for the quantitative determination of protein-DNA binding even when the protein is non-fluorescent, like the RPA protein used.

#### 4.4 Discussion

Here we show that we have established a single molecule monitoring procedure using scanning confocal fluorescence microscopy on agarose gel-based samples, to visualize and quantify biomolecular interactions under physiological and equilibrium conditions. As a model system we used a well-defined reaction

intermediate from the NER pathway, *i.e.* the binding of the damage verifiers XPA and RPA to a ds-DNA duplex containing a 30 nt bubble. We used a 5' Cy3.5 fluorescently labeled DNA substrate and GFP-tagged XPA, which was overproduced in *E.coli*, purified to near homogeneity and shown to be fully functional in *in vivo* NER.

The properties of the gel are such that protein-bound DNA can be distinguished easily from unbound DNA. Uncomplexed DNA bubble-substrates diffuse freely within the agarose matrix. Binding to proteins results in DNA immobilization, which can be quantified. After assembly of protein-DNA complexes, colocalization of the GFP-label (attached to the XPA-protein) with the Cy3.5-label on the DNA is observed by simultaneously exciting both fluorophores and detecting the emission in two spectrally separated channels. Because the concentration of the components can be controlled and their interaction quantified this method should be widely applicable to the study of protein-DNA interactions at the single molecule level in equilibrium conditions.

The observed low affinity of XPA for bubble-DNA, as determined here on the single molecule level, is in agreement with already reported binding affinities from biochemical methods (5,10-12). Although the EGFP label has a similar size as the XPA protein, no interference with the XPA binding affinity is expected, because of the positive result in the functionality test. Also the enhancement of XPA binding by the RPA protein is in good correspondence with results reported from ensemble measurements (5-9,11,12,23). So far only one single molecule fluorescence study has been published on NER proteins. In this study autocorrelation methods were applied to reveal conformational dynamics of individual XPA-DNA complexes on two different time scales (27). A 55-bp ds-DNA substrate was used with a 5'-fluorescein considered as a lesion for DNA-repair. The difference in approach as well as the interest in other aspects of individual NER-complexes makes it difficult to compare with our results. From biochemical methods it has been demonstrated that the bubble-DNA substrate used is a relevant model substrate for some steps of the NER mechanism (18). The XPA-DNA binding reaction studied here is obviously only a starting point for single molecule analysis of the NER reaction. We expect to obtain new information on the NER mechanism studying authentic NER-specific damages and additional protein components.

We can conclude from our results so far that aspects of complicated biological processes, like NER, can be analyzed on a single molecule level using confocal fluorescence microscopy and GFP fusion proteins. We will extend our studies to describe the dynamics of interactions between NER-components and DNA. In addition, our home-built microscope setup is able to measure dynamics and properties of single macromolecular interactions, using fluorescence resonance

energy transfer between proper spectral variants of GFP (such as CFP and YFP) fused to different NER proteins (28). The time resolution of data acquisition in our setup allows us to determine interaction dynamics on a time-scale of 10  $\mu$ s. Our results so far and the planned expansion to dynamic studies clearly indicate an exciting future role for single molecule confocal fluorescence microscopy to provide new insight into the molecular mechanisms of vital biological reactions.

## 4.5 References

1. Sugasawa, K., Ng, J., Masutani, C., van der Spek, P.J., Eker, A.P.M., Hanaoka, F., Bootsma, D., and Hoeijmakers, J.H.J. (1998) Xeroderma pigmentosum group C protein complex is the initiator of global genome nucleotide excision repair. *Mol. Cell*, **2**, 223-232
2. Houtsmuller, A.B., Rademakers, S., Nigg, A.L., Hoogstraten, D., Hoeijmakers, J.H., and Vermeulen, W. (1999) Action of DNA repair endonuclease ERCC1/XPF in living cells. *Science*, **284**, 958-961
3. de Laat, W.L., Jaspers, N.G.J., and Hoeijmakers, J.H.J. (1999) Molecular mechanism of nucleotide excision repair. *Genes Dev.*, **13**, 768-785
4. Araujo, S.J., and Wood, R.D. (1999) Protein complexes in nucleotide excision repair. *Mutat. Res.*, **435**, 23-33
5. Hey, T., Lipps, G., and Krauss, G. (2001) Binding of XPA and RPA to damaged DNA investigated by fluorescence anisotropy. *Biochemistry*, **40**, 2901-2910
6. Buschta-Hedayat, N., Buterin, T., Hess, M.T., Missura, M., and Naegeli, H. (1999) Recognition of nonhybridizing base pairs during nucleotide excision repair of DNA. *Proc. Natl. Acad. Sci. USA*, **96**, 6090-6095
7. Li, L., Peterson, C.A., Lu, X., and Legerski, R.J. (1995) Mutations in XPA that prevent association with ERCC1 are defective in nucleotide excision repair. *Mol. Cell. Biol.*, **15**, 1993-1998
8. Mu, D., Wakasugi, M., Hsu, D.S., and Sancar, A. (1997) Characterization of reaction intermediates of human excision repair nuclease. *J. Biol. Chem.*, **272**, 28971-28979
9. Stigger, E., Drissi, R., and Lee, S.-H. (1998) Functional analysis of human replication protein A in nucleotide excision repair. *J. Biol. Chem.*, **273**, 9337-9343
10. Jones, C.J., and Wood, R.D. (1993) Preferential binding of the xeroderma pigmentosum group A complementing protein to damaged DNA. *Biochemistry*, **32**, 12096-12104
11. Wang, M., Mahrenholz, A., and Lee, S.-H. (2000) RPA stabilizes the XPA-damaged DNA complex through protein-protein interaction. *Biochemistry*, **39**, 6433-6439
12. Wakasugi, M., and Sancar, A. (1999) Order of assembly of human DNA repair excision nuclease. *J. Biol. Chem.*, **274**, 18759-18768
13. Hoeijmakers, J.H.J. (2001) Genome maintenance mechanisms for preventing cancer. *Nature*, **411**, 366-374
14. Segers-Nolten, G.M.J., Wyman, C., Wijgers, N., Vermeulen, W., Lenferink, A.T.M., Hoeijmakers, J.H.J., Greve, J. and Otto C. (2002) Scanning confocal fluorescence microscopy for single molecule analysis of Nucleotide Excision Repair complexes, *Nucl. Acids Res.*, **30**, 4720-4727

15. Henricksen, L.A., Umbricht, C.B., and Wold, M.S. (1994) Recombinant replication protein A: expression, complex formation and functional characterization. *J. Biol. Chem.*, **269**, 11121-11132
16. de Laat W.L., Appeldoorn, E., Sugasawa, K., Weterings, E., Jaspers, N.G., and Hoeijmakers, J.H. (1998) DNA-binding polarity of human replication protein A positions nucleases in nucleotide excision repair. *Genes Dev.*, **12**, 2598-2609.
17. Vermeulen, W., van Vuuren, A.J., Chipoulet, M., Schaeffer, L., Appeldoorn, E., Weeda, G., Jaspers, N.G., Priestley, A., Arlett, C.F., and Lehmann, A.R. et al. (1994) Three unusual repair deficiencies associated with transcription factor BTF2(TFIID): evidence for the existence of a transcription syndrome. *Cold Spring Harb Symp Quant Biol.*, **59**, 317-329
18. Matsunaga, T., Park, C.H., Bessho, T., Mu, D., and Sancar, A. (1996) Replication protein A confers structure-specific endonuclease activities to the XPF-ERCC1 and XPG subunits of human DNA repair excision nuclease. *J. Biol. Chem.*, **271**, 11047-11050
19. Eker A.P., Vermeulen, W., Miura N., Tanaka K., Jaspers N.G., Hoeijmakers J.H., and Bootsma D. (1992) Xeroderma pigmentosum group A correcting protein from calf thymus. *Mutat Res.* **274**, 211-24
20. Garcia-Parajo, M.F., Veerman, J.-A., Segers-Nolten, G.M.J., de Grooth, B.G., Greve, J, and van Hulst, N.F. (1999) Visualising individual green fluorescent proteins with a near field optical microscope. *Cytometry*, **36**, 239-246
21. Garcia-Parajo, M.F., Segers-Nolten, G.M.J., Veerman, J.-A., Greve, J., and van Hulst, N.F. (2000) Real-time light-driven dynamics of the fluorescence emission in single green fluorescent protein molecules. *Proc. Natl. Acad. Sci.*, **97**, 7237-7242
22. Dickson, R.M., Cubitt, A.B., Tsien, R.Y., and Moerner, W.E. (1997) On/off blinking and switching behaviour of single molecules of green fluorescent protein. *Nature*, **388**, 355-358
23. He, Z., Henricksen, L.A., Wold, M.S., and Ingles C.J. (1995) RPA involvement in the damage-recognition and incision steps of nucleotide excision repair. *Nature*, **374**, 566-569
24. Patrick, S.M., and Turchi, J.J. (2002) Xeroderma pigmentosum complementation group A protein (XPA) modulates RPA-DNA interactions via enhanced complex stability and inhibition of strand separation activity. *J. Biol. Chem.*, **277**, 16096-16101
25. Iakoucheva, L.M., Walker, R.K., van Houten, B., and Ackerman, E.J. (2002) Equilibrium and stop-flow kinetic studies of fluorescently labeled DNA substrates with DNA repair proteins XPA and replication protein A. *Biochemistry*, **41**, 131-143
26. Kim, C., Paulus, B.F., and Wold, M.S. (1994) Interactions of human replication protein A with oligonucleotides. *Biochemistry*, **33**, 14197-14206
27. Lu, H.P., Iakoucheva, L.M., and Ackerman, E.J. (2001) Single-molecule conformational dynamics of fluctuating noncovalent DNA-protein interactions in DNA damage recognition. *J. Am. Chem. Soc.*, **123**, 9184-9185 (37)
28. Brasselet, S., Peterman, E.J.G., Miyawaki, A., and Moerner, W.E. (2000) Single-molecule fluorescence resonant energy transfer in calcium concentration dependent cameleon. *J. Phys. Chem B*, **104**, 3676-3682

# 5

## SINGLE MOLECULE STUDY on NUCLEOTIDE EXCISION REPAIR:

### DNA-BINDING SPECIFICITY of XPA, RPA and XPC

*In this chapter we extend our single molecule confocal study on Nucleotide Excision Repair complexes to a more detailed investigation of the DNA binding specificity of the XPA, RPA and XPC protein. The binding affinity of XPA/RPA for bubble-DNA, ds-DNA and ss-DNA was determined. XPC binding to cholesterol damaged and undamaged bubble-DNA and ds-DNA was studied.*

## 5.1 Introduction

In the previous chapter we showed the single molecule results for binding of EGFP-XPA to Cy3.5 labeled 90-bp bubble-DNA, containing a 30-bp unpaired central region, in the presence and absence of the RPA protein (1). In agreement with bulk data we found a substantial increase in DNA binding affinity of XPA in combination with RPA. In literature reports the XPA protein alone was shown to display only a slight preference for binding to damaged or partly unpaired DNA over unmodified double-strand DNA (2-6). More specific binding to damaged DNA was observed for the combination of XPA and RPA, indicating a possible role for XPA together with RPA in the initial, damage recognizing stage of NER (4,5,7,8). The reported results with respect to single-strand DNA binding of XPA are contradictory. In some papers a higher affinity for single-strand than for double-strand DNA is mentioned (4,5,9), while others (6,10) report the opposite.

Another NER protein supposed to be involved in damage recognition is the XPC protein. The human XPC protein has a molecular mass of 125 kD and occurs *in vivo* always associated with the 58 kD hHR23B protein. In *in vitro* repair assays the XPC/hHR23B was found to be the first damage-sensing factor (11). This suggestion is supported by the observation with various methods of specific binding with high affinity of XPC/hHR23B to damaged DNA (12-14). Nevertheless there are indications that damage recognition by the XPC/hHR23B complex is not sufficient to initiate the NER reaction. Probably other NER proteins are needed to verify the presence of a damage before the NER reaction proceeds. As possible candidates for damage verification the XPA/RPA combination has been proposed (15,16).

Here we want to study on the single molecule level the specificity for binding of the XPA and RPA proteins to other DNA substrates than bubble-DNA (see chapter 4). We determined and compared the XPA binding affinity for bubble-DNA, ds-DNA, ss-DNA and four-way junction DNA in the presence and absence of the RPA protein. A four-way junction DNA substrate was included in this study because a strong interaction of the XPA protein with DNA junctions was reported recently (10). It was not observed that RPA had an enhancing effect on the affinity of XPA binding to DNA junctions.

Because of the possible involvement of both the XPA/RPA proteins and the XPC/hHR23B complex in the damage recognition part of NER, we also studied the DNA binding specificity of the XPC/hHR23B complex. The XPC/hHR23B protein complex was combined with undamaged ds-DNA and bubble-DNA as well as with a damaged version of both types of DNA. The damage in the DNA substrate was a cholesterol molecule that replaced a thymine nucleotide. The



substitution used was a cholesterol type-A (17), known to be recognized by NER proteins as a damage. In Figure 5.1.1 schematically the position of the XPC/hHR23B is indicated in a possible NER complex together with Cy3.5-labeled damaged DNA and the EGFP label on XPC.

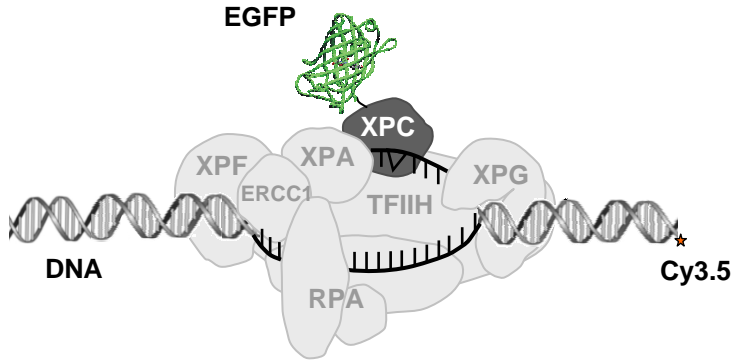


**Fig.5.1.1.** Position of XPC/hHR23B protein (indicated as XPC) in a possible NER complex built up on a 90-'bp' damaged DNA molecule. In this case the damage (triangle) is a cholesterol modification.

## 5.2 Materials and Methods

### Proteins

#### EGFP-XPA

EGFP-XPA was prepared, purified and tested for functionality as described in paragraph 4.2.

#### RPA

The recombinant human RPA complex, utilized in our studies, purified from *E.coli* cells was kindly provided by M. Modesti and A. Janicijevic (Genetics, Rotterdam)(18,19).

#### EGFP-XPC/hHR23B

The EGFP-XPC/hHR23B protein complex was kindly provided by K. Sugawara, RIKEN, Institute of Physical and Chemical Research, Saitama 351-0198, Japan. The protein was produced as FLAG-EGFP-XPC/hHR23B-His<sub>6</sub> protein. Briefly, insect cells were infected with FB1 virus containing FLAG-EGFP-XPC cDNA. The cell extract was purified on Heparin-Sepharose and anti-FLAG agarose. Then the FLAG-EGFP-XPC protein was combined with recombinantly produced hHR23B-His<sub>6</sub> protein to reconstitute FLAG-EGFP-XPC/hHR23B-His<sub>6</sub> complexes

(20). For further purification of the FLAG-EGFP-XPC/hHR23B-His<sub>6</sub> complexes a second Heparin column was used and a Ni-chelating column.

### **DNA substrates**

In binding experiments with the XPA and RPA protein the following Cy3.5 labeled DNA substrates were used: single-strand 90-nt DNA (purchased from DNA Technology A/S, Aarhus, Denmark) and double-strand 90-bp DNA (prepared as described in paragraph 3.2.1). The four-way junction DNA was labeled with Cy3.5 and Cy5. (prepared as described in paragraph 3.1.2). For the experiments described in this chapter only the Cy3.5 label was relevant, the Cy5 label was present to enable single molecule FRET experiments as described in paragraph 3.1.1.

In binding reactions with the EGFP-XPC/hHR23B protein a double-strand 90-bp DNA substrate was used containing a cholesterol (CHO) modification (17). The double-strand 90-bp CHO-DNA was prepared from a 90 nucleotide oligomer containing a cholesterol molecule instead of a thymine nucleotide at position 60 from the 5'-end (Eurogentec, Maastricht, the Netherlands) and the same 5'-Cy3.5 labeled oligomer as used for the double-strand DNA preparation without a modification.

It means that the cholesterol modification is located at position 31 from the 5'-Cy3.5 labeled end. A Cy3.5 labeled 90-bp bubble-DNA containing a cholesterol damage was prepared by combining the same cholesterol containing oligomer as used for preparation of the double-strand DNA with a partly complementary Cy3.5 labeled 90 nucleotide oligomer. The resulting bubble-DNA contains a 30-nt central unpaired region with the cholesterol modification inside the bubble region at the position of the fifth nucleotide from the junction to double-strand DNA.

Also a Cy3.5 labeled double-strand 90-bp DNA substrate and a 90-bp bubble-DNA without a modification was used in combination with EGFP-XPC/hHR23B. Preparation of both DNA substrates was as described for Cy3.5 labeled double-strand DNA in paragraph 3.2.1.

### **EGFP-XPA binding to different DNA substrates**

Binding reactions were performed as described in paragraph 4.2.

### **EGFP-XPC/hHR23B binding to different DNA substrates**

EGFP-XPC/hHR23B was combined with Cy3.5-labeled double-strand 90-bp DNA or bubble-DNA, with or without a cholesterol modification in a molar ratio of 1:20. During incubation the EGFP-XPC/hHR23B concentration was approximately  $3 \times 10^{-9}$  M and DNA concentration was  $6 \times 10^{-8}$  M in a 5  $\mu$ l volume

of 25 mM Hepes, 0.2 mM EDTA, 120 mM NaCl, 20 mM KCl, 7 mM MgCl<sub>2</sub>, pH 7.5. Incubation was performed for 30 min. at 30° C.

### Sample preparation for confocal microscopy

Samples from binding reactions between EGFP-XPA and DNA in the presence and absence of RPA were prepared as described in paragraph 4.2.

Samples from binding reactions between EGFP-XPC/hHR23B and DNA were diluted to concentrations of approximately  $5 \times 10^{-10}$  M with respect to EGFP-XPC at 30° C in molten low melt agarose, 1% (w/v) in 25 mM Hepes, 0.2 mM EDTA, 120 mM NaCl, 20 mM KCl, 7 mM MgCl<sub>2</sub>, pH 7.5.

### Scanning confocal fluorescence microscopy

Confocal measurements were performed as described in paragraph 4.2.

## 5.3 Results

### Preparation of cholesterol containing DNA substrates

In Figure 5.3.1 the electrophoresis result is shown of the annealing products for preparation of 90-bp double strand DNA and bubble-DNA containing a cholesterol modification on an 8% polyacrylamide gel.

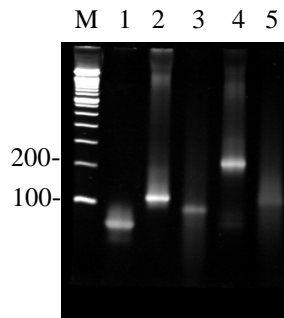


**Fig.5.3.1.** Result of electrophoresis of cholesterol containing DNA preparations. Samples were run on an 8% non-denaturing polyacrylamide gel in 1X TBE buffer (0.09 M Tris-borate, 2 mM EDTA, pH 8.0) and ethidium bromide stained. Lane M: 100-bp ds-DNA marker; lane 1: cholesterol 90-nt oligomer; lane 2: Cy3.5-ds-90bp-cholesterol-DNA; lane 3: Cy3.5-90-nt-oligomer used to prepare ds-90-bp-cholesterol-DNA; lane 4: Cy3.5-90-bp-bubble-cholesterol-DNA; lane 5: Cy3.5-90-nt-oligomer used to prepare 90-bp-bubble-cholesterol-DNA.

From the gel we can conclude that the preparations mainly consist of the desired products. In this figure we can observe a similar difference in electrophoretic mobility between CHO-bubble-DNA (lane 4) and the CHO-ds-90-bp analogue (lane 2) as observed for the non-cholesterol containing DNA preparations, shown

already in paragraph 3.2.2. There is no contamination visible with single strand DNA, only a fraction of less than 10% of the DNA is located in the higher molecular mass side of the gel, probably consisting of combinations of more than two strands of DNA. On the basis of the electrophoresis results the quality of the DNA preparations was considered to be sufficient for use without further purification.

### Single molecule analysis of XPA/RPA/DNA complexes

The results for XPA binding to double-strand and single-strand DNA in the presence and absence of RPA are summarized in Table 5.3.1 and Figure 5.3.2, together with the results from binding to the 90-bp bubble-DNA already described in paragraph 4.3 (1). Results concerning EGFP-XPA interaction with four-way junction DNA have been omitted because no complex formation could be detected from this combination.

	90-bp bubble-DNA		90-bp ds-DNA		90-nt ss-DNA	
	+ RPA	- RPA	+ RPA	- RPA	+ RPA	- RPA
% EGFP-XPA colocalized	31.8±0.8	10.1±0.5	26.5±1.0	7.7±0.9	21.4±1.1	5.5±0.5
$K_D$ (nM)	21±3.4	89±14	27±4.6	119 ± 28	36 ± 6.6	171 ± 35
# EGFP-XPA molec. analyzed	4352	4340	2928	995	1819	1770
# image pairs analyzed	351	361	304	114	206	202

**Table 5.3.1.** Results from analysis of scanning confocal images from complexes of EGFP-XPA and Cy3.5-labeled DNA substrates (ratio 1:20) in a 1% agarose matrix with simultaneous excitation and emission detection of EGFP and Cy3.5 label in the presence and absence of RPA protein. In the presence of RPA the ratio between EGFP-XPA, RPA and DNA was 1:1:20. Statistical errors are indicated.

From these results it appears that the affinity of the XPA protein is only slightly higher for bubble-DNA ( $K_D$  89 ± 14 nM) than for completely double-strand DNA ( $K_D$  119 ± 28 nM). The lowest affinity was observed for the reaction of EGFP-XPA with single-strand DNA ( $K_D$  171 ± 35 nM). Our equilibrium dissociation constants for binding of only XPA to double-strand and single-strand DNA correspond most closely to literature data obtained from gel mobility assays (6). With this non-equilibrium method a  $K_D$  value was reported of 83 nM for XPA binding to double-strand 49-bp DNA and of 217 nM for binding to single-strand 49-mers. In another report, with only qualitative data obtained with the same technique, a slightly higher affinity of XPA for bubble-DNA than for single-

strand DNA was mentioned (10). From this result they concluded that probably not only the single-strand character of a lesion determines XPA binding. Helical deformations like bending and/or kinking accompanying a bubble-DNA structure, may be recognized too.

Our data indicate that the XPA protein alone binds with low affinity and without a clear preference for binding to any of the DNA substrates used.

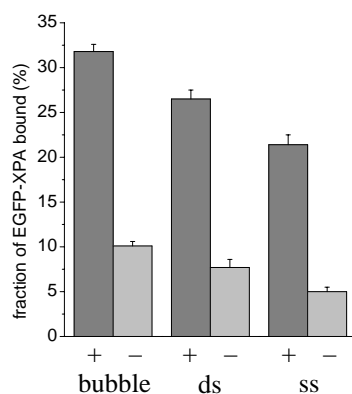


**Figure 5.3.2.** Results from analysis of scanning confocal images from complexes of EGFP-XPA and Cy3.5-labeled DNA substrates (ratio 1:20) in a 1% agarose matrix with simultaneous excitation and emission detection of EGFP and Cy3.5 label in the presence (dark gray bars) and absence of RPA protein (light gray bars). In the presence of RPA the ratio between EGFP-XPA, RPA and DNA was 1:1:20.

**Literature data on XPA/DNA binding** Not all literature reports on XPA binding to different DNA substrates are in agreement. An equilibrium method based on detection of fluorescence quenching resulted in a dissociation constant of  $24.4 \pm 2.5$  nM for binding of XPA to 50-bp double-strand DNA (21). Upon interaction of XPA with single-strand DNA the fluorescence intensity changes were too small to calculate an accurate  $K_D$ . The combination of XPA with 50-bp double-strand DNA containing a 4-bp bubble resulted in a  $K_D$  of  $158 \pm 4.1$  nM, indicating weaker binding to mismatched DNA than to single-strand and double-strand DNA.

From an equilibrium anisotropy study on complex formation of XPA with 36-bp double-strand DNA a significantly higher  $K_D$  appeared of  $1150 \pm 84$  nM and for the single-strand equivalent a  $K_D$  of  $355 \pm 38$  nM (4). Here the affinity of XPA is even 3-4 times higher for single-strand than for double-strand DNA. With the same technique a  $K_D$  of  $380 \pm 45$  nM was obtained for binding of XPA to a 36-bp DNA substrate containing a 6-bp bubble. These data indicate that methods as well as types of DNA substrates used are quite diverse. Also salt concentrations and reaction temperatures were different, resulting in data that are not directly

comparable. In Table 5.3.2 an overview is given of our XPA/DNA binding data together with the available literature data.

single molecule	$K_D$ (nM)	EMSA (6)	$K_D$ (nM)	fluor. quenching (21)	$K_D$ (nM)	fluor. anisotropy (4)	$K_D$ (nM)
bubble-30/90	89	-	-	bubble-4/50	158	bubble-6/36	380
ds-90-bp	119	ds-49bp	83	ds-50-bp	24.4	ds-36-bp	1150
ss-90-nt	171	ss-49-nt	217	ss-50-nt	-	ss-36-nt	355

**Table 5.3.2.** Comparison of our single molecule XPA/DNA binding results with literature data. The bubble-DNA substrates are named bubble- $x/y$ , where  $x$  is the number of unpaired base pairs forming the bubble, and  $y$  is the total length of the DNA in base pairs. EMSA means Electrophoretic Mobility Shift Assay.

In the presence of RPA we observed a similar tendency for XPA-DNA binding than without RPA. In general we can conclude that RPA enhances the binding of XPA to DNA. Several other investigators also observed this effect with different methods. Although hardly any quantitative data are presented, apparently these reports show a larger difference in binding specificity between helix-distorted and non-distorted DNA substrates (5,8,10,22-24) than measured with our equilibrium single molecule method.

**RPA/DNA binding** In the confocal images measured from XPA/RPA/DNA binding reactions we also determined the fractions of immobilized Cy3.5-labeled DNA colocalized and non-colocalized with EGFP-XPA. The colocalized DNA fraction consists of complexes of EGFP-XPA  $\pm$  RPA and DNA, while the non-colocalized fraction consists of RPA-DNA complexes. In chapter 4 (1) we already mentioned for bubble-DNA that 71.9% of immobilized bubble-DNA is present in complex with EGFP-XPA or EGFP-XPA and RPA. Then a 28.1% fraction of immobilized bubble-DNA was present as RPA/bubble-DNA complexes. For double-strand 90-bp DNA we determined a fraction of 37.5% of bound DNA in complex with only RPA. Binding to the single-strand 90-nt oligomer resulted in a 27.5% fraction of bound-DNA complexed to RPA. The resulting ratio's for DNA/XPA/RPA to DNA/RPA complexes for bubble-DNA, ds-DNA and ss-DNA are respectively 2.6, 1.7 and 2.7. This is rather surprising because the RPA protein is known to bind preferentially to single-strand DNA. Preassembly of XPA/RPA complexes may explain the relatively low fraction of RPA/DNA complexes observed. Binding of the XPA/RPA complexes to single-strand or partly single-strand DNA may be more stable than to double-strand DNA. Faster dissociation

of XPA from the instable XPA/RPA complexes on double-strand DNA may result in a relatively larger fraction of RPA/DNA complexes.

### Single molecule analysis of XPC/hHR23B/DNA complexes

The image pairs obtained from scanning confocal microscopy were analyzed for the presence of colocalized intensities from emission of EGFP-XPC and Cy3.5-DNA. The results for EGFP-XPC/hHR23B binding to double-strand DNA with and without a cholesterol modification and bubble-DNA with a cholesterol modification are summarized in Table 5.3.3 and Figure 5.3.3. The combination of EGFP-XPC/hHR23B with unmodified bubble-DNA did not result in images suitable for analysis. In the images a lot of EGFP-XPC/hHR23B aggregation occurred, such that analysis for colocalization of fluorescence was not possible.

	90-bp ds-DNA		90-bp-bubble-DNA	
	+ CHO	- CHO	+ CHO	- CHO
% EGFP-XPC colocalized	42.2 ± 3.4	26.3 ± 2.8	41.1 ± 2.8	–
K <sub>D</sub> (nM)	13 ± 3.8	28 ± 7.5	14 ± 3.5	–
# EGFP-XPC molecules analyzed	360	323	530	–
# image pairs analyzed	45	43	40	–

**Table 5.3.3.** Results from analysis of scanning confocal images from complexes of Cy3.5-labeled DNA substrates with and without a cholesterol modification and EGFP-XPC/hHR23B in a 1% agarose matrix with simultaneous excitation and emission detection of EGFP and Cy3.5 label. The ratio between EGFP-XPC/hHR23B and DNA was 1:20. Statistical errors are indicated.

From the single molecule results obtained from the reaction between the EGFP-XPC/hHR23B complex and different DNA substrates we can conclude that EGFP-XPC/hHR23B binds more specifically to double-strand DNA containing a cholesterol damage than to unmodified double-strand DNA. The equilibrium dissociation constant for binding to undamaged DNA ( $28 \pm 7.5$  nM) is twice the K<sub>D</sub> for cholesterol damaged DNA ( $13 \pm 3.8$  nM). If the main function of the XPC protein indeed is recognition of damaged DNA sites then it is likely that the protein displays a stronger affinity for damaged over undamaged DNA. Obviously the structural distortion produced by the cholesterol damage, even

within a double-strand environment, is sufficient for specific binding of EGFP-XPC/hHR23B (16). On the other hand there is no difference in affinity between complex formation with cholesterol modified double-strand and bubble-DNA. From investigations with DNA containing only a small 5-bp bubble, XPC/hHR23B binding was shown to be independent of the presence of a damage (16). Possibly our results for complex formation of EGFP-XPC/hHR23B with bubble-DNA containing a cholesterol damage indicate more the recognition of unpaired bases than specific binding to the cholesterol modification. Our results may also be influenced by DNA end-binding of EGFP-XPC/hHR23B. Other researchers reported this phenomenon too (13,16).

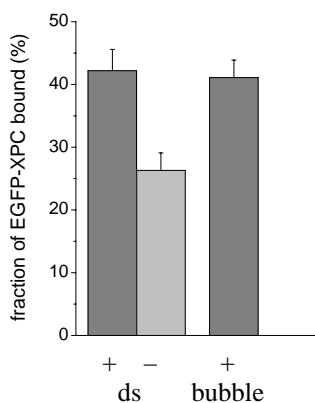


**Figure 5.3.3.** Results from analysis of scanning confocal images from complexes of Cy3.5-labeled double-strand and bubble-DNA substrates with (dark gray bars) and without (light gray bar) a cholesterol (CHO) damage and EGFP-XPC/hHR23B in a 1% agarose matrix with simultaneous excitation and emission detection of EGFP and Cy3.5 label. The ratio between EGFP-XPC/hHR23B and DNA was 1:20.

**Literature data on XPC/DNA binding** The absolute  $K_D$  values obtained with our single molecule method are somewhat higher than those obtained by other investigators. With electrophoretic gel-shift assays  $K_D$  values for XPC/hHR23B binding to undamaged 49-bp (7) and 60 bp (14) double-strand DNA were determined to be 5 nM. Binding to UV-damaged DNA resulted in dissociation constants of 0.12 nM (7) for 49-bp DNA, 4 nM (14) for 60-bp DNA, and 7 nM (12) for 136-bp DNA. With fluorescence anisotropy measurements at equilibrium conditions  $K_D$  values of  $10 \pm 3$  nM were obtained for binding to undamaged DNA and  $1.1 \pm 0.3$  nM for binding to a 6-bp unpaired region within 36-bp double-strand DNA (13). They also showed that UV-induced 6,4-photoproducts were bound with a 30x higher affinity ( $K_D$   $0.5 \pm 0.2$  nM) than cyclobutane dimers ( $K_D$   $16 \pm 2$  nM). Like mentioned for XPA binding, also the literature data available for XPC binding are hard to compare, because of application of different methods and various DNA substrates. In Table 5.3.4 our single molecule results are shown together with literature data.



single molecule	$K_D$ (nM)	EMSA	$K_D$ (nM)	fluor. anisotropy (13)	$K_D$ (nM)
ds-90-bp+CHO	13	UV-damaged (7) ds-49-bp (14) ds-60-bp (12) ds-136-bp	0.12 4 7	Bubble 6/36 6,4-PP 36-bp CPD 36-bp	1.1 0.5 16
ds-90-bp-CHO	28	(7) ds-49bp (14) ds-60bp	5	ds-36bp	10
bubble-30/90+CHO	14				

**Table 5.3.4.** Comparison of our single molecule results with literature data. All measurements were performed at 30 °C. The bubble-DNA substrates are named bubble-*x/y*, where *x* is the number of unpaired base pairs forming the bubble, and *y* is the total length of the DNA in base pairs. EMSA means Electrophoretic Mobility Shift Assay. 6,4-PP is a pyrimidine(6,4)pyrimidone photoproduct, CPD is cyclobutane pyrimidine dimer.

## 5.4 Discussion and Conclusions

**XPA/RPA** The combination of XPA +/- RPA with four-way junction DNA did not result in any colocalization of DNA and protein. Because the conformation of the four-way junction depends largely on the Mg-ion concentration (25-27), we performed binding reactions in the presence of 0-10 mM MgCl<sub>2</sub>. Still no complexes could be detected, not with XPA alone, nor with RPA or with a combination of XPA and RPA. That our results do not correspond to published data (10) may be because of a difference in buffer composition, base composition and length of the arms of the DNA junction. To verify XPA/RPA binding to four-way junction DNA with our single molecule method it is recommended to use identical DNA and reaction conditions as in literature.

Considering the bubble-DNA as a model for damaged DNA (28), it is surprising that we detect only a small difference in binding specificity between bubble-DNA and double-strand DNA even in the presence of RPA. If the XPA/RPA couple indeed plays a role early in NER, where damage recognition and verification takes place (15), a higher selectivity would be conceivable. Possibly our results are influenced by binding of proteins not only to the non-hybridized bubble region but also non-specific binding to the ends of the DNA may occur. In contrast to our equilibrium method, in non-equilibrium methods, like electrophoretic mobility shift assays (8,10,22,23) and surface immobilization methods (5,24), non-specifically formed complexes may dissociate before they can be visualized. For the RPA protein preferential end-binding to single-strand

oligomers has been suggested (29). Assessment of the extent of non-specific DNA end-binding is feasible by performing competition experiments with an excess of unlabeled DNA. Saturation of the non-specific binding sites may result in more pronounced specific binding.

In the binding reactions of XPA/RPA with different DNA substrates the ratio of DNA/XPA/RPA to DNA/RPA complexes was not equal. Possibly the RPA and XPA protein preassemble before they bind to DNA. Upon DNA binding, a conformational change in the XPA/RPA/DNA complex may disrupt the XPA interaction, resulting in remaining RPA/DNA complexes (30). The interaction of XPA/RPA with ds-DNA may be weaker than with bubble-DNA and ss-DNA, resulting in a faster dissociation of the XPA protein. Also free RPA may bind to the DNA. From our data so far it is hard to draw definite conclusions on the exact mechanism of binding of XPA and/or RPA to these particular DNA substrates.

The literature data mentioned illustrate that XPA/RPA/DNA complex formation has not yet been completely characterized. No published data from single molecule methods are available on DNA substrate specificity of NER proteins.

**EGFP-XPC/hHR23B** If the XPC protein is involved in primary recognition of damaged DNA sites then a strong damage discrimination capacity is expected. Considering this role somewhat lower dissociation constants may be expected than obtained from our single molecule experiments. Probably by eliminating non-specific DNA binding, more specific XPC binding may be revealed resulting in lower  $K_D$  values. Like suggested for a more precise determination of  $K_D$  values for XPA/RPA binding to DNA, also for EGFP-XPC/hHR23B binding, competition experiments in the presence of an excess unlabeled DNA may be useful. Specific binding to cholesterol-containing bubble-DNA may be revealed from competition experiments with unlabeled bubble-DNA.

**Comparison of XPA/RPA and XPC/hHR23B binding to DNA** Comparison of the equilibrium dissociation constants for binding of EGFP-XPC/hHR23B to cholesterol damaged DNA ( $K_D$   $13 \pm 3.8$  nM) and for binding of the XPA/RPA combination to bubble-DNA ( $K_D$   $21 \pm 3.4$  nM) reveals a somewhat higher DNA-binding affinity for EGFP-XPC/hHR23B. The affinity for undamaged double-strand DNA is equal for EGFP-XPC/hHR23B ( $K_D$   $28 \pm 7.5$  nM) and for XPA/RPA ( $K_D$   $27 \pm 4.6$  nM). Unfortunately it is not possible to compare directly the binding of EGFP-XPC/hHR23B and the XPA/RPA couple to undamaged bubble-DNA. Analysis for colocalization of protein and DNA was bothered by a strong aggregation of EGFP-XPC/hHR23B observed in recorded images. There may be a relation between the aggregation and the presence of the There may be a relation between the aggregation and the presence of the unmodified

bubble-DNA. This phenomenon however has not yet been sufficiently studied to draw definite conclusions.

In our single molecule experiments the EGFP-XPC/hHR23B complex appears to be more selective for DNA damages than the XPA/RPA combination. The EGFP-XPC/hHR23B has a two times higher affinity for damaged DNA ( $K_D$   $13 \pm 3.8$  nM) than for undamaged DNA ( $K_D$   $28 \pm 7.5$  nM). For binding of the XPA/RPA proteins to bubble-DNA we determined a  $K_D$  of  $21 \pm 3.4$  nM, while binding to double-strand DNA resulted in only a slightly higher  $K_D$  of  $27 \pm 4.6$  nM. This indicates that the XPC/hHR23B complex has a higher damage discriminating capacity than the XPA/RPA couple. It means that our results are in line with the proposed mechanism that damage recognition is performed by XPC/hHR23B complex and damage verification by the XPA/RPA combination (15,16,31).

The confocal fluorescence microscopy results described in this chapter corroborate the results and conclusions from chapter 4. The extension from protein-DNA binding (1, and chapter 4) to assessment of DNA binding specificity (chapter 5) resulted in a confirmation of the potential of our single molecule method. In paragraph 3.2 we compared the diffusion rates of the different DNA substrates within the same 1% agarose medium as used in the protein binding experiments. From the diffusion results it appeared that there is no significant difference in diffusion rate between the bubble-DNA and double-strand DNA. Diffusion of single-strand DNA in the gel was only 1.5 times faster. The observed diffusion properties indicate that the conditions during our confocal measurements are not significantly different for the types of DNA used. It is an extra verification of the reliability of our method.

Even from a biological process as complicated as Nucleotide Excision Repair relevant information can be gained on the single molecule level. In future experiments the influence of XPA/RPA on XPC/hHR23B binding to damaged DNA may be studied, from which conflicting data have been published from biochemical methods (7,13). Physical interaction of XPA with XPC/hHR23B was recently demonstrated (31). In a single molecule AFM study the XPC/hHR23B appeared to bind DNA preferentially at the site of damage and to induce a bend in the DNA whether or not the protein is bound to a site of damage (32). In this study no evidence was found for direct recognition of bent DNA complex bound by XPC/hHR23B. Soon single molecule methods may provide important information additional to the knowledge gained so far from ensemble methods.

### **Acknowledgement**

We thank K. Sugawara for kindly providing the EGFP-labeled XPC/hHR23B complex.

## 5.5 References

1. Segers-Nolten, G.M.J., Wyman, C., Wijgers, N., Vermeulen, W., Lenferink, A.T.M., Hoeijmakers, J.H.J., Greve, J., and Otto, C. (2002) Scanning confocal fluorescence microscopy for single molecule analysis of nucleotide excision repair complexes. *Nucl. Acids Res.*, **30**, 4720-4727
2. Jones, C.J., and Wood, R.D. (1993) Preferential binding of the xeroderma pigmentosum group A complementing protein to damaged DNA. *Biochemistry*, **32**, 12096-12104
3. Kuraoka, I., Morita, E.H., Saijo, M., Matsuda, T., Morikawa, K., Shirakawa, M., and Tanaka, K. (1996) Identification of a damaged-DNA binding domain of the XPA protein. *Mutat. Res.*, **362**, 87-95
4. Hey, T., Lipps, G., and Krauss, G. (2001) Binding of XPA and RPA to damaged DNA investigated by fluorescence anisotropy. *Biochemistry*, **40**, 2901-2910
5. Wang, M., Mahrenholz, A., and Lee, S.-H. (2000) RPA stabilizes the XPA-damaged DNA complex through protein-protein interaction. *Biochemistry*, **39**, 6433-6439
6. Lao, Y., Gomes, X.V., Ren, Y., Taylor, J.-S., and Wold, M.S. (2000) Replication protein A interactions with DNA. III. Molecular basis of recognition of damaged DNA. *Biochemistry*, **39**, 850-859
7. Wakasugi, M., and Sancar, A. (1999) Order of assembly of human DNA repair excision nuclease. *J. Biol. Chem.*, **274**, 18759-18768
8. Buschta-Hedayat, N., Buterin, T., Hess, M.T., Missura, M., and Naegeli, H. (1999) Recognition of nonhybridizing base pairs during nucleotide excision repair of DNA. *Proc. Natl. Acad. Sci. USA*, **96**, 6090-6095
9. Eker, A.P., Vermeulen, W., Miura, N., Tanaka, K., Jaspers, N.G., Hoeijmakers, J.H.J., and Bootsma, D. (1992) Xeroderma pigmentosum group A correcting protein from calf thymus. *Mutat. Res.*, **274**, 211-224
10. Missura, M., Buterin, T., Hindges, R., Hübscher, U., Kaspárková, J., Brabec, V., and Naegeli, H. (2001) Double-check probing of DNA bending and unwinding by XPA-RPA: an architectural function in DNA repair. *EMBO J.*, **20**, 2001
11. Sugasawa, K., Ng, J.M.Y., Masutani, C., Iwai, S., van der Spek, P.J., Eker, A.P.M., Hanaoka, F., Bootsma, D., and Hoeijmakers, J.H.J. (1998) Xeroderma pigmentosum group C protein complex is the initiator of global genome nucleotide excision repair. *Mol. Cell*, **2**, 223-232
12. Batty, D., Rapic-Otrin, V., Levine, A.S., and Wood, R.D. (2000) Stable binding of human XPC complex to irradiated DNA confers strong discrimination for damaged sites. *J. Mol. Biol.*, **300**, 275-290
13. Hey, T., Lipps, G., Sugasawa, K., Iwai, S., Hanaoka, F., and Krauss, G. (2002) The XPC-HR23B complex displays high affinity and specificity for damaged DNA in a true-equilibrium fluorescence assay. *Biochemistry*, **41**, 6583-6587
14. Reardon, J.T., Mu, D., and Sancar, A. (1996) Overproduction, purification, and characterization of the XPC subunit of the human DNA repair excision nuclease. *J. Biol. Chem.*, **271**, 19451-19456
15. Hoeijmakers, J.H.J. (2001) Genome maintenance mechanisms for preventing cancer. *Nature*, **411**, 366-374

16. Sugasawa, K., Okamoto, T., Shimizu, Y., Masutani, C., Iwai, S., and Hanaoka, F. (2001) A multistep damage recognition mechanism for global genomic nucleotide excision repair. *Genes & Dev.*, **15**, 507-521
17. Mu, D., Hsu, D.S., and Sancar, A. (1996) Reaction mechanism of human DNA repair excision nuclease. *J. Biol. Chem.*, **271**, 8285-8294
18. Henricksen, L.A., Umbricht, C.B., and Wold, M.S. (1994) Recombinant replication protein A: expression, complex formation and functional characterization. *J. Biol. Chem.*, **269**, 11121-11132
19. de Laat W.L., Appeldoorn, E., Sugasawa, K., Weterings, E., Jaspers, N.G., and Hoeijmakers, J.H. (1998) DNA-binding polarity of human replication protein A positions nucleases in nucleotide excision repair. *Genes Dev.*, **12**, 2598-2609).
20. Masutani, C., Araki, M., Sugasawa, K., van der Spek, P.J., Yamada, A., Uchida, A., Maekawa, T., Bootsma, D., Hoeijmakers, J.H.J., and Hanaoka, F. (1997) Identification and characterization of XPC-binding domain of hHR23B. *Mol. Cell. Biol.*, **17**, 6915-6923
21. Iakoucheva, L.M., Walker, R.K., van Houten, B., and Ackerman, E.J. (2002) Equilibrium and stop-flow kinetic studies of fluorescently labeled DNA substrates with DNA repair proteins XPA and replication protein A. *Biochemistry*, **41**, 131-143
22. Stigger, E., Drissi, R., and Lee, S.-H. (1998) Functional analysis of human replication protein A in nucleotide excision repair. *J. Biol. Chem.*, **273**, 9337-9343
23. He, Z., Henricksen, L.A., Wold, M.S., and Ingles C.J. (1995) RPA involvement in the damage-recognition and incision steps of nucleotide excision repair. *Nature*, **374**, 566-569
24. Li, L., Peterson, C.A., Lu, X., and Legerski, R.J. (1995) Mutations in XPA that prevent association with ERCC1 are defective in nucleotide excision repair. *Mol. Cell. Biol.*, **15**, 1993-1998
25. Duckett, D.R., Murchie, A.I.H., Diekmann, S., von Kitzing E., Kemper, B., and Lilley, D.M.J. (1988) The structure of the Holliday junction and its resolution. *Cell*, **55**, 79-89
26. Clegg, R.M., Murchie, A.I.H., Zechel, A., Carlberg, C., Diekmann, S., and Lilley, D.M.J. (1992) Fluorescence resonance energy transfer analysis of the structure of the four-way DNA junction. *Biochemistry*, **31**, 4846-4856
27. Clegg, R.M., Murchie, A.I.H., and Lilley, D.M.J. (1994) The solution structure of the four-way DNA junction at low-salt conditions: a fluorescence resonance energy transfer analysis. *Biophys. J.*, **66**, 99-109
28. Matsunaga, T., Park, C.H., Bessho, T., Mu, D., and Sancar, A. (1996) Replication protein A confers structure-specific endonuclease activities to the XPF-ERCC1 and XPG subunits of human DNA repair excision nuclease. *J. Biol. Chem.*, **271**, 11047-11050
29. Kim, C., Paulus, B.F., and Wold, M.S. (1994) Interactions of human replication protein A with oligonucleotides. *Biochemistry*, **33**, 14197-14206
30. Patrick, S.M., and Turchi, J.J. (2002) Xeroderma pigmentosum complementation group A protein (XPA) modulates RPA-DNA interactions via enhanced complex stability and inhibition of strand separation activity. *J. Biol. Chem.*, **277**, 16096-16101
31. You, J.-S., Wang, M., and Lee, S.H. (2002) Biochemical analysis of damage recognition process in nucleotide excision repair. *J. Biol. Chem.*, epub ahead of print

32. Janićijević, A., Sugawara, K., Shimizu, Y., Hanaoka, F., Wijgers, N., Djurica, M., Hoeijmakers, J.H.J., and Wyman, C. (2003) DNA bending by the human damage recognition complex XPC-HR23B. *DNA Repair*, **2**, 325-336

# 6

## GENERAL DISCUSSION and FUTURE PROSPECTS

*In this chapter our single molecule fluorescence results will be discussed in view of future applications in the study of NER.*

## 6.1 Confocal fluorescence microscope

The results presented in this thesis demonstrate that it is well possible to obtain relevant information from complicated biological systems with single molecule confocal fluorescence microscopy. The particular confocal microscope used in this study satisfies the requirements with respect to optical sensitivity and resolution to enable good quality single molecule detection.

To accomplish simultaneous multi-color excitation a prism setup was included, consisting of two identical prisms and a retroreflector. Due to the particular design of the prism setup convenient selection of combinations of excitation wavelengths has been realized. The orientation of the prisms can be precisely tuned to achieve optimal overlap of selected wavelengths, which is essential in the distance determination between individual molecules. A small misalignment will cause a systematic error in the localization of molecules. The systematic error can be calibrated accurately by simultaneous detection in two channels of photons scattered by small gold particles upon illumination with two different wavelengths during scanning.

So far we applied linearly polarized excitation, resulting in dipole orientation related excitation efficiencies. To excite all molecules independent of their dipole orientations with equal efficiencies circular polarized excitation is preferable. With multi-color excitation this is however not simply achieved by including a  $\frac{1}{4}\lambda$ -plate. In our setup we have available for excitation wavelengths from 457 nm to 647 nm. With one  $\frac{1}{4}\lambda$ -plate it was not possible to obtain circularly polarized light over the whole wavelength region. Possibly a Fresnel rhomb quarter wave retarder is more suitable for this purpose, because it performs the conversion from linear to circular polarization practically wavelength independent. However, if it is positioned in the detection path the polarization of the emitted light will not be maintained. So selective detection on polarization of the emission will not be possible then.

In the existing configuration a dichroic beam splitter is used for spectral separation of emitted wavelengths for detection with two APD's. Consequently only two different wavelength regions can be detected simultaneously. Currently we are implementing in the setup a spectrograph in combination with a CCD camera to enhance the flexibility in the selection of relevant spectral detection regions. The result will be that every pixel of a measured image will contain a complete fluorescence spectrum. Moreover, in the spectrograph-CCD configuration only alignment on one pinhole is required, which is a simplification compared to the situation with two pinholes and APD's. The possibilities of the setup will be even expanded more by implementation of a blue light source, like a 410 nm laser diode, in particular for more efficient excitation of ECFP.



## **6.2 Fluorophores**

The single molecule fluorescence results presented in this thesis demonstrate that every fluorescent label has its own typical fluorescence characteristics. All fluorophores included, whether GFP mutants, Cy dyes or Alexa dye, display intensity fluctuations during emission on different time scales. Still GFP mutants are very attractive because of the unique possibility to fuse them to a partner protein in a 1:1 ratio by mild recombinant techniques. Other 1:1 protein-labeling techniques usually require mutagenesis too, to insert, delete or change certain amino acid residues for creation of a single site for labeling. At present single molecule labeled DNA can be purchased from many suppliers, who couple fluorophores to DNA during routine DNA-synthesis. A continuously increasing range of dyes is available for this purpose. The fluorescence on-times of the individual fluorophores studied appeared to be very limited. In general low excitation intensities result in longer on-periods and a higher recovery of photons. In single molecule measurements with organic dyes removal of oxygen should be considered to prolong the duration of emission.

In the search for fluorescent labels with most stable and long-living fluorescence the development of nanocrystals or quantum dots (1,2) appeared to be very promising. Nanocrystals or quantum dots are small semiconductor nanocrystalline objects with diameters that can be fine-tuned from 2 to 10 nm. Their emission wavelength can be tuned by means of material composition and size from UV to infrared. By exciting quantum dots of different size with one wavelength, emission will occur at different wavelengths. Therefore they are very attractive for applications that need multi-color detection. Because one wavelength can be used for excitation there are no effects of chromatic aberrations in the excitation path. Quantum dots show similar or slightly lower quantum yields than organic dyes, but they have larger absorption cross-sections and reduced photobleaching rates. However they also suffer from blinking. They exhibit dark states that last from microseconds to seconds. Still labeling of biomolecules with single quantum dots is not easily achieved. The surface area of a single quantum dot is large enough for linking to multiple biomolecules. Similar methods for coupling to quantum dots are used as for immobilization of biomolecules to surfaces, like silanization and crosslinking (1,3). No biological applications of labeling with single quantum dots have been reported yet.

### **6.3 Alternative optical single molecule methods to study NER**

Here we have shown the possibilities of confocal fluorescence microscopy to study aspects of NER. As already mentioned in paragraph 1.3 NSOM would provide better spatial resolution than confocal fluorescence microscopy. This would improve the localization accuracy of individual components within a NER complex. Considering the size of proposed NER complexes the additional resolution offered by NSOM will be desired. As soon as good quality NSOM measurements can be performed in liquid environment the technique will become more attractive for single molecule biological applications, including NER. Better resolution as well as higher detection efficiency is also offered by 4-pi fluorescence microscopy.

Another possibility would be to study NER complexes with a combined confocal and AFM setup equipped with a metal tip. After identification of a labeled protein from the fluorescence signal, the metal tip may be used to quench or enhance the fluorescence. For quenching or enhancement it is required that the probe and the molecule are in close proximity. In this way it is possible to determine the position of a molecule with much higher precision than the diffraction limit. If proteins within a complex are labeled with different fluorophores, the dye molecules may be quenched or enhanced separately, providing high-resolution information about the distance between the molecules. Also dynamical interactions within a complex, resulting in a change in distance between the tip and a fluorophore, may be monitored from the quenching or enhancement of the fluorescence. By using the metal AFM tip as a nano-tool, individual proteins within complexes may be manipulated. This kind of experiments may provide information about interaction forces between different NER proteins and between proteins and DNA.

### **6.4 Confocal single molecule microscopy and NER**

The applicability of confocal fluorescence microscopy in monitoring dynamic changes of biomolecules is demonstrated from the single molecule FRET data shown from surface immobilized DNA molecules labeled with a donor Cy3.5 and acceptor Cy5 (paragraph 3.1.1) molecule. In view of planned FRET experiments on ECFP-labeled XPA and EYFP-labeled ERCC1/XPF this is a promising result.

With higher excitation intensities than applied in the diffusion experiments in paragraph 3.2 it may be possible to observe FRET from diffusing donor and acceptor labeled molecules. Without any changes in the setup fluorescence correlation spectroscopy (FCS) can be performed to detect fluorescence intensity

fluctuations as a result of dynamic processes on the molecular scale. Also protein-DNA binding may be studied from diffusing complexes with FCS as an alternative for the DNA-immobilization experiments performed in agarose. Upon diffusion of complexes of EGFP-labeled NER proteins and Cy3.5-labeled DNA through the confocal volume, fluorescence intensity will appear simultaneously in the EGFP and the Cy3.5 detection channel.

### Model for initial steps of NER as proposed from confocal single molecule fluorescence results

Figure 6.3.1 gives an author's impression of the initial steps of NER based on the confocal single molecule results described in this thesis, taking into account reported protein-protein interactions (4).

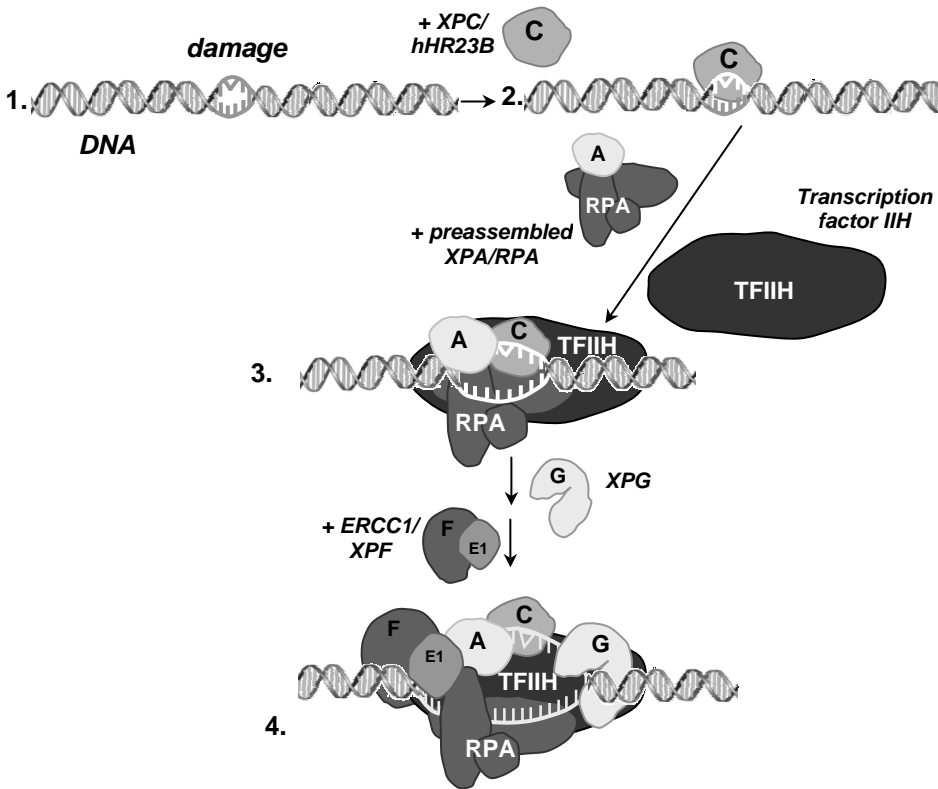


**Fig. 6.3.1.** Proposed model for the first steps of the NER process. 1. A damage induces a helix distortion. 2. The XPC/hHR23B complex recognizes the damage. 3. A preassembled XPA/RPA complex is attracted to the damaged site together with TFIIH. 4. A fully opened DNA complex (24-32 nt) is created by a combined action of RPA and TFIIH. Subsequently XPG is positioned on the 3'-side and ERCC1/XPF to the 5' side of the damage.

The confocal single molecule fluorescence observations included in the model are summarized below:

- in chapter 5 we concluded from equilibrium dissociation constants that the XPC protein has a higher ‘damage’ discriminating ability than the XPA/RPA combination.
- in the XPA/RPA/DNA binding experiments we observed a fraction of DNA in complex with only RPA. This fraction seemed to be dependent on the type of DNA present. We proposed that XPA and RPA may preassemble before binding and that the resulting XPA/RPA/DNA complexes are more stable with single-strand (containing) DNA.
- in the ERCC1/XPF binding experiments to bubble-DNA (paragraph 3.3) we observed that ERCC1/XPF binding is accomplished only in the presence of RPA. Therefore it is likely that there are contacts between ERCC1/XPF and RPA after DNA binding.

So far we studied a limited number of NER proteins on the single molecule level. For further single molecule research on NER complex formation additional recombinant NER-GFP fusion proteins are in production.

Future investigations will include:

- investigation of complex formation in the presence of both XPA/RPA and XPC
- study of interaction between ERCC1-EYFP/XPF and ECFP-XPA by monitoring FRET. As a model FRET-compound the ERCC1-EYFP/ECFP-XPF is in production.
- NER complex formation on DNA containing real damages, like T-T dimers or (6-4)-photoproducts.
- to enable real-time observation of association and dissociation of proteins a different sample preparation method needs to be developed. It is not practical to introduce proteins or other components within a gel environment.

Regardless of the complexity of the mechanism, apparently Nucleotide Excision Repair proteins are able to search very efficiently through the huge genome for damages with a high level of discrimination. To resolve completely the mechanism still a lot of investigations are required from single molecule as well as from ensemble biochemical methods. If we consider NER to take place in vivo within an environment of closely packed chromatin it is even more astonishing that repair is accomplished in such a reliable way as it obviously does. Single molecule studies on NER within a nucleosome environment will be extremely challenging. It may be feasible to study the interaction of fluorescently labeled NER proteins with mononucleosomes, reconstituted from histone octamers and damaged DNA.

## 6.5 References

1. Chan, W.C., Maxwell, D.J., Gao, X., Bailey, R.E., Han, M., and Nie, S. (2002) Luminescent quantum dots for multiplexed biological detection and imaging. *Curr Opin Biotechnol.*, **13**, 40-46
2. Lacoste, T.D., Michalet, X., Pinaud, F., Chemla, D.S., Alivisatos, A.P., and Weiss, S. (2000) Ultrahigh-resolution multicolor colocalization of single fluorescent probes. *Proc. Natl. Acad. Sci. USA*, **97**, 9461-9466
3. Goldman, E.R., Anderson, G.P., Tran, P.T., Mattoussi, H., Charles, P.T., and Mauro, J.M. (2002) Conjugation of luminescent quantum dots with antibodies using an engineered adaptor protein to provide new reagents for fluoroimmunoassays. *Anal. Chem.*, **74**, 841-847
4. Hoeijmakers, J.H.J. (2001) Genome maintenance mechanisms for preventing cancer. *Nature*, **411**, 366-374



## Summary

Confocal fluorescence microscopy is particularly well-known from the beautiful images that have been obtained with this technique from cells. Several cellular components could be nicely visualized simultaneously by staining them with different fluorophores. Not only for ensemble applications but also in single molecule research confocal fluorescence microscopy became a popular technique. In this thesis the possibilities are shown to study a complicated biological process, which is Nucleotide Excision Repair (NER), on the single molecule level with confocal fluorescence microscopy. In chapter one an introduction is given in single molecule fluorescence, properties of fluorescent labels and immobilization methods. Also the NER process is described and the configuration of the confocal fluorescence microscope used.

In chapter 2 the single molecule characteristics of the fluorescent labels used in the course of this thesis work are presented as observed with confocal fluorescence microscopy. Typical single molecule fluorescence observations are shown, like blinking and bleaching features. GFP mutants and chemical dyes, like Cy dyes and Alexa dye, are compared for their single molecule applicability. It appears that every fluorophore has its own typical characteristics. In general we can conclude that it is favorable to excite fluorescent molecules with low intensity to keep the molecules in an emissive state as long as possible and to collect the maximum number of photons. For Cy dyes we demonstrate that removal of oxygen is beneficial to prolong on-times. On the single molecule level Alexa dyes appear to be less attractive than expected from ensemble properties.

Chapter 3 is an illustration of the possibilities of single molecule fluorescence measurements to study the structure, dynamics and interactions of molecules. Results obtained from Cy3.5 and Cy5 double-labeled 4-way junction DNA indicate the potential of single-pair FRET not only to study the configuration of molecules, but also the dynamics of interactions between molecules. The results on DNA diffusion show that not only from immobilized molecules interesting information can be gained with confocal fluorescence microscopy. Our setup offers the possibility for FCS measurements too. DNA immobilization in agarose by protein binding is demonstrated by using fluorescently labeled (ERCC1-EYFP/XPF) as well as non-fluorescent proteins (RPA). In the last paragraph of chapter 3 the accuracy to localize individual fluorescent molecules in confocal images is investigated. It appears that fluorescent molecules can be localized within a diffraction-limited spot with an accuracy of a few tens of nanometers, dependent on the intensity, the signal to background ratio and the number of pixels in a spot.

In chapter 4 results are shown from the application of single molecule fluorescence microscopy to the study of the vitally important NER system. The correspondence of the results obtained from XPA and XPA/RPA binding to a model bubble-DNA substrate with bulk results indicate that relevant information can be obtained with single molecule fluorescence methods. In particular the enhancement of XPA/DNA binding in the presence of RPA shows the significance of our single molecule gel immobilization method.

In chapter 5 the experiments with XPA/RPA are extended to investigate the specificity of binding to different DNA substrates. XPA binding was low with all DNA substrates included, while RPA always had an enhancing effect. The XPC/hHR23B complex was shown to have a higher damage discriminating capability than the XPA/RPA combination. In literature similar results have been reported from ensemble experiments.

Chapter 6 gives a general discussion on single molecule fluorescence aspects in relation with NER. Possibilities for future single molecule NER experiments are suggested.



## Samenvatting

Confocale fluorescentie microscopie is vooral bekend vanwege de schitterende afbeeldingen van cellen, die met deze techniek verkregen zijn. Meerdere cellulaire componenten kunnen tegelijkertijd zichtbaar gemaakt worden door te labelen met verschillende fluoroforen. Niet alleen voor toepassingen in bulk, maar ook voor de bestudering van individuele moleculen is confocale fluorescentie microscopie een populaire techniek geworden. In dit proefschrift wordt getoond wat de mogelijkheden zijn van confocale fluorescentie microscopie voor de bestudering van een ingewikkeld biologisch proces, het nucleotide excisie herstel proces (NER), op het niveau van één enkel molecuul. In hoofdstuk 1 wordt fluorescentie van individuele moleculen geïntroduceerd, evenals eigenschappen van verschillende fluorescerende labels en methoden voor het immobiliseren van moleculen. Ook het NER proces wordt beschreven en de bouw van de gebruikte confocale fluorescentie microscoop.

In hoofdstuk 2 worden de karakteristieke eigenschappen weergegeven van individuele fluorescerende labels, die toegepast zijn in het onderzoek beschreven in dit proefschrift, zoals ze waargenomen zijn met confocale fluorescentie microscopie. Typische kenmerken van individuele fluorescerende moleculen worden getoond, zoals het afwisselend aan en uitgaan (blinker) en het discrete blekings gedrag. Mutanten van GFP zijn vergeleken met chemische Cy and Alexa labels, wat betreft hun toepasbaarheid in metingen aan individuele moleculen. Het blijkt dat elk fluorofoor zijn eigen typische fluorescentie eigenschappen heeft. In algemene zin kunnen we concluderen dat het gunstig is om fluorescerende moleculen aan te slaan met lage intensiteit om zodoende de moleculen zo lang mogelijk in een emitterende toestand te houden en zoveel mogelijk fotonen te verzamelen. Voor Cy kleurstoffen laten we zien dat de aan-periodes aanzienlijk verlengd kunnen worden als zuurstof verwijderd wordt. Op het niveau van individuele moleculen blijken Alexa labels minder geschikt te zijn dan verwacht was op grond van hun eigenschappen in bulk.

Hoofdstuk 3 illustreert de mogelijkheden van metingen aan individuele moleculen voor de bestudering van de structuur en het dynamisch gedrag van moleculen, alsook voor het vaststellen van interacties tussen moleculen. Resultaten verkregen met Cy3.5 and Cy5 dubbel-gelabeled DNA geven niet alleen het vermogen aan van FRET voor bestudering van de configuratie van individuele moleculen, maar ook voor het observeren van dynamische interacties tussen moleculen. Resultaten verkregen met diffunderend DNA geven aan dat niet alleen van geïmmobiliseerde moleculen interessante informatie verkregen kan worden met confocale fluorescentie microscopie. Onze microscoop biedt tevens de mogelijkheid om FCS metingen te doen. Immobilisatie van DNA in agarose door middel van eiwit

binding wordt aangetoond door fluorescerende (ERCC1-EYFP/XPF) alsook niet-fluorescerende eiwitten (RPA) te gebruiken.

In de laatste paragraaf van hoofdstuk 3 wordt onderzocht wat de nauwkeurigheid is, waarmee individuele fluorescerende moleculen in confocale afbeeldingen gelokaliseerd kunnen worden. Het blijkt dat de positie van fluorescerende moleculen binnen een diffractie gelimiteerde spot bepaald kan worden met een nauwkeurigheid van enkele tientallen nanometers, afhankelijk van de intensiteit, de signaal-achtergrond verhouding en het aantal pixels in een spot.

In hoofdstuk 4 worden resultaten getoond van de toepassing van confocale fluorescentie microscopie voor de bestudering van individuele moleculen die deel uitmaken van het NER systeem, waarvan het goed functioneren voor ons van levensbelang is. De resultaten verkregen van XPA en XPA/RPA binding aan een model bubble-DNA substraat zijn vergelijkbaar met resultaten van bulk experimenten. Dit geeft aan dat het mogelijk is om relevante informatie te verkrijgen met methoden waarbij fluorescentie van individuele moleculen gedetecteerd wordt. In het bijzonder de toename van XPA/DNA binding in aanwezigheid van RPA geven de betekenis aan van onze gel immobilisatie methode.

In hoofdstuk 5 worden de experimenten met XPA/RPA uitgebreid om de specificiteit van de binding aan verschillende DNA substraten te onderzoeken. Er bleek weinig binding van XPA te zijn aan alle gebruikte DNA substraten, terwijl RPA steeds een toename van XPA binding tot gevolg had. Het XPC/hHR23B complex bleek een hoger vermogen te hebben om schades in DNA vast te stellen dan de XPA/RPA combinatie. In de literatuur zijn vergelijkbare resultaten beschreven van experimenten gedaan in bulk.

In hoofdstuk 6 wordt een algemene beschouwing gegeven van aspecten van fluorescentie van individuele moleculen met betrekking tot NER. Er worden mogelijkheden aangegeven voor toekomstige experimenten aan individuele NER complexen.

**List of abbreviations**

AFM	atomic force microscopy
APD	avalanche photodiode
bp	basepair
CCD	charge coupled device
cDNA	complementary DNA
CHO	cholesterol
CPD	cyclobutane pyrimidine dimer
DNA	desoxyribonucleic acid
ds-DNA	double-strand DNA
DTT	dithiothreitol
$\epsilon$	extinction coefficient
ECFP	enhanced cyan fluorescent protein
EGFP	enhanced green fluorescent protein
EMSA	electrophoretic mobility shift assay
ERCC1	excision repair cross complementation group 1 protein
EYFP	enhanced yellow fluorescent protein
FCS	fluorescence correlation spectroscopy
FLAG	Asp-Tyr-Lys-Asp-Asp-Asp-Lys epitope
FRAP	fluorescence recovery after photobleaching
FRET	fluorescence resonance energy transfer
FWHM	full width half maximum
GFP	green fluorescent protein
Hepes	4-(2-Hydroxyethyl)piperazine-1-ethanesulfonic acid
His <sub>6</sub> HA	6 histidine stretch + heamagglutine epitope
IPTG	isopropyl $\beta$ -D-1-thiogalactopyranoside
ISC	intersystem crossing
K <sub>D</sub>	equilibrium dissociation constant
kDa	kilo Dalton
$\lambda$	wavelength
n	refractive index
NA	numerical aperture
NER	nucleotide excision repair
NHS	N-hydroxy-succinimide
Ni-NTA	nickel-nitrilo-triacetate
NP-40	nonionic detergent
NSOM	near field scanning optical microscopy
nt	nucleotide
6,4-PP	pyrimidine(6,4)pyrimidone photoproduct,
PAA	polyacrylamide
PAGE	polyacrylamide-gelelectrophoresis
PBS	phosphate buffered saline

*List of abbreviations*

---

PCR	polymerase chain reaction
Q	quantum yield
RPA	replication protein A
SDS	sodiumdodecylsulphate
ss-DNA	single-strand DNA
TAE	0.04 M Tris-acetate, 1 mM EDTA, pH 8.0
TBE	0.09 M Tris-borate, 2 mM EDTA, pH 8.0
TFIIH	transcription factor IIH
TIRFM	total internal reflection microscopy
UDS	unscheduled DNA synthesis
wt-GFP	wild-type GFP
XPA-G	Xeroderma pigmentosum group A to G protein
XRCC4	X-ray cross complementation protein 4

## Nawoord

In februari 1997 benaderde Jan (G.) mij met de vraag of ik interesse had om een promotieonderzoek te gaan doen. Daarna heeft hij die vraag nog vaak herhaald, steevast eindigend met: *De druppel holt de steen uit, niet door geweld, maar door dikwijls te vallen (Gutta cavat lapidem, non vi, sed saepe cadendo!)*. Na de nodige bedenktijd, kwam ik uiteindelijk tot de conclusie dat het wel tijd werd voor een nieuwe uitdaging, na een geslaagd triplo voortplantings-experiment. Het tot stand komen van dit proefschrift bewijst dan ook dat het spreekwoord uiteindelijk bewaarheid is geworden. Jan, bedankt voor de gelegenheid die je me geboden hebt om deze stap te zetten. Dankzij verschillende geldbronnen die je wist aan te boren, zoals het fonds Vrouwen aan de UT, was het mogelijk om mij 'vrij' te maken voor het promotieonderzoek.

Tijdens het onderzoek hebben we steeds nauw samengewerkt met de groep van Jan Hoeijmakers, afdeling Genetica, Erasmus Universiteit Rotterdam. Een groot gedeelte van 1998 heb ik zelfs full-time mogen doorbrengen in het Rotterdamse lab om te proberen mijn eigen GFP fusie-eiwitten te produceren. Jan (H.), bedankt voor de gastvrijheid. Ik kijk nog steeds met veel plezier terug op deze intensieve, maar zeer leerzame periode. De hulp, inzet en het enthousiasme van jou, Wim, Suzanne, Claire en Nils heb ik zeer gewaardeerd, ook in de tijd daaropvolgend.

Binnen BFT werd ik opgenomen in de groep van Kees (O.), die mij toestond om de Raman microscoop te 'mis'bruiken voor single molecule fluorescentie. Hij heeft de bouw van een nieuwe confocale fluorescentie microscoop mogelijk gemaakt, waarmee ik vele 'exciting' metingen heb kunnen doen. Tijdens het promotieonderzoek is Kees steeds mijn aanspreekpunt geweest. Kees, bedankt hiervoor en ik hoop dat hieraan met deze promotie geen einde komt.

Omdat ik met mezelf heb afgesproken maar één pagina uit te trekken voor het nawoord, moet ik me beperken wat betreft het noemen van namen. Daarom wil ik graag tegen alle aardige, behulpzame, leuke, geïnteresseerde, poëtische, handige, creatieve, zorgzame, gezellige (ex)medewerkers en (ex)studenten van BFT, zeggen: BEDANKT!

Toch wil ik een paar mensen apart noemen: Aufried, zonder jou waren de confocale metingen nooit tot stand gekomen. Je was onvermoeibaar in het aanhoren en beantwoorden van al mijn 'gezeur' over allerlei details in de opstelling. Roel, 'jouw' prisma-gedeelte is voor mij nog steeds de parel van de microscoop. De sample-houder en andere onderdelen functioneerden erg goed, dankzij het precisie-werk van Hans (de B.) Als kamergenoot was Natallia altijd de klos voor het beantwoorden van alle mogelijke fysische vragen (spasibo). Tijdens de eindfase van het schrijven was het telkens weer Anthony die spontaan hielp allerlei moeilijkheden met programma's, figuren, kleuromzettingen, etc. op te lossen.

En alweer komen de mensen die verdienen als eerste genoemd te worden, achteraan. Het zijn mijn ouders geweest die mij de kans hebben gegeven om 'door te leren'. Pa en Ma, bedankt voor jullie steun en interesse. Ondanks de ingrijpende, trieste gebeurtenis binnen de familiekring, heb ik steeds duidelijk de belangstelling van alle familieleden gemerkt, niet in het minst van Marian zelf. Het staat buiten kijf dat een goed verzorgde thuissituatie onontbeerlijk is om onbekommerd te kunnen werken. Jos, de vanzelfsprekendheid waarmee jij allerlei taken op je genomen hebt is bewonderenswaardig. Tim, Marijn en Lex, jullie flexibele houding, meelevende en verrassende kijk op de zaak (denk je nou echt dat iemand dat leest....?) heeft mij steeds goed gedaan.

Ine

## **Curriculum vitae**

Ine Segers-Nolten werd geboren op 21 juli 1956 te Oldenzaal. In 1974 behaalde zij het Gymnasium- $\beta$  diploma aan het Twents Carmel lyceum te Oldenzaal. Vervolgens deed zij de HNWO (Hoger Natuur Wetenschappelijk Onderwijs) opleiding aan de Analistenschool te Groningen, die zij in 1978 met gunstig gevolg afsloot. In het kader van deze opleiding werd een afstudeeronderzoek gedaan bij de Afdeling Plantenfysiologie van de Rijks Universiteit Groningen. Aansluitend kwam zij in 1978 in dienst bij het Academisch Ziekenhuis Groningen, afdeling Nucleaire Geneeskunde, waar zij als biochemisch analist assisteerde in een promotieonderzoek naar de toepasbaarheid van hormoon-behandelingen in de bestrijding van borstkanker. In 1981 kreeg zij een aanstelling als analist aan de Universiteit Twente, faculteit Technische Natuurkunde, groep Biofysische Technieken, geleid door prof. dr. J. Greve. Tot 1998 vervulde zij deze functie, waarna zij als AIO aan een promotie-onderzoek begon, onder leiding van dr. C. Otto en prof. dr. J. Greve. Het onderzoek werd gefinancierd door de Stichting Technische Wetenschappen (STW) en werd uitgevoerd in nauwe samenwerking met de afdeling Genetica van de Erasmus Universiteit te Rotterdam, geleid door prof. dr. J.H.J. Hoeijmakers. Het promotie-onderzoek betrof de bestudering van individuele fluorescerende moleculen en de toepassing ervan in de bestudering van het nucleotide excisie herstel mechanisme. De resultaten van dit werk zijn beschreven in dit proefschrift.